AN ABSTRACT OF THE THESIS OF

Moon H. Lee for the degree of Doctor of Philosophy

in Mechanical Engineering presented on August 14, 1984

Title: Fatigue Life, Fatigue Crack Propagation and Fracture Toughness Study of 7075 Aluminum Alloy Subjected to Thermomechanical Processing

Redacted for Privacy

Abstract approved: ______________________
Dr. Murli Saletore

Due to its high strength/weight ratio, 7075 aluminum alloy has been widely used as an aerospace material. However, it has relatively low fatigue strength and low fracture toughness in the T6 condition. Thermomechanical processing, including pre-cyclic loading and stretching at high and ambient temperatures, has been investigated with the aim of improving these properties.

Fatigue life tests show that all four thermomechanical processes investigated increase the fatigue life at low stress levels, but cause a reduction at high stress levels.

The effect of the precipitate free zone (PFZ) width on the fatigue crack propagation rate and fracture toughness has also been investigated. The fatigue crack propagation rate of the alloy with a wide PFZ was found to be approximately the same as that of the alloy with a narrow PFZ under similar conditions of cyclic loading.

The alloy with the wide PFZ demonstrated a greater value of fracture toughness than that shown by the alloy with the narrow PFZ.

These experimental results have been analyzed taking recently proposed theoretical models into account.

Transmission electron microscopy showed that a large number of dislocations were generated within the soft PFZ areas as a result of the cyclic pre-loading. This is believed to contribute to the increase in fatigue life at low applied stress levels.

Scanning electron microscopy has shown an intergranular fracture mode for the alloy with the narrow PFZ and a dimple rupture mode for the alloy with the wide PFZ.

Fatigue Life, Fatigue Crack Propagation and Fracture Toughness Study of 7075 Aluminum Alloy Subjected to Thermomechanical Processing

by

Moon H. Lee

A THESIS

submitted to

Oregon State University

in partial fulfillment of
the requirements for the
degree of

Doctor of Philosophy

Completed August 14, 1984

Commencement June 1985

APPROVED:

Redacted for Privacy

Assistant Professor of Mechanical Engineering in charge of major

Redacted for Privacy

Head of Department of Mechnical Engineering

Redacted for Privacy

Dean of Graduate School

Date thesis is presented August 14, 1984

Typed by Donna Lee Norvell-Race for Moon H. Lee

ACKNOWLEDGMENTS

This work would have been impossible without:

- my parents' absolute love toward me,
- my family members' profound belief in me,
- consistent support by my wife, Kyung-Sook,
- continuous financial aid from department head, Dr. J. W. Welty,
- enlightening guidance from my advisor, Professor M. Saletore,
- sincere encouragements from my committee members, Professor P. Burke, Professor T. Kennedy, Professor R. Thresher and Professor E. Fichter.

Also, I would like to give my deep gratitude to J. Bauffer, A. Brickman, L. Sundberg, C. Svenson, A. Soedner and P. Romans for their technical assistance and advice.

TABLE OF CONTENTS

LIST OF FIGURES

LIST OF TABLES

Fatigue Life, Fatigue Crack Propagation and Fracture Toughness Study of 7075 Aluminum Alloy Subjected to Thermomechanical Processing

I. INTRODUCTION

Since the adoption of precipitation hardening procedures for high strength aluminum alloys, 7075 aluminum alloy [1,2,3] has been used in aerospace applications because of its high strength/weight ratio and relatively good ductility with T6 tempering. However, it has relatively poor fatigue strength and low fracture toughness.

The low fracture toughness and poor fatigue properties are attributed to the metallurgical inhomogeneities such as second phase particles, grain-boundaries and precipitate free zones which cause early crack nucleation or inhomogeneous slip distribution [4].

As one way to improve the fracture toughness and fatigue properties, thermomechanical processing (the combination of thermal processing and mechanical processing: TMP) has been developed. Since the advent of TMP, it has been investigated and used for aluminum alloys including 7075 aluminum alloy.

One of the main purposes of TMP in 7075 aluminum alloy has been to homogenize slip distribution. One of the most widely used types of TMP is rolling before final aging. This TMP reduces precipitate free zone length by creating grain boundary steps or homogenizes the dislocation distribution. This promotes the precipitation during the final aging process. However, this conventional TMP could not eliminate the precipitate free zone totally, thus did not improve the fatigue properties of the alloy satisfactorily. Cyclic pre-loading as TMP is a new concept which has shown positive results in some studies, but has not been investigated extensively.

Furthermore, cyclic pre-loading at elevated temperature, which is theoretically more plausible, has not been investigated at all. Cyclic pre-loading at elevated temperature has the following advantages [5]:

1. Vacancies which are necessary for precipitation are generated at elevated temperature by cyclic loading.
2. Peierls-Nabarro force is smaller at elevated temperature than at room temperature.

Therefore, it would be useful to examine the fatigue properties of 7075 aluminum alloy subjected to cyclic loading at high temperature.

Although this type of TMP improves the fatigue life, it remains in doubt that such TMP will reduce the fatigue crack propagation rate, an important parameter in modern design [6,7]. From this point of view, the fatigue crack propagation study becomes necessary.

Furthermore, a precipitate free zone, which is devoid of precipitates, develops in 7075 aluminum alloy. This PFZ is unavoidable in 7075 aluminum alloy and its width can be easily changed by a slight change in aging temperature or in the solution treating temperature.

Some investigations have been conducted into the microstructural factors which affect fatigue crack propagation or fracture toughness such as grain size, inclusions or degree of aging. However, there do not seem to have been any investigations into the effect of PFZ width changes on the fatigue crack propagation rate or fracture toughness. Recently, a theoretical model has been proposed to help estimate the fracture toughness of alloys which develop precipitate free zones.

Considering the above points, it is necessary and important for practical and academic purposes to study the effects of PFZ width on fatigue life, fatigue crack propagation and fracture toughness. In addition, the fracture mode of the alloy plays an important role in fracture toughness. Therefore, it is felt to be worthwhile to study the fracture of the alloys subjected to thermomechanical processing.

II. LITERATURE SURVEY

II.1 7075 Aluminum Alloy

Aluminum-based alloys are classified by their major alloying elements and tempering. The major alloying elements present in 7075 aluminum alloy are zinc, magnesium and copper. The composition of 7075 aluminum alloy is shown in Table 1.

7075-T6 is one of the high strength aluminum alloys and is tempered after solution treatment, at 120°C for 24 hours to obtain the maximum strength and good ductility. 7075-T651 is the alloy which has been T6 tempered and stretched 1-3% to relieve the residual stresses.

This alloy has been used as an aerospace material extensively because of its high strength/weight ratio, good ductility and good corrosion resistance [1].

The hardening mechanism of 7075 aluminum alloy is mainly precipitation hardening combined with some solid solution hardening. The major precipitation mechanism is as follows:

$$\text{G-P zone} \rightarrow \eta' \rightarrow \eta$$

G-P zones are formed in the very early stage of precipitation. The planar array of Cu atoms which are coherent with the matrix are formed.

η' is the metastable semi-coherent precipitate whose chemical composition is $Mg(Zn)_2$. The η' precipitates form prime strengthening particles in the matrix.

η is the incoherent precipitate which forms as an equilibrium state of η'. Other forms of precipitates are second phase particles. These second phase particles are detrimental to mechanical properties including fatigue properties and fracture toughness and occur in sizes large enough to be seen by optical microscopy.

Another type of precipitate, dispersoids, is formed from Cu or Mn. These elements are added to control the grain-size and to prevent recrystallization.

II.2 Precipitate Free Zone

II.2.1 The Origin of the Precipitate Free Zone

The precipitate free zone (PFZ) occurs frequently in age-hardening alloys including 7075 aluminum alloy. The origin of the PFZ was investigated by Thomas [14] and others [15-17], who found that the depletion of vacancies around the grain-boundary leads to the formation of the PFZ.

When the alloy is quenched from the solution treatment temperature, the concentration of the vacancies is not uniform around the grain boundaries. The concentration of vacancies is very low near the grain boundary and increases gradually away from it. The profile of the concentration of vacancies is shown in Figure 1:

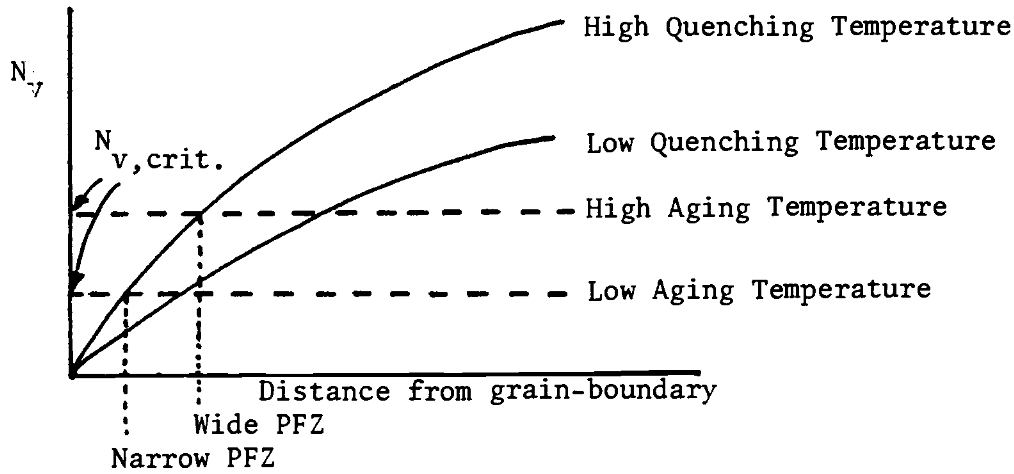

FIGURE 1. Profile of vacancy concentration near the grain boundary with different quenching temperatures

The nucleation of precipitates does not occur if the concentration of vacancies is below the critical value. Therefore, precipitates will not form near the grain boundary if the concentration of vacancies is below the critical value. This critical concentration of vacancy ($N_{v,crit.}$) increases as the aging temperature increases. Therefore, it is expected that a wider PFZ will be formed at higher aging temperatures with the same quenching temperature and the same quenching rate rather than at low aging temperatures.

Starke [18] discussed the effect of quenching temperature on the width of the PFZ. Unwin [16] and Nicholson [19] studied the origin of the PFZ considering both vacancy depletion and solute depletion.

II.2.2 The Effect of the PFZ on Mechanical Properties

The fact that plastic deformation occurs preferentially within the PFZ was noted by Thomas and Nutting [14]. Later, Sedricks [20] confirmed the phenomenon using transmission miscroscopy.

Recently, Abe [21] examined the mechanical properties of Al-Zn-Mg alloy and found that work-hardening rate and elongation change markedly with PFZ width thus confirming the occurrence of preferential plastic deformation within the PFZ. Lütjering [22] studied the fatigue and fracture of aluminum alloys with PFZ and discussed possible fracture mechanisms.

Welpman [23] also examined the fatigue properties in high strength aluminum alloys with PFZ and found some improvements in fatigue life by thermomechanical processing. However, the crack propagation rate was found to increase by the same TMP. Cornish [24] investigated the relationships between mechanical properties and PFZ width and found that U.T.S., Y.S. and elongation all decrease as PFZ width increases.

II.3 Thermomechanical Processing

Various kinds of thermomechanical processing (TMP) have been investigated [25,26,27] to improve the fatigue properties in 7000 series aluminum alloys. TMP can be defined as the combination of mechanical deformation and thermal treatment during the final processing of age-hardenable aluminum alloys.

Many investigators have employed deformation prior to or during the aging process. This deformation introduces additional nucleation sites for precipitation which could improve mechanical properties, including fatigue characteristics.

Osterman [28] showed that fatigue strength of 7075 aluminum alloy could be increased substantially by TMP and observed that the principal requirement for high-cycle fatigue resistance is the ability of the alloy to deform by homogeneous slip. Homogeneous deformation of age-hardened alloys requires a homogeneous microstructure. TMP of age-hardening alloys offers the possibility of homogeneous slip by introducing uniform dislocation distribution in the matrix. Di Russo [29] developed TMP procedures for improving ductility and fracture toughness of 7000 series alloys.

Alder [30] examined heat-treatments on fatigue properties. Ryu [31] examined the effect of double heat-treatment and reported some improvement in fatigue life at low stress levels. Nunomura [32] reported that extremely underaged or extremely overaged alloy showed improved fatigue strength despite a low value of yield strength.

Recently, a new concept of TMP was proposed by Weissman and coworkers [33,34]. Weissman showed that fatigue life of a single crystal can be markedly extended by judicious control of the dislocation substructure developed during cyclic loading. Lu and Weissman [35] found recently that cyclic deformation before aging in Al-6.5 Zn alloy improved fatigue resistance by introducing dislocation tangles within the PFZ. Lu [35] also examined tensile deformation at elevated temperature before aging and found a significant improvement in fatigue resistance at low stress levels.

However, the concept of cyclic pre-loading and tensile deformation at high temperature as thermomechanical processing has not been tested in the 7075 aluminum alloy system.

II.4 Fatigue Life Studies

II.4.1 S-N Curve

The oldest and most widely used method to study fatigue properties is the S-N curve. The S-N curve or Wöhler curve can be obtained by plotting the stress amplitude used for cyclic loading against the total number of cycles at which the fatigue specimen failed.

The mathematical expression for this curve can be expressed by the following equation [36]:

$$\sigma_a = \sigma_f'(2N_f)^e$$

where σ_a : stress amplitude

σ_f' : fatigue strength coefficient

e : exponent of S-N curve

N_f : fatigue life

In recent years, sophisticated instruments have been developed to control cyclic deformation in order to obtain the $\Delta\varepsilon_t$ - 2N curve, which is similar to the S-N curve. This curve is described by the Manson-Coffin equation whose mathematical expression is as follows [37]:

$$\frac{\Delta\varepsilon_t}{2} = \frac{\sigma_f'}{E}(2N_f)^b + \varepsilon_f'(2N_f)^c$$

where $\frac{\Delta\varepsilon_t}{2}$: total strain amplitude

N_f : total fatigue life at failure

σ_f' : fatigue strength coefficient

E : Young's modulus

ε_f' : fatigue ductility coefficient

b : fatigue strength exponent

c : fatigue ductility exponent

From this S-N curve or Manson-Coffin curve, fatigue crack nucleation or fatigue crack propagation can be studied simultaneously without a lot of facilities or at much expense.

At high stress levels or in the large strain amplitude regime, the fatigue crack initiates immediately and most of the fatigue life is consumed by fatigue crack propagation. On the contrary at low stress levels or in the low strain amplitude regime, most of the fatigue life is consumed by fatigue crack initiation. From this point of view, the S-N curve would be the first step to study in order to investigate fatigue properties because it gives information about both fatigue crack nucleation and fatigue crack propagation.

Generally, the S-N curve obtained using load control is used in the study of high strength materials which are metallurgically and cyclically stable and the $\frac{\Delta\varepsilon_t}{2}$ - $2N_f$ curve is used for ductile or cyclically unstable materials and for low cycle fatigue tests.

II.4.2 Sites for Crack Nucleation

A fair amount of experimental observation has shown that the fatigue crack in a homogeneous material invariably initiates at the free surface of the specimen. Four types of nucleation sites are frequently observed [38-40]:

1. Fatigue slip band caused by slip concentration within the grain
2. Grain boundaries in the case of high strain fatigue
3. Surface inclusions
4. Precipitate free zone near the grain boundary.

The feature common to all the above possible nucleation sites is the plastic strain concentration at or near the surface. Therefore, the most important task in improving resistance to fatigue crack nucleation is to determine where the crack nucleates in specific alloy systems and to prevent the concentration of local plastic strain at the nucleation site.

In this study, it is known from the literature that 7075 aluminum alloy has a weak PFZ, which consequently appears to offer the most probable site for fatigue crack nucleation.

II.4.3 Fatigue Crack Nucleation Models

Many fatigue crack nucleation models have been proposed in the literature [41-44]. The idea common to these crack nucleation models is that slip steps which form from dislocation motion to the surface contribute to form persistent slip bands (PSB) which probably lead to fatigue crack nucleation.

Mughrabi [45] discussed the dislocation structure of PSB and found that PSB consist of hard dislocation rich veins and soft dislocation poor channels.

The basic idea of Fujita's model [41] is the accumulation of defects which have been produced by cyclic deformation. Laird's model [42] proposes that the grain boundary hinders plastic deformation and that the strain concentration at the grain boundary leads to the formation of microcracks. Laird proposed that the fatigue crack nucleates at the grain boundary. The grain boundary hinders plastic deformation and plastic instability can occur on a micro scale in such a way that the depth of a crease at the grain boundary deepens with increasing number of cycles until the strain concentration of the crease becomes so large that the crease constitutes a microcrack.

However, in precipitation hardening alloys the crack nucleation mechanism would be different from others because of its distinctive PFZ which is much weaker than the matrix. McEvily [46] discussed the crack initiation model within the PFZ of an age-hardening alloy. He found that extensive cold working prior to aging strengthens the grain boundary region and changes the mode of failure from intercrystalline to transcrystalline, leading to an improvement in fatigue properties.

Glysler [40] proposed that if the alloy forms intense slip bands due to the presence of coherent particles, crack initiation will occur at large slip offsets on the specimen surface and that if the alloy exhibits a soft PFZ along the grain boundary, crack initiation will start along these highly deformed boundary regions. He reported that slip homogenization and grain-boundary alignment led to improved resistance to fatigue crack nucleation.

Among these models, Lynch's model [44] appears to be most suitable for material which has a soft region around the grain boundary such as the PFZ.

II.4.4 Lynch's Model for Crack Nucleation

Lynch's model [44] for crack nucleation is particularly based on material which has soft layers, such as the PFZ. Lynch made a model specimen to simulate the soft layer by adhesively bonding a sheet of annealed aluminum between blocks of age-hardened Al-Zn-Mg alloy and then subjecting it to fatigue by reversed torsion. He found that under compression, discrete ribbons of softer material were extruded from the surface, or produced a step at the surface along one of the soft layer/hard-zone interface. These are shown in Figure 2.

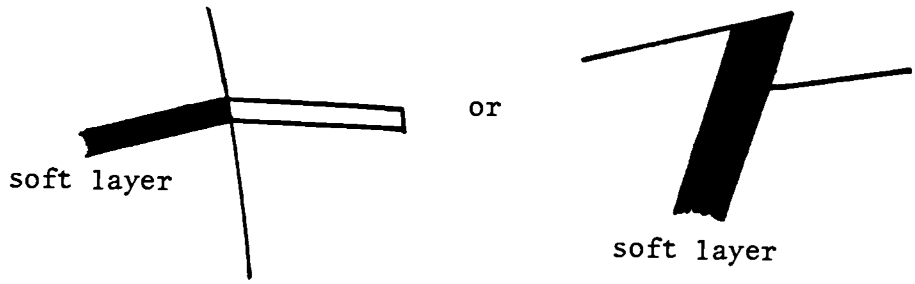

FIGURE 2. Extrusion of soft layer and boundary step in simulated microstructure from Lynch's model

He also reported that extrusions and intrusions at grain boundaries were particularly prevalent at intermediate and low strain amplitude in torsional fatigue. From this model it appears to be important to strengthen or remove the soft layers in the alloy in order to increase the fatigue life, at least at low stress levels.

II.4.5 Microstructural Factors which Affect Crack Nucleation in Aluminum Alloys with PFZ

II.4.5.1 Alloying elements

The variation of the solute content (Zn+Mg) did not change PFZ width, however, titanium [47] and silver [48] additions have been shown to reduce the PFZ width. Chen and Judd [49] reported that the addition of titanium to a Al-Zn-Mg alloy reduced the amount of grain boundary precipitation and thus reduced the width of the PFZ from 0.6μ to 0.3μ and from 4μ to 0.8μ, with quenching media of air and brine, respectively.

Polmear [50] reported that in Al-Zn-Mg alloys, the presence of silver stimulated precipitation within the grains so that very fine precipitates were formed which were much more evenly dispersed, particularly in the vicinity of the grain boundary. Considering these reports and the fact that zirconium (Zr) has similar atomic properties, it would be expected that 7050 aluminum alloy which has 0.1 percent Zr will have improved fatigue properties. This idea may be supported by the fact that the fatigue strength of 7050 aluminum alloy is 40 Ksi, which is far greater than that of 7075 alloy which does not contain Zr [120].

II.4.5.2 Grain-size reduction

Many investigators have studied grain-size reduction as a possible solution to improving fatigue crack nucleation resistance. Glysler [40], Lütjering [22] and Sanders [51] have reported such improvement in high strength aluminum alloys.

Sanders pointed out that grain refinement is especially beneficial in the low cycle fatigue regime because of an increase in ductility by grain refinement. However, it is generally believed from these investigators' results that grain refinement increased fatigue life in both low cycle and high cycle fatigue.

Grain-size refinement is especially attractive because the grain-size can be controlled during ingot processing [52] and because it improves the other mechanical properties such as strength, fracture toughness, and ductility.

II.4.5.3 Degree of aging

Degree of aging is the most important as well as the easiest parameter to control in the precipitation hardening of an aluminum alloy. Therefore, it is also important to appreciate the effect of degree of aging on fatigue crack nucleation.

The degree of aging is directly related to the coherency of the precipitates with the matrix. The coherent precipitates are sheared by dislocations and this results in a local decrease in the resistance to further dislocation motion and leads to concentration of slip. Such concentrated slip may lead to early crack nucleation in the slip band.

When the alloy is overaged, dislocations no longer shear the precipitates but bypass them. Therefore, strain localization is removed and the deformation becomes more homogeneous. This results in smaller offsets at the surface and delays the fatigue crack nucleation phenomenon [53].

Sanders and Starke [54] also reported that overaging of an Al-Zn-Mg-Zr alloy resulted in the best low cycle fatigue resistance and this was attributed to the increased homogeneity of slip resulting from the occurrence of dislocations looping as the primary deformation mechanism.

II.4.5.4 Thermomechanical processing

Thermomechanical processing has been investigated as a possible means to improve resistance to fatigue crack nucleation by many investigators [55-61]. TMP introduces steps into the grain boundaries and reduces the slip length within the PFZ with corresponding improvement in the resistance to fatigue crack nucleation.

The other purpose of TMP is to align the grain boundary by rolling. If these thermomechanically processed alloys are aged to have non-shearable precipitates and PFZ, only the PFZ inclined to the stress axis will be subjected to preferential deformation and the occurrence of fatigue crack nucleation will be reduced.

The main purpose of TMP in a precipitation hardening alloy system is to provide the uniform dislocation structure which provides the nucleation sites for further precipitation. In addition, TMP provides more homogeneous deformation by facilitating slip initiation throughout the matrix.

II.4.5.5 Cyclic pre-loading as TMP

According to Lynch's fatigue crack initiation model, it is obvious that a weak PFZ around the grain boundary becomes the most probable intrusion site. From this point of view, there are two possible ways to prevent the formation of such intrusions.

One way is to reduce the width and length of the PFZ, which can be obtained by grain-size reduction, TMP or alloying element addition as discussed in the previous sections. The other way is to strengthen the soft PFZ. Weissman and coworkers [33] began to investigate the effect of cyclic loading on aluminum single crystals and reported an extended fatigue life for both the high and low strain amplitude fatigue regimes. Later, Kiritani [34] reported that the dislocations produced by cyclic loading with a stress amplitude below the elastic limit were limited to the zone adjacent to the grain boundary in Al-6.5% Zn alloy and reported that the dislocations were generated from the grain boundary and that fatigue life at low stress levels was increased substantially by cyclic loading.

II.5 Fatigue Crack Propagation Studies

II.5.1 General Description of Fatigue Crack Propagation

In general, fatigue crack propagation (FCP) studies [62] include near threshold fatigue crack propagation (ΔK_{th}) [63-64], linear FCP range (mid-ΔK regime) [65-67] and unstable crack propagation (Fracture Mechanics).

The linear FCP range is widely described as Paris' law [68] shown below:

$$\frac{da}{dN} = A(\Delta K)^m$$

where, $\frac{da}{dN}$: fatigue crack growth rate

A : constant

ΔK : stress intensity factor range

m : constant

Since the advent of Paris' equation, most FCP studies have been done in the linear region of the $\frac{da}{dN}$ vs. ΔK curve because crack propagation can be controlled and monitored in this region.

The effects of microstructure [69-76] on FCP have been investigated by many investigators because of its practical importance in 7075 aluminum alloy.

II.5.2 Effect of Microstructure

Fatigue crack propagation is generally divided into Stage I [77] and Stage II [78] propagation. Stage I crack propagation is when the fatigue crack propagates on a plane oriented at approximately 45° to the stress axis within several grains.

Stage II crack propagation is when the crack propagates in the direction normal to the loading direction. Most fatigue crack propagation studies are concerned with Stage II crack propagation because Stage I crack propagation is usually considered as crack nucleation.

Fatigue crack propagation rate (FCPR) is affected by many factors which originate inherently in the material processing or from the results of deliberate control of microstructure. For example, grain boundaries, stacking fault energy, PFZ and rolling texture belong to the first category. Thermomechanical processing, impurities, degree of aging and pre-loading belong to the second category. There are other factors which affect FCPR significantly such as temperature [79], environment [80], state of stress [81], loading sequence [82], and mean stress [83].

II.5.2.1 The effect of degree of aging on fatigue crack propagation

Crack propagation resistance has been observed to be significantly higher for an underaged microstructure containing shearable precipitates in comparison with an overaged microstructure with non-shearable precipitates [71,73].

This improvement in underaged condition crack propagation resistance is attributed to the increased tendency for reversed slip of dislocations due to the greater incidence of planar slip behavior.

The number of dislocations which are able to leave the material to form extrusions depends strongly on the degree of slip planarity. For example, if the cross-slip process takes place and increases either by high stacking fault energy or due to the presence of non-shearable precipitates, some dislocations will move out of the original slip plane. This would result in an enhanced FCPR in the overaged condition.

II.5.2.2 Effect of grain-size on fatigue crack propagation

Some investigators have studied the effect of grain-size on FCPR in 7075 aluminum alloy [84,85].

For the small ΔK range, Lindigkeit [86] found that an increase in grain-size increased the ΔK_{th} in vacuum considerably. This result was explained on the basis of reversed slip of dislocations within the plastic zone of the propagating fatigue crack. The situation can be visualized as shown in Figure 3.

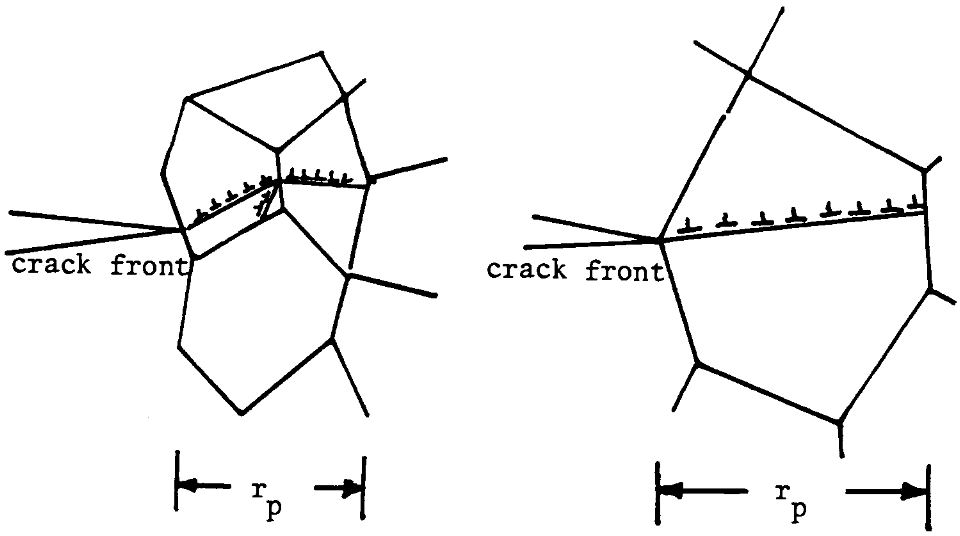

FIGURE 3. Reversed slip process of dislocations within plastic zone of propagating fatigue crack

For the large ΔK range, where the maximum plastic zone size exceeds the grain-size, small grain-sized material has less degree of reversed slip because more grain boundaries are present in the plastic zone. Therefore, small grain-sized material will have a higher FCPR than large grain-sized material.

II.5.2.3 Effect of pre-deformation on fatigue crack propagation

Kang [87] has investigated the effect of plastic deformation on FCPR in high strength aluminum alloys. He observed an increase in the crack propagation rate of 2024-T351 aluminum alloy subjected to pre-deformation. As a reason for this behavior, Kang stated that the cyclic ductility of the material is decreased as a consequence of the pre-deformation and that crack propagation becomes faster according to the cumulative damage model proposed by McClintock [88].

Schijve [89] has studied the effect of pre-strain on the crack propagation behavior of 2024 aluminum alloy and observed an increase in the FCPR along with an increase in the amount of pre-strain.

Cyclic predeformation has also been observed to increase the FCPR of high strength aluminum alloys and was explained by Schulte [90] as follows:

1. Due to the cyclic hardening of the material, the cyclic yield stress increases above the yield strength of non-predeformed material. This leads to a smaller plastic zone size ahead of the crack tip. Furthermore, the capability of the material to deform plastically decreases with increasing amounts of predeformation. Both lead to a reduction of the crack opening load level.

2. The cyclic predeformation causes a high dislocation density. In contrast to monotonic predeformation, cyclic predeformation of the specimen leads to the formation of inhomogeneous slip bands which increase the FCPR.

II.5.2.4 Effect of stacking fault energy on fatigue crack propagation

Awatani [91] and others [92] have studied the effect of stacking fault energy (SFE) on the fatigue properties. Avery [93] proposed that the boundaries of the cell structure that develops in high SFE material offer the preferred route for crack propagation.

For low SFE material, the dislocations accumulate on the active slip plane and they are difficult to move due to the difficulty of cross-slip. Laird [94] regarded the great work-hardening capacity of low SFE alloys to be the controlling factor in resisting crack tip deformation, assuming that the plastic blunting process occurs.

From these considerations, FCPR of a low SFE alloy is expected to be smaller than the FCPR of a high SFE alloy, and some experimental evidence does support this assumption [91-94].

II.5.2.5 The effect of PFZ on fatigue crack propagation

There have been some investigations done showing that PFZ width affects the fracture toughness [93] and that the PFZ length which can be controlled by grain-size control, does affect fatigue crack propagation or fracture toughness [86].

However, there has been no direct investigation into or model proposed regarding the effect of PFZ width on fatigue crack propagation. Some studies have investigated the effect of PFZ width on fracture toughness [22]. The above offers some clues that PFZ width might also affect the FCPR. In addition, there is no direct evidence available as to how the crack propagates in a material that has a PFZ around the grain boundary, except that Lütjering [22] has speculated that the fatigue crack propagates through the matrix in the low ΔK regime and along the PFZ in the high ΔK regime.

II.5.3 Fatigue Crack Propagation Models

Since it has been reported that the length of the fatigue crack is related exponentially to the number of stress cycles, and that the rate of the crack propagation bears a similar relationship [96,97] to the stress level, various crack propagation models have been reported to interpret or to predict the fatigue crack propagation rate in many different alloy systems.

Tomkins [98] has developed a simple theory to assess quantitatively, the mechanism of fatigue crack propagation in metals. Irving [99] has reviewed Paris' law and compared it with the experimental results, and introduced a crack propagation rate equation considering fracture toughness and threshold stress intensity factor range.

Katz [100] has investigated the fatigue crack growth mechanism in 7075 aluminum alloy and Beevers [101] has examined FCP behavior of various metals and alloys at low stress intensity levels. Kaisand [102] has tried to relate low cycle fatigue properties and the fatigue crack growth rate and has proposed a model based on the J-integral. However, Laird's [75] plastic blunting model is the most popular one due to its wide applicability including to plastics.

II.6 Plane Strain Fracture Toughness Studies

II.6.1 The Effect of Microstructure on Fracture Toughness

Fracture toughness of aluminum alloys is generally affected by the factors which affect other mechanical properties such as yield strength or true fracture strain.

Hahn and Rosenfield [103] have developed a model and equation to predict the fracture toughness from the other mechanical properties as follows:

$$K_{IC} = [LE\sigma_y n^2 \varepsilon_f]^{\frac{1}{2}}$$

where, K_{IC} : plane strain fracture toughness

L : constant

E : Young's modulus

σ_y : yield strength

n : strain hardening exponent

ε_f : true fracture strain

From the above equation it is expected that K_{IC} will be affected by microstructural factors which affect the other mechanical properties of the material. For example, grain-size, degree of aging, grain texture, TMP or PFZ which affect strength will also affect the fracture toughness. There have been attempts to understand the role of grain-size [104], PFZ [105], grain boundary precipitates [106], dispersoids [107], and of strengthening precipitates [108] in the context of fracture toughness.

Especially in aluminum alloys, such as the 7000 series alloy system, which develops a weak PFZ, there appears to be a high probability that the PFZ width would affect fracture toughness.

II.6.2 The Effect of PFZ on Fracture Toughness

Hornbogen [109] has developed a model and modified the Hahn-Rosenfield equation by assuming that plastic deformation is restricted to a planar soft zone in order to predict the fracture toughness of precipitation hardened aluminum alloys containing a narrow soft zone at the grain boundaries. Hornbogen's equation is expressed as follows:

$$K_{IC} = [L_i E \sigma_{yi} n_i^2 \varepsilon_{fi} \frac{d}{D}]^{\frac{1}{2}}$$

where, L : empirical constant with the dimension of length

ε_f : elongation at fracture

n : work-hardening exponent

E : Young's modulus

i : stands for intercrystalline and characterizes the mechanical properties of soft zone at grain-boundary

d : width of precipitate free zone

D : average grain-size

From this equation, it can be seen that K_{IC} will be larger for the alloy with a larger PFZ width if the other mechanical properties are comparable. Also, from the above equation it is obvious that the strain-hardening capacity is an important factor in fracture toughness, playing a more important role than the yield strength or true fracture strain.

Recently, Ludka [110] has reported that the fracture toughness of 7000 series alloys depends on the coarseness of matrix slip and the strength differential between the matrix and precipitate free zone, i.e., ($\sigma_M - \sigma_{PFZ}$). Ludka states that the smaller ($\sigma_M - \sigma_{PFZ}$) is, the more favorable the overall deformation would be. In other words, for large PFZ widths the strain would be equally dissipated by the grain-matrix and PFZ. This may retard the void formation in the PFZ giving rise to a larger fracture toughness in the alloy with a wide PFZ than in the alloy with a narrow PFZ.

II.6.3 The Effect of Grain-size and Shape

Hahn and Rosenfield [103] have studied the metallurgical factors that affect fracture toughness of aluminum alloys and have found that fracture toughness decreases with increasing grain-size in the under-aged as well as in the over-aged alloy.

Thompson [108] has studied 7075 aluminum alloy sheet and has reported that grain-size and shape were found to affect the toughness strongly. The plane strain fracture toughness at a given yield strength level was found to vary by a factor of three between fully recrystallized, coarse equiaxed grain structure and unrecrystallized structure.

For 7075-T651 aluminum alloy, it has been shown that fracture toughness for the L-T direction is larger than that for the T-L direction.

III. EXPERIMENTAL PROCEDURE

III.1 Material

The material investigated was 7075 aluminum alloy obtained from Alcoa. Chemical composition of as-received alloy was analyzed and is shown in Table 1. All the specimens were cut in a longitudinal direction which is parallel to the rolling direction for tensile tests, fatigue life tests, fatigue crack propagation tests and plane strain fracture toughness tests. The rolling texture was revealed by metallographic techniques as shown in three dimensions in Figure 4.

III.2 Thermomechanical Processing

Four different thermomechanical processing (TMP) procedures have been used in the preparation of specimens for testing the fatigue life of 7075 aluminum alloy. These include cyclic pre-loading at high and room temperatures, cyclic pre-loading combined with T6 tempering and stretching at high temperature. The designations are as follows:

FHT: The fatigue specimens were cyclically loaded for 100,000 cycles with ± 7 Ksi at 150° ± 10°C and then aged at 120°C for 24 hours.

FRT: The fatigue specimens were cyclically loaded for 100,000 cycles with ± 7 Ksi at room temperature and then aged at 120°C for 24 hours.

TABLE 1. Composition of as-received 7075 aluminum alloy from Alcoa

Elements	Composition (w/o)
Copper	1.62
Iron	.17
Manganese	.02
Silicon	.15
Magnesium	2.77
Zinc	5.16
Chromium	.19
Titanium	.05
Other elements	< .15
Aluminum	Remainder

—— ROLLING DIRECTION ⟶

FIGURE 4. Three-dimensional microstructure of 7075 aluminum alloy revealing rolling texture

FT6: The fatigue specimens were aged at 120° ± 10°C and cyclically loaded at the same time for 24 hours.

As received, one-inch thick plate was cut into 1"x1"x8" blocks and solution treated in a muffler-type furnace at 460° ± 15°C for two hours and water-quenched within 10 seconds after taking it out from the furnace. This short holding time guaranteed that the quenching rate was fast enough for precipitation hardening of 7075 aluminum alloy.

Artificial aging was performed in an aging bath containing mineral oil. The aging temperature was controlled within ± 2° accuracy.

III.2.1 Cyclic Pre-loading at High Temperature: FHT

Smooth fatigue specimens were mounted in an MTS closed-loop system with special grips provided by the MTS corporation for flat-end smooth fatigue specimens. This type of grip minimizes the possible bending of a fatigue specimen in tension-compression loading. Electrical resistance tape, which can be used for heating metals, was wrapped around the specimen. The specimen temperature was controlled by variable transformer within ± 10°C accuracy.

The fatigue specimens were cyclically loaded at 150°C at one-third of the yield strength of the solution-treated alloy, which is approximately 7 Ksi, by load control, for 100,000 cycles at 10 Hertz.

After this cyclic pre-loading the specimens were artificially aged at 120°C for 24 hours for maximum strength.

III.2.2 Cyclic Pre-loading at Room Temperature: FRT

Experimental procedures to prepare FRT specimens were the same except that cyclic pre-loading was done at room temperature instead of at elevated temperature.

III.2.3 Cyclic Pre-loading Combined with T6 Tempering: FT6

Smooth fatigue specimens were cyclically pre-loaded at 120°C for 24 hours using ± 7 Ksi at 1 Hertz. After cyclic pre-loading, T6 tempering was done to achieve maximum strength.

III.2.4 Stretching at High Temperature: SH5

The flat-end smooth fatigue specimens which could be later tested for fatigue life were mounted with specially designed grip on the Instron tensile testing machine. The specimens were heated by the heating tape to 150°C, then plastically deformed five percent using 0.2 inch/minute cross-head speed. These stretched specimens were aged at 120°C for 24 hours for T6 tempering.

III.3 Heat Treatment for Precipitate Free Zone

The solution-treated specimens were aged at 177°C for two hours to obtain the alloy with a wide precipitate free zone, and at 150°C for two hours to obtain the alloy with a narrow precipitate free zone.

III.4 Fatigue Life Tests

III.4.1 Testing System

An MTS closed-loop hydraulic system which has a maximum load capacity of 22,000 lbs. was used for the fatigue life tests. The alignment between load cell and the actuator was checked by rotating the actuator with the tip of a dial gage in contact with it and by reading the displacement of the dial gage. These tests showed the MTS system to be in satisfactory condition, according to A.S.T.M. E-647 [9].

III.4.2 Specimen Design

Flat-end smooth fatigue specimens were designed according to A.S.T.M. (E-606) [10] and MTS specifications. The shape and dimensions of the smooth fatigue specimen are shown in Appendices 1 and 2. The surface of the gage section was carefully prepared in order to have the same surface condition for all specimens.

The machined specimen surface was found with 600 grit abrasive paper and polished longitudinally with polishing paste of 45 μm, 6 μm and 1 μm particle size in sequence to remove all machining scratches.

III.4.3 Test Procedures

Special grip (Model 643.65) for flat-end smooth fatigue specimens, which were designed for MTS, were used to minimize the possible misalignment and bending during the fatigue tests. The specimens were mounted according to the procedures described in MTS specifications [11] to prevent possible slippage during fatigue tests. The load cell was checked by proof ring and found to be accurate within the limits of experimental error.

Load control was used throughout the tests in order to minimize instrumental error. Frequency of 10 Hertz was used for ± 30 Ksi and ± 40 Ksi stress levels. Six Hertz was used for ± 50 Ksi cyclic loading. Completely reversed cyclic loading of sine wave form was applied for all the tests. The test environment was air at room temperature with ambient humidity.

III.5 Fatigue Crack Propagation Test: FCP Test

III.5.1 Equipment

Fatigue crack propagation (FCP) tests were conducted using the MTS closed-loop hydraulic system according to A.S.T.M. E-647. MTS clip gage Model 632.02B-20 was used for monitoring the growth of the crack. Strip chart recorder with a sensitivity of 0.01 volt was also used to record the data.

III.5.2 Specimen Design

A special grip for FCP specimens was designed according to A.S.T.M. E-647. The compact tension specimens with W=2 inches were designed according to the same specification. The shape and dimensions of the grip and of the compact tension specimen are shown in Appendices 3-7.

III.5.3 Test Procedures

The compact tension specimen with machined notch was fatigue pre-cracked according to the specification A.S.T.M. E-647. The length of the pre-crack was 3-5 mm long at the outer edge of the specimen. The FCP specimens were cyclically loaded by load control with R=0.1 and frequency of 10 Hertz. The crack length was monitored by clip gage attached to the mouth of the machined notch. The voltage output from the clip gage was recorded automatically on a strip chart recorder. To eliminate possible error, the settings of the MTS system and the voltage range in the recorder were kept the same for all the tests. For example, S_m = 0.792 Kips and S_a = 0.638 Kips were used for load control. Ten percent of full-scale of strain (10% F.S.) was selected for strain control using the clip gage.

The actual crack length was measured visually and with a crack propagation gage (Model CPA01) to calibrate the voltage output from the clip gage with the actual crack length.

III.5.4 (da/dN) Calculation and Related Computer Program

The output voltage from the clip gage, which is linearly proportional to clip gage displacement, was correlated with the number of cycles applied with load control. The output voltages from the clip gage were converted to the actual crack lengths to calculate the crack growth rates.

From the curve of the crack length versus the number of cycles, fatigue crack propagation rates were determined using the incremental polynomial method described in A.S.T.M. E-647. The original FORTRAN language program was converted to BASIC language for use on a microcomputer. To test the validity of the program, the BASIC version of the program was tested with sample data and was found to give exactly the same result as that obtained using the FORTRAN program.

Stress intensity factors were calculated using Strawley's equation [12] for compact tension specimens (refer to III.6.4). From the ΔK and (da/dN) obtained from the experiments and seven-point polynomial method, log ΔK versus (da/dN) were plotted on semi-logarithmic paper.

The BASIC version of the program and computer outputs are shown in Appendices 58-62.

III.6 Plane Strain Fracture Toughness Test

III.6.1 Equipment

The MTS closed-loop hydraulic system and the clip gage were used with an X-Y recorder. Ramp control was used to maintain a loading rate of 100 lbs./sec throughout the test.

III.6.2 Specimen Design

Compact tension specimens were designed for plane strain fracture toughness tests according to the A.S.T.M. E-399. The shape of the compact tension specimen is shown in Appendix 8 and the dimensions are shown in Appendix 10. The special grips for this compact tension specimen were also designed according to the same A.S.T.M. specification. The shape and the dimensions of the grips are shown in Appendices 9 and 11.

III.6.3 Test Procedures

The pre-crack was made by cyclic loading in order to obtain a sharp crack front. The typical fatigue pre-crack is shown in Appendix 12. A very sharp fatigue pre-crack was made according to

A.S.T.M. E-399, except that the length was shorter than that specified. However, the total crack length was long enough to be used in Strawley's equation [12] to obtain the K_{IC} value. Strawley's equation can be used to calculate the plane strain fracture toughness when the crack length is greater than 0.2W.

A loading rate of 100 lb./second was used to generate a load versus crack opening distance plot on the X-Y recorder. All the settings of the equipment, including the recorder, were kept the same for all the K_{IC} tests in order to eliminate any possible equipment related errors.

III.6.4 K_{IC} Calculation and the Computer Program

P_Q was obtained from the load versus crack opening distance plot. This P_Q was then used to calculate the K_{IC} value using the following equation:

$$K_Q = \frac{P_Q}{BW^{\frac{1}{2}}} \left[(2+a/w)\left\{0.866+4.64\left(\frac{a}{w}\right) - 13.32\left(\frac{a}{w}\right)^2 + 14.72\left(\frac{a}{w}\right)^3 - 5.6\left(\frac{a}{w}\right)^4\right\}\right] / \left(1 - \frac{a}{w}\right)^{3/2}$$

where, K_Q : candidate fracture toughness

P_Q : the load at fast fracture

a : total crack length

w : width of compact tension specimen

The calculated K_Q values were tested in order to be accepted as K_{IC} values considering plastic zone size.

III.7 Tensile Test

III.7.1 Equipment

An Instron machine was used to obtain the load versus cross-head displacement curve.

III.7.2 Specimen Design

Standard tensile specimens were machined according to A.S.T.M. E-8 [13]. The dimensions of the specimen are shown in Appendix 13. All the specimens were machined with the longitudinal direction parallel to the rolling direction. The intermediate step tensile test of the thermomechanically processed specimens was performed before the final T6 tempering, using the flat-end smooth fatigue specimen directly with a specially designed adapter for the Instron machine.

III.7.3 Test Procedures

Tensile tests of as-received T651 and T6 tempered alloys were carried out using a maximum load of 10,000 lbs. and cross-head speed of 0.2 inch/minute with a chart speed of 2 inches/minute.

All the test conditions were kept the same for all the tensile tests. The load cell was checked with standard weights and was found to be within experimental error. The dimensions of the special adapter for the Instron tensile test machine are shown in Appendix 14.

III.8 Transmission Electron Microscopy

A Phillips 300 transmission electron microscope was used at

100 KV for all the specimens. Thin disc-type specimens were cut from the middle section of the original fatigue specimen with a slow cutter. The initial thickness was approximately 20/1000 inch. This thin disc was electropolished to a thickness of 1/1000 - 2/1000 inch in a solution of 20 percent perchloric acid and 80 percent ethyl alcohol. A small circular specimen was punched from this disc with a punching machine to fit the T.E.M. specimen holder.

A twin-jet electropolisher was used to electropolish and thin down the disc until tiny holes appeared and joined together. Two parts methanol plus one part nitric acid was used for jet electropolishing and the temperature was kept below -20°C in order to obtain a uniform thin section. The low temperature was obtained by using a mixture of acetone and dry ice. Some specimens were ground before the first electropolishing step.

III.9 Scanning Electron Microscopy

An AMR Model 1000 scanning electron microscope was used to examine the fracture surface of the tensile specimens and the final fracture zones of the compact tension specimens used in the fracture toughness tests. Compact tension specimens were directly observed with the low stage mounting equipment of the S.E.M. Tensile test specimens were cut and mounted on a small disc which was connected electrically by silver paste. Striation spacings were observed in the fatigue crack propagation zone of the FCP specimens at a point 0.35 inch from the machined notch, where ΔK was calculated to be 17 Ksi$\sqrt{\text{in}}$.

III.10 Metallography

Standard metallographic techniques and standard dark room techniques were used to examine the rolling texture and the microstructure of the thermomechanically processed 7075 aluminum alloys. Keller's agent was used as an etchant with various etching times ranging from 30 seconds to two minutes.

IV. RESULTS AND DISCUSSION

IV.1 Thermomechanical Processing (TMP)

IV.1.1 Concepts of Thermomechanical Processing

Thermomechanical processing (TMP) or thermomechanical treatment (TMT) generally refers to the combination of mechanical deformation and various thermal treatments during the final processing of materials.

TMP is particularly attractive in age-hardening aluminum alloys because it provides uniform distribution of dislocations and jogged grain-boundaries which act as nucleation sites for precipitation. Ordinarily, TMP has been performed by rolling or stretching the material before the final aging of 7075 aluminum alloy.

In 7075 aluminum alloy, a precipitate free zone develops around the grain boundary even though the width of the PFZ is reduced by an alloying element such as copper. Furthermore, there is experimental evidence that plastic deformation concentrates within this weak PFZ. Therefore, it is necessary to eliminate the PFZ or reduce the PFZ width in order to improve the mechanical properties, including fatigue properties, especially fatigue crack nucleation.

However, Kiritani and Weissman [34,35] have reported that cyclic pre-loading generates dislocations from the grain boundaries and reverses the motion of dislocations toward the grain boundaries. This mutual interactien of dislocations provides a dense accumulation of dislocations near the grain boundaries. Recently, Lu and Weissman [35] have reported that fatigue life was improved by cyclic pre-loading with small stress amplitude.

The stress level of the cyclic pre-loading was chosen to be about 7 Ksi, which is one-third of the yield stress of the solution-treated alloy. This low stress level was large enough to generate dislocations from the grain-boundary but not large enough for dislocations to proceed beyond the PFZ [35].

From this point of view, cyclic pre-loading can be a powerful tool to strengthen the weak PFZ which is responsible for nucleating the fatigue crack in 7075 aluminum alloy. In addition, the effect of temperature on the cyclic pre-loading has never been studied, even though high temperature is expected to be beneficial (Refer to IV-1-2).

IV.1.2 Cyclic Pre-loading at High Temperature (FHT)

In this study, cyclic pre-loading was applied at 150°C, which is above the critical solvus temperature. This cyclic pre-loading at elevated temperature is beneficial because it helps dislocations to glide easily from the grain-boundaries and thus gives a uniform dislocation distribution around the grain boundaries to strengthen the PFZ. In addition, high temperature provides more vacancies which help to nucleate precipitates around the grain boundaries.

Transmission electron micrographs of cyclically pre-loaded specimens show many dislocations around the grain boundaries (refer to Section IV.7).

IV.1.3 Cyclic Pre-loading at Room Temperature (FRT)

Cyclic pre-loading with a stress amplitude of 7 Ksi was applied to the fatigue specimen at room temperature after solution treatment in order to generate a uniform dislocation structure at the grain boundaries. Room temperature processing was used to compare the results with FHT thermomechanical processing. It was observed that fewer dislocations were generated from the grain boundaries at room temperature than in FHT thermomechanical processing (refer to Section III.3).

Comparing yield stress and ultimate tensile stress of the FRT with FHT, FRT showed lower yield and ultimate tensile stress value than the FHT did. This could be so because the FRT generated fewer dislocations than the FHT. Y.S. and U.T.S. values are shown in Table 2.

After cyclic pre-loading the specimens were aged artificially at 120°C for 24 hours to obtain the maximum strength for this type of alloy. As can be seen from Appendix 15, the Y.S. and U.T.S. of the FRT were higher than those of conventional T6 tempered alloy. This increase in Y.S. and U.T.S. is rationalized by the fact that precipitation was facilitated by the dislocations generated and the dislocation tangles within the PFZ.

IV.1.4 Cyclic Pre-loading Combined with T6 Tempering (FT6)

FT6 thermomechanical processing was prepared by applying cyclic

TABLE 2. Yield strength and ultimate tensile strength of 7075 aluminum alloys which have been thermo-mechanically processed

7075 Aluminum alloys	Y.S. (Ksi)	U.T.S. (Ksi)
T651 (LT)	82	91
T651 (TL)	72	83
Solution treated (after 5 days passed)	53	81
T6 (L)	71	80
FHT	29	52
FHT + T6	58	68
FRT	24	52
FRT + T6	78	90
FT6	75	86
SH5	78	86
PFZ#1 (immediately after artificial aging)	35	40
PFZ#2 " "	26	32

stress of ± 7 Ksi at one or two Hertz at a temperature of 120°C for 24 hours. The main purpose of this thermomechanical processing was to apply cyclic loading at the temperature at which the maximum strength of this alloy can be achieved in order to accommodate the precipitation to the dislocations generated by cyclic loading.

Studies have shown that the application of stress can change the habit plane of precipitation in aluminum single crystals [119]. This idea was adopted for the polycrystals of this study to change the habit plane of the precipitates by applying tensile and compressive stresses. This would make the precipitates more randomly oriented in the matrix. The cyclic pre-loading also generates the vacancies which are necessary for precipitation above the critical temperature.

However, this kind of TMP has never been investigated even though it has a strong theoretical basis for the improvement of fatigue properties. Y.S. and U.T.S. were determined to be 75 Ksi and 86 Ksi, respectively, aftet FT6 thermomechanical processing.

These strengths are close to those obtained with T651 tempering which is the most widely used one. Therefore, it appears to be possible to improve the fatigue properties by this TMP while maintaining the high strength of the alloy.

IV.1.5 Stretching at High Temperature (SH5)

SH5 thermomechanical processing was carried out by applying five percent monotonic plastic deformation at 150°C. This type of TMP has been studied for Al-6.5 Zn alloy by Lu and Weissman [35] and they found that the fatigue life was noticeably increased.

Plastic deformation at room temperature provides uniform dislocation structure throughout the matrix and these dislocations provide the nucleation sites for precipitation. This increase in the amount of precipitation helps strengthen possible weak regions and thus delay crack nucleation.

However, in the SH5 thermomechanical processing, plastic deformation was carried out at elevated temperature. High temperature plastic deformation is beneficial because the Peierls-Nabarro stress is lower at high temperature and the dislocations can glide more freely than at room temperature. Consequently, dislocations are distributed more uniformly at high temperature than at low temperature. This retards the formation of persistent slip bands which are known to result in nucleation of cracks.

After five percent plastic elongation at elevated temperature, the specimen was aged at 120°C for 24 hours to obtain the maximum strength of this alloy. The yield strength and ultimate tensile strength were determined to be 78 Ksi and 86 Ksi, respectively.

IV.1.6 Thermal Treatment for Precipitate Free Zone Formation (PFZ#1 and PFZ#2)

Thermal treatments designated as PFZ#1 and PFZ#2 were carried out to study the effect of the precipitate free zone on mechanical properties, fatigue properties and fracture toughness.

The width of the PFZ can be controlled in two different ways. First, the quenching rate can be changed by changing quenching temperature, thereby changing the diffusion rate of the solutes and vacancies to the grain boundaries. This change in diffusion rate of solutes or vacancies gives rise to the variation of PFZ width.

The other method is to change the aging temperature, thereby changing the gradient of vacancy concentration which controls PFZ width (refer to Section III.2).

In this study, PFZ width was controlled by changing the aging temperature. For example, 7075-PFZ#1 was prepared by aging the specimen at 150°C for two hours and 7075-PFZ#2 was prepared by aging at 177°C for two hours. These aging temperatures were selected so that 7075-PFZ#1 and 7075-PFZ#2 alloys would have comparable yield strength [95].

The PFZ width of 7075-PFZ#1 alloy was determined to be 800 Å and that of 7075-PFZ#2 was determined to be 2000 Å with the aid of transmission electron microscopy.

Compared to a PFZ width of 570 Å for T6 tempered alloy, PFZ#1 and PFZ#2 have relatively large PFZ widths. This is due to the higher aging temperatures used for PFZ#1 and PFZ#2 than that normally used for T6 tempered alloy. The grain-sizes of PFZ#1 and PFZ#2 were determined to be A.S.T.M. grain-size No. 8 for both alloys. The mechanical properties of these alloys are shown in Appendix 15.

Metallography (Appendices 16 and 17) showed that more grain-boundaries precipitates were present in PFZ#1 than in PFZ#2 and this may have caused the relatively large fraction of intergranular fracture mode in the fracture surfaces examined by scanning electron microscope. However, the yield strength and ultimate tensile strength of PFZ#1 were found to be somewhat larger than those of

PFZ#2. Therefore, the fracture mode may be due to factors other than just weak grain boundaries caused by grain-boundary precipitates (refer to IV.6.2).

The details of the mechanical properties, fracture mode, fatigue crack propagation, fracture toughness and their relationship to the microstructure will be discussed in later sections.

IV.2 Material and Tensile Tests

IV.2.1 As-received 7075-T651 Alloy

Standard tensile test specimens were machined according to A.S.T.M. E-8 to obtain the mechanical properties of the 7057-T651 aluminum alloy.

Tensile tests were performed on an Instron tensile test machine for the as-received T651 tempered alloys with longitudinal direction parallel to the loading direction as a reference. The yield strength and ultimate tensile strength were determined to be 72 Ksi and 83 Ksi, respectively. In the transverse direction, the Y.S. and U.T.S. were found to be 82 Ksi and 91 Ksi, respectively. These values are reasonably close to the values given in Metals Handbook [120].

The tensile test specimen exhibited 10 percent elongation to failure and the fracture plane occurred at an angle of 45° to the loading axis. SEM examination showed that the failure occurred by the ductile dimple mode.

IV.2.2 Tensile Test of Solution-treated Alloy

Tensile test was performed after the solution treatment. However, some degree of natural aging occurred during the period between the solution treatment and the tensile testing. This probably increased the strength of the solution-treated alloy to some extent.

The Y.S. and U.T.S. were determined to be 53 Ksi and 81 Ksi, respectively. The elongation of 11 percent was higher than average, and metallography showed the specimen to have an equiaxed grain structure after solution treatment.

IV.2.3 Tensile Test of T6-aged Alloy

Yield strength and ultimate tensile strength were determined for the T6-tempered alloys to be 71 Ksi and 80 Ksi, respectively (Appendix 18). These values were very close to the values given in Metals Handbook. From this comparison, it is evident that the solution treatment and artificial aging procedures used in this study are acceptable.

IV.2.4 Tensile Test of FHT Alloy

Thermomechanically processed FHT specimens were tensile tested immediately after cyclic pre-loading at elevated temperature in order to eliminate the natural aging that could occur before the tensile test was carried out.

The Y.S. and U.T.S. were determined to be 29 Ksi and 52 Ksi, respectively. These Y.S. and U.T.S. values are significantly greater than those from obtained in the solution-treated condition and are due to the artificial aging carried out for approximately three hours (this is the period of cyclic pre-loading), and to the dislocations generated during the cyclic loading at elevated temperature.

After the cyclic pre-loading, the specimens were aged at 120°C for 24 hours to attain the T6 condition prior to further fatigue life tests.

Tensile tests were also performed after T6 tempering. The Y.S. and U.T.S. were determined to be 58 Ksi and 68 Ksi, respectively. This U.T.S. value was relatively smaller than that obtained with the normal T6 tempered alloy. This decrease was probably caused by the overaging which occurred during the cyclic pre-loading at 150°C for two hours. The load-displacement curves obtained before and after aging to the T6 condition are shown in Appendices 19 and 20.

IV.2.5 Tensile Test of FRT Alloy

Thermomechanical processing called FRT was prepared by applying a cyclic pre-loading stress of ± 7 Ksi at room temperature. The cyclic stress amplitude was determined to be approximately one-third of the Y.S. of the solution-treated alloy. After FRT thermomechanical processing, the Y.S. and U.T.S. were determined to be 24 Ksi and 52 Ksi, respectively. These Y.S. and U.T.S. values were somewhat lower than those of the FHT alloy.

These lower strength values of the FRT alloy are speculated to be caused by fewer dislocations being generated in FRT processing or by the fact that dislocation glide was less easy at room temperature than at high temperature.

After T6 aging of this FRT thermomechanically processed alloy, tensile testing showed a Y.S. of 78 Ksi and U.T.S. of 90 Ksi. These values are very close to the values associated with T651 aged alloy.

From these tensile tests, it is would appear that cyclic preloading creates dislocations and strengthens the material. The original load-displacement curves of the tensile tests are shown in Appendices 21 and 22.

IV.2.6 Tensile Test of FT6 Alloy

A tensile test was performed with the FT6 thermomechanically processed 7075 aluminum alloy. The yield strength and ultimate tensile strength were determined to be 75 Ksi and 86 Ksi, respectively.

The load-displacement curve is shown in Appendix 23.

IV.2.7 Tensile Test of SH5 Alloy

The tensile test of the SH5 thermomechanically processes 7075 aluminum alloy was conducted on the Instron machine. The yield strength and ultimate tensile strength were determined to be 78 Ksi and 86 Ksi, respectively. The load-displacement curve is shown in Appendix 24.

IV.2.8 Tensile Tests of PFZ#1 and PFZ#2 Alloys

Tensile tests of PFZ#1 and PFZ#2 specimens were conducted immediately after the heat-treatment. The Y.S. and U.T.S. of PFZ#1 were determined to be 35 Ksi and 40 Ksi, respectively. The Y.S. and U.T.S. of PFZ#2 were determined to be 26 Ksi and 32 Ksi, respectively.

The load-displacement curves are shown in Appendices 25 and 26.

IV.3 Fatigue Life Studies

Fatigue life tests were conducted for four different thermomechanically processed 7075 aluminum alloys under load control and the results obtained were compared with those of aged alloy. All thermomechanically processed and T6-aged alloys showed Wöhler-type S-N curves with fatigue lives ranging from 10^4 cycles to 10^6 cycles for applied stress amplitudes of 50, 40 and 30 Ksi.

Stress amplitudes and fatigue lives for thermomechanically processed alloys and T6-aged alloys are shown in Table 3.

Stress amplitude versus fatigue life for these alloys plotted on semi-logarithmic scale are shown in Appendices 27-31.

Completely reversed cyclic loading ($R = -1$) was applied to the smooth fatigue specimens with stress amplitudes of 30, 40 and 50 Ksi.

From the various types of thermomechanical processings investigated, FHT showed the best high-cycle fatigue life at the stress amplitude of 30 Ksi. The other three thermomechanically processed alloys showed a noticeable increase in fatigue life at 30 Ksi level.

It is generally agreed that the fatigue life at low stress levels (high-cycle fatigue regime) is mostly spent in crack nucleation and Stage I crack propagation. Therefore, the fatigue life at low stress levels would seem to reflect the characteristics of the crack initiation stage.

From Appendix 28 it can be seen that FHT processing caused an increase of approximately one-half of an order of magnitude in the

TABLE 3. Fatigue lives for thermomechanically processed 7075 aluminum alloy (number of cycles)

Alloys (7075-X)	Stress Amplitude (Ksi)		
	30	40	50
T6	66,856	28,176	13,980
FHT + T6	1,132,370 318,832 130,784 161,228 187,462	33,502	9,846
FRT + T6	129,878	29,909	8,553
FT6	118,908	26,400	5,028
SH5	96,689	36,180	8,479
T651	224,655	62,553	22,537
PFZ#1	114,092	21,565	4,947
PFZ#2	74,379	29,789	11,273

fatigue life at a stress amplitude of 30 Ksi. This increase in fatigue life is thought to be due to the improved resistance to fatigue crack nucleation. As noted in the literature survey, there has been speculation and some experimental results to the effect that plastic deformation occurs preferentially in the soft precipitate free zone around the grain boundaries in 7075 aluminum alloy. Therefore, it is very likely that persistent slip bands form within the PFZ more easily and that fatigue cracks initiate from these persistent slip bands.

In addition, the PFZ generally appears to occur in conjunction with grain-boundary precipitates that are not coherent with the matrix. Based on the above, it would appear to be necessary to remove the soft PFZ or strengthen it, in order to retard fatigue crack initiation.

Several different approaches have been adopted to accomplish the foregoing objective. For example, the addition of alloying elements such as Ti or Ag could reduce the width of the PFZ in the Al-Zn-Mg alloy system. Thermomechanical processing such as rolling could form jogs in the grain boundaries and reduce slip length.

Another approach is dual heat-treatment which is the method of aging the alloy at two different temperatures for different periods of time in order to promote precipitation.

However, cyclic pre-loading as a TMP had not been studied until Lu and Weissman [35] examined Al-6.5% Zn alloy recently and reported an increase in fatigue life. In this study, cyclic preloading at high temperature was examined in an attempt to strengthen the weak PFZ by generating dislocations from the grain boundaries.

IV.3.1 Fatigue Life Study of FHT Alloy

The thermomechanically processed alloy, FHT, was processed as discussed in the TMP section. An elevated temperature of 150°C was used for the cyclic pre-loading in order to allow easier dislocation glide.

At elevated temperatures, coherent thermal atomic motion, corresponding to dislocation oscillation, helps dislocations in overcoming the Peierls-Nabarro energy barrier. In addition, thermal atomic motion helps smooth out the potential troughs and hills along close-pack rows. This reduces the Peierls-Nabarro stress.

This theoretical consideration seems to be substantiated by the fact that more dislocations were generated from the grain boundaries in the alloy that was cyclically pre-loaded at high temperature than in the alloy pre-loaded at room temperature. Transmission electron micrographs show a greater density of dislocations in the FHT specimen than in the FRT specimen (refer to Section IV.7).

The fatigue life at 30 Ksi level was somewhat increased over the -T6 condition. This increase in fatigue life is speculated to be due to the reduction or elimination of soft PFZ areas. This experimental result also supports the model that fatigue cracks nucleate within the weak PFZ in 7075 aluminum alloy.

Furthermore, there is another factor which should be considered in an effort to explain the increase in fatigue life. It is generally accepted that high-cycle fatigue properties improve when the material becomes stronger. If this is true, the lower strength of FHT as compared with the T6-aged alloy should result in increased crack initiation or reduced fatigue life at low stress levels. However, the fatigue life of FHT at low stress levels was found to be improved.

The strength, which comes mostly from matrix precipitates, does not significantly affect crack nucleation or fatigue strength at low stress level. Instead, the characteristics of the PFZ will be the major factor affecting crack initiation. From this point of view it appears that characteristics around the grain boundaries play a predominant role in the crack initiation behavior of 7075 aluminum alloy.

At high stress levels, the fatigue life was found to decrease when compared with the fatigue life of the T6-aged alloy. This result would appear to be due to the fact that cyclic pre-loading increases the rate of crack propagation and that at high stress levels, cracks initiate early, and most of the life is spent in the crack propagation stage.

IV.3.2 Fatigue Life Study of FT6 Alloy

FT6 processing, which included the application of cyclic preloading at 120°C for 24 hours with a stress amplitude of 7 Ksi, behaved in a fashion similar to that demonstrated by the FHT and FRT alloys.

The increase in fatigue life at low stress levels was not significant. However, while indicating a level of fatigue life similar to that of the T6 alloy at the 40 Ksi level, there is a tendency towards an increase in life at the 30 Ksi level.

Although the overall improvement in fatigue life was not significant this type of TMP may prove to be useful since standard T6 aging was conducted simultaneously with cyclic pre-loading. This procedure is believed to accommodate precipitates at possible crack nuclei that may be formed at the early stages by dislocation movement (refer to Section IV.1.4).

IV.3.3 Fatigue Life Study of SH5 Alloy

This SH5 alloy was processed by stretching plastically by five percent at 150°C. The S-N curve shows trends similar to those of the other thermomechanically processed alloys (Appendix 29).

IV.3.4 Fatigue Life Study of PFZ#1 and PFZ#2 Alloys

Fatigue life tests were performed as described in the earlier sections. As can be seen from Appendices 30 and 31, PFZ#1 and PFZ#2 showed approximately the same fatigue life. From these results, it is appropriate to say that a two-fold difference in the width of the PFZ is not a significant factor in fatigue life.

IV.4 Fatigue Crack Propagation Studies

IV.4.1 Fatigue Crack Propagation of Plastically Deformed and Non-deformed Alloys

The fatigue crack propagation rate (FCPR) was determined for

7075-T651 and compared with that for 7075-T6 aluminum alloy to study the effect of deformation on FCPR.

FCPR of both T651 and T6-aged alloys were studied for the mid-ΔK range from ΔK=13 Ksi$\sqrt{in}$ to ΔK=24 Ksi$\sqrt{in}$. (da/dN) versus log ΔK was plotted in semi-logarithmic paper. It shows a linear relationship between log (da/dN) and log ΔK. The da/dN was obtained by the incremental polynomial method described in A.S.T.M. E-647.

The (da/dN) versus ΔK plots of 7075-T651 and 7075-T6 are shown in Appendices 32 and 33, respectively. From these figures, it can be seen that the FCPR of 7075-T651 is about one-half of an order of magnitude greater than that of 7075-T6, indicating that the FCPR of plastically deformed alloy is significantly greater than that of non-deformed alloy.

Two models for FCP of the predeformed condition have been proposed, i.e., "damage accumulation model" and "crack tip blunting model." According to the damage accumulation model [88], predeformation reduces the remaining plastic deformation capability of the material. This reduction in deformation capability reduces the residual deformation on the fracture surface behind the propagating crack. Therefore, the crack opens earlier in the predeformed material than in the non-deformed material.

The crack tip blunting model [94] states that the higher yield strength caused by predeformation will induce a smaller plastic zone size and consequently less crack closure, which leads to a higher crack growth rate than for the non-deformed material.

In this study it was observed from tensile tests, that the

Y.S. of 7075-T651 was higher than that of 7075-T6. Therefore, the crack tip blunting model can be applied to explain the higher FCPR of the T651-aged alloy as compared with that of the T6-tempered alloy.

Furthermore, the fatigue life at high stress levels was determined to be shortened for the cyclically pre-loaded alloy. This implies that the FCPR of the cyclically pre-loaded alloy is higher than that of the non-deformed alloy.

However, tensile tests showed a lower value of Y.S. for the alloy cyclically pre-loaded at high temperature as compared with the T6-aged alloy. From these results, it can be said that the "damage accumulation model" seems to be more generally applicable than the "crack tip blunting model" in explaining the increased FCPR of plastically deformed alloy.

In this study, cyclic pre-loading and stretching gave rise to shorter fatigue lives at high stress levels. This is indicative of higher FCPR for the thermomechanically processed alloys. In addition, it is of interest to note that T651 processing increased the fatigue life in comparison with T6-aging, but the FCPR of T651-aged alloy was substantially higher than that of the T6-aged alloy.

These results give rise to the dilemma that TMP can improve the fatigue life at low stress levels at the expense of a decrease of fatigue life at high stress levels, due to the high FCPR associated with the latter. From this point of view, TMP would appear to be beneficial only for low cyclic stress levels, or for the high-cycle fatigue regime in the 7075 aluminum alloy system investigated.

IV.4.2 Fatigue Crack Propagation Study of Alloys with Different PFZ Widths

Thermal treatment is one of the methods to control PFZ width in 7075 aluminum alloy. For example, PFZ width was increased by increasing aging temperature. However, FCP behavior has not been previously studied in alloys that have different widths of the PFZ.

From Appendices 30 and 31, it can be seen that PFZ#1 and PFZ#2 had approximately the same fatigue lives. A FCP study was also conducted to determine fatigue crack propagation rates of PFZ#1 and PFZ#2 alloys.

In this investigation, fatigue crack propagation was studied for the alloy with 800 Å PFZ width (PFZ#1), and 2000 Å PFZ width (PFZ#2). However, it was necessary to keep the other microstructural factors reasonably similar in order to permit comparison fatigue crack growth rates of alloys with different widths of the PFZ.

The Y.S. and U.T.S. were not the same in both alloys but they were comparable (refer to Section IV.2). The grain-size of both PFZ#1 and PFZ#2 was also comparable.

From Appendices 34 and 35, it can be seen that the FCPR of PFZ#2 was not significantly different from that of PFZ#1 in the mid-ΔK range.

There have been attempts to correlate fatigue life test results with FCP test results. However, in this study it was only possible to correlate qualitatively because the fatigue life tests were conducted under load control. However, the trend, obvious from both experiments, is that a wider PFZ permits a greater degree of residual plastic deformation on the fracture surface behind the propagating crack, in accordance with the damage accumulation model. Also, in comparing the tensile test results of PFZ#1 and PFZ#2, it is seen that PFZ#2 has a higher strain hardening capacity than PFZ#1. The higher strain-hardening capacity, in turn, would indicate less damage accumulation in the material.

From these speculations, it is expected that the alloy with a wide PFZ would show a lower FCPR than would the alloy with a narrow PFZ. This probably furnishes one way to test the damage accumulation model suggested by McClintock.

IV.5 Plane Strain Fracture Toughness Studies

Load versus crack opening distance plots are shown in Appendices 36-40.

IV.5.1 Plane Strain Fracture Toughness of 7075-T651 and 7075-T6 Alloys

Plane strain fracture toughness of 7075-T651 aluminum alloy was determined to be 22 Ksi$\sqrt{in}$ for the T-L direction and 25 Ksi$\sqrt{in}$ for L-T direction as shown in Table 4 and Appendices 36-40.

The K_{IC} value determined by this study for the alloy is close to the K_{IC} value given in the ASM Metals Handbook.

The plane strain fracture toughness of the alloy in the T6-aged condition was determined to be 40 Ksi$\sqrt{in}$, which is much greater than the K_{IC} value of T6 from other sources [111]. However, this

TABLE 4. P(Q) and K_{IC} values of 7075-T6, 7075-T651 and experimental PFZ#1 and PFZ#2 aluminum alloys

Alloys (7075-X)	P(Q) (Kips)	K_{IC} (Ksi$\sqrt{in}$)
T651 (L)	6.27	22
T651 (T)	7.70	25
T6	9.68	40
PFZ#1	9.90	35
PFZ#2	11.66	39

discrepancy could be explained by the fact that the T6-aged condition was prepared by solution treatment of as-received T651 material, followed by water quenching and artificial aging at 120°C for 24 hours. This T6 processing resulted in an equiaxed recrystallized structure, which has a relatively lower Y.S. and U.T.S. when compared with the commercial 7075-T6 aluminum alloy which has pancake-shaped grains.

Thompson [108] has reported that this difference in grain shape probably gives rise to the difference in the values for fracture toughness. The results also show that, in general, a higher tensile strength material possesses a lower K_{IC} value.

IV.5.2 Plane Strain Fracture Toughness of PFZ#1 and PFZ#2 Alloys

The plane strain fracture toughness of the alloy with 800 Å wide PFZ, PFZ#1, was determined to be 35 Ksi$\sqrt{in}$ and K_{IC} for the alloy with 2000 Å wide PFZ, PFZ#2, was found to be 39 Ksi$\sqrt{in}$.

From this result it would seem to follow that the alloy with a wide PFZ has a large K_{IC} value, indicating that the PFZ width is one of the metallurgical factors that affect the fracture toughness of 7075 aluminum alloy.

There have been some investigations of fracture toughness in the context of grain size or TMP. However, these studies were only concerned with the length of the PFZ, and not the width. Therefore, it is interesting to note the difference in K_{IC} due to a variation in PFZ width.

Hornbogen [109] has recently published a model for the estimation of fracture toughness values and has developed an equation for an alloy that has a soft region around the grain boundaries. Since 7075 aluminum alloy belongs to this category due to the presence of the PFZ, Hornbogen's model is applicable to the K_{IC} results obtained for PFZ#1 and PFZ#2 alloys.

Hornbogen has modified Hahn's equation to include the factor of PFZ width and has reported the following equations:

$$K_{ICi} = [L_i E\sigma_{yi} n_i^2 \varepsilon_{fi}^2 (\frac{d}{D})]^{\frac{1}{2}}$$

and $$K_{IC} = K_{ICi} P_i + K_{ICt}(1-P_i)$$

where,

L	:	constant
E	:	Young's modulus
σ_y	:	yield strength
n	:	strain-hardening coefficient
e_f	:	true fracture strain
d	:	PFZ width
D	:	grain-size
i	:	stands for intercrystalline
t	:	stands for transcrystalline
P	:	relative portion

Assuming PFZ width, d, is the only factor that is different for PFZ#1 and PFZ#2, K_{IC} values were compared in an attempt to test the model.

From the calculations, K_{IC} for PFZ#2 is expected to be 59 Ksi$\sqrt{in}$

which is larger than the experimental result, 39 Ksi$\sqrt{in}$. From this calculation, it can be said that the contribution to the fracture toughness due to a soft PFZ is about 20 percent.

At this stage, it is difficult to state, with any degree of certainty, that Hornbogen's model is indeed correct. However, the model would appear to be a useful tool for the estimation of fracture toughness for alloys containing precipitate free zones.

IV.6 Scanning Electron Microscopy

IV.6.1 SEM Study of Fatigue Crack Propagation

Fatigue striation spacings were measured at a point 0.35 inch away from the machined notch for each FCP test specimen. The stress intensity factor range at this point was determined to be 17 Ksi$\sqrt{in}$.

From Appendices 41 and 42, it is obvious that the striation spacing of the T651-aged alloy is approximately three times larger than that of T6-aged alloy. The striation spacing of the alloys was measured to be 0.50 μm for 7075-T6 and 1.50 μm for 7075-T651.

From these scanning electron micrographs, it can be seen that the FCPR for 7075-T651 is approximately three times greater than that of 7075-T6. This ratio is approximately the same as the ratio of da/dN between 7075-T651 and 7075-T6. (da/dN) for $\Delta K = 17$ Ksi$\sqrt{in}$ was determined to be 4×10^{-5} inch/cycle for 7075-T6 and 1.2×10^{-4} inch/cycle for 7075-T651.

However, the values of striation spacing for PFZ#1 and PFZ#2 were approximately the same, as shown in Appendices 43 and 44. As can be seen in Appendix 45, the crack front propagated in various directions due to the different orientations of grains and the relative differences in their strengths. This appendix also shows a difference in striation spacing in different directions indicative of a range of FCPR.

It is also observed that the fatigue stiration are of a ductile type, typical of 7075 aluminum alloy.

IV.6.2 SEM Study of Fracture Surfaces

As reported by many other investigators, the fracture mode of 7075 aluminum alloy in the plane strain condition is observed to be of the ductile dimple mode [112,113,114]. Microvoids frequently initiate at second phase particles or inclusions and join together to fracture, representative of the ductile dimple mode.

As shown in Appendices 46 and 47, a wide range of dimple sizes are observed on the fracture surface. Some investigators [114] have reported that the number of large dimples increases as the purity of the alloy increases, while some others [115,116] have reported that the dimple size increases with the coarsening of the grain boundary precipitates. Kirman [95] has observed the depth of dimples and reported that the depth of the dimple may be influenced by the width of the PFZ.

From Appendices 48 and 49, it can be stated that the dimple size increases as the PFZ width increases. This result is especially interesting because Ludka [110] has recently stated that $(\sigma_m - \sigma_{PFZ})$ is an important factor affecting the mode of fracture. Based on this concept, it is speculated that a wider PFZ has less tendency to form a crack path due to the coalescence of microvoids and, hence, the formation of larger dimples. On the contrary, a narrow PFZ provides an easier crack path for intergranular fracture and leads to the formation of small dimples. These speculations are shown schematically in Figure 5.

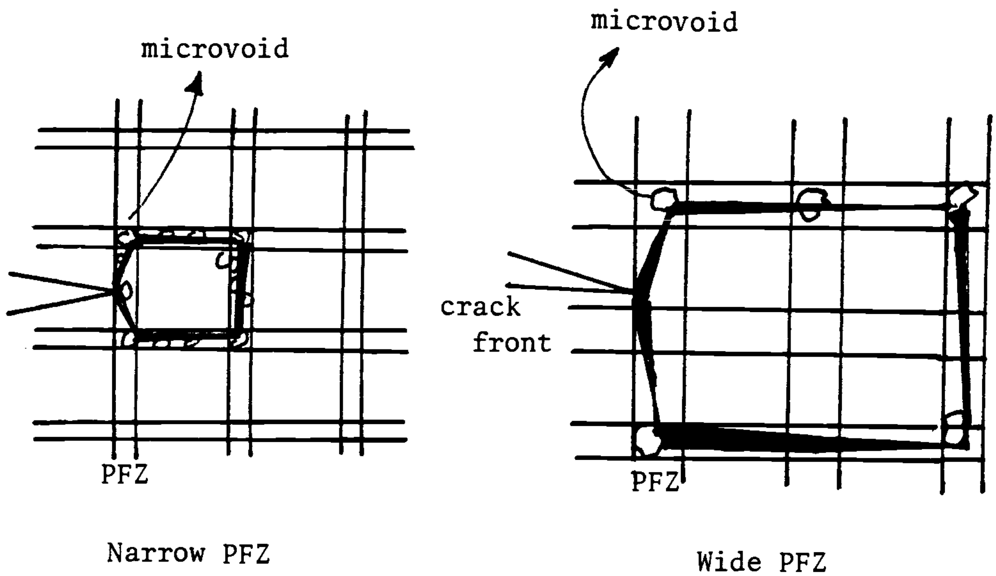

FIGURE 5. The origin of various dimple sizes for various widths of precipitate free zone applying Ludka's model

Furthermore, Ludka's speculation is found to be reasonable in light of the intergranular fracture mode of the tensile test specimen of PFZ#1 which has a high value of $(\sigma_m - \sigma_{PFZ})$, due to its narrow PFZ width. PFZ#2 showed a ductile dimple mode of fracture as did other thermomechanically processed aluminum alloy specimens, as shown in Appendix 51.

However, the fracture surfaces of PFZ#2 exhibited no signs of intergranular fracture as shown in Appendix 41, even though it has larger grain boundary precipitates. This is probably due to the small value of $(\sigma_m - \sigma_{PFZ})$. Kirman [95] has reported that the dimple size increases with an increase in grain boundary precipitate size. However, this conclusion does not appear to be supported by the present experimental results.

From this study, Ludka's model appears to be more plausible than Kirman's statement regarding dimple size as an explanation of the present experimental results.

IV.7 Transmission Electron Microscopy

IV.7.1 TEM Study of Thermomehanically Processed 7075 Aluminum Alloys

Appendix 52 shows a transmission electron micrograph of FHT alloy after cyclic pre-loading but before the fatigue left test. Round and plate-shaped η' phases are present after T6-aging. This micrograph also shows a dislocation that has passed through an η' phase particle that is semi-coherent with the matrix. Another dislocation has passed half-way through an η' particle.

Also, it can be seen at the lower left corner that dislocation bands have formed around and from the second phase particles which give rise to stress concentrations.

Appendix 53 shows a TEM photograph of FRT alloy. This micrograph shows that numerous dislocations have been generated from the grain boundaries and distributed uniformly through the matrix. This is normally to be expected after any thermomechanical processing is done. A number of precipitates particles are shown to be nucleated at the dislocations in the matrix.

Appendix 54 shows the precipitate free zone around the grain boundary and discontinous grain-boundary precipitates. The width of the PFZ was determined to be 570 Å. This micrograph clearly shows that even T6-aging of 7075 aluminum alloy leads to the development of the distinctive precipitate free zone. Dislocations generated by small cyclic loading from the grain boundary, and that lead to an increase in strength of the PFZ, are also visible.

IV.7.2 TEM Study of PFZ#1 and PFZ#2 Alloys

Appendix 55 is a transmission electron micrograph of PFZ#1. This shows the 800 Å width of the PFZ, and continuous grain-boundary precipitation, which is responsible for the intergranular fracture mode discussed earlier. It is also evident that precipitate size near the grain boundary is larger than that at a distance from the grain boundary.

Appendix 56 shows a transmission electron micrograph of PFZ#2. This micrograph shows the PFZ, 2000 Å in width, and discontinuous grain boundary precipitates.

IV.7.3 TEM Study after Fatigue Life Testing

Appendix 57 is a transmission electron micrograph of FHT alloy after the fatigue-life test under an alternating stress of 50 Ksi. This micrograph shows a large dislocation band that was formed during fatigue cycling.

These dislocation bands often lead to crack initiation at the surface by the formation of intrusions.

V. CONCLUSIONS

1. The width of the precipitate free zone can be controlled by varying the aging temperature with fixed aging time rather than changing quenching temperature.

2. Cyclic pre-loading at one-third of the Y.S. of the solution-treated material at room temperature or at high temperature increased the fatigue life at low stress levels to some degree, but did not significantly affect the life at high stress levels.

3. A new type of thermomechanical processing, FT6, was examined for 7075 aluminum alloy and showed a tendency towards an increase in fatigue life at low stress levels.

4. With the exception of FHT, all types of thermomechanical processing investigated increased the U.S. and U.T.S. as compared with the standard T6 aging of 7075 aluminum alloy, due to the promotion of nucleation of precipitates at dislocations created by mechanical processing.

5. Cyclic pre-loading at a low stress amplitude generated a large number of dislocations around the grain-boundaries at elevated and at room temperatures. This is believed to be the main reason for the small increase observed in high-cycle fatigue life.

6. The width of the PFZ was determined by TEM to be 800 Å for the alloy aged at 150°C for two hours (7075-PFZ#1) and 2000 Å for the alloy aged at 177°C for two hours (7075-PFZ#2).

7. The fatigue crack propagation rate was studied for 7075-T651 and 7075-T6. FCPR of 7075-T651 was approximately four times greater than that of 7075-T6 and the damage accumulation model is applied to explain this.

8. The fatigue life of the alloy with narrow PFZ was not found to be significantly different from that of the alloy with wide PFZ at low applied stress levels.

9. Fatigue crack propagation rates have been determined for 7075-PFZ#1 and 7075-PFZ#2. It was found that 7075-PFZ#2 exhibited approximately the same rate of crack propagation as that shown by 7075-PFZ#1.

10. Plane strain fracture toughness of 7075-T651 and 7075-T6 were determined to be 22 Ksi$\sqrt{in}$ and 39 Ksi$\sqrt{in}$, respectively.

11. Plane strain fracture toughness of 7075-PFZ#1 and 7075-PFZ#2 were determined to be 35 Ksi$\sqrt{in}$ and 39 Ksi$\sqrt{in}$, respectively. These results were found to correlate fairly well with a recently proposed model [109].

12. SEM studies showed a tendency towards intergranular fracture for 7075-PFZ#1 and ductile dimple fracture for 7075-PFZ#2. This result would appear to confirm the recently proposed concept [110] that the strength differential between the matrix and the PFZ would affect the fracture toughness, and hence the mode of fracture.

13. BASIC version of an incremental polynomial computer program for determining the crack propagation rate was developed and utilized for analysis of the data.

VI. SUGGESTIONS FOR FURTHER RESEARCH

1. It has been known and confirmed that a higher aging temperature gives a wider precipitate free zone than a lower aging temperature. However, it is necessary to establish a quantitative relationship between the aging temperature and the PFZ width in 7075 aluminum alloy and other alloy systems.

   In addition it is worthwhile to investigate the effect of the width of the PFZ on the mechanical properties in other alloy systems where a PFZ develops in order to help predict the fatigue and fracture properties.

   It is also recommended that the effect of alloying elements other than Ti and Ag to control the PFZ width be examined.

2. Only a few experimental results have been reported regarding the effects of cyclic pre-loading on aluminum alloy. This study showed some positive results of cyclic pre-loading by increasing the high-cycle fatigue life in 7075 aluminum alloy. Therefore, cyclic pre-loading at low stress levels needs to be investigated as a possible solution for the improvement of fatigue life in other alloy systems that develop a PFZ.

   Furthermore, simultaneous cyclic pre-loading with aging is suggested for study in Al-Cu alloy system. The change in precipitate structure and distribution by cyclic loading may be interesting to study and may be used in developing a new thermomechanical processing technique for the above alloy.

3. It has been qualitatively recognized that the crack propagation rate is affected by the PFZ width in 7075 aluminum alloy. However, it is suggested that the effect of the PFZ width on fatigue crack propagation be the subject of further study.

   It is also important to determine what factors are the most important microstructural parameters affecting fatigue crack propagation behavior in 7075 and other aluminum alloys at ambient and elevated temperatures.

4. Fatigue crack initiation at ΔK_{th} levels needs to be investigated for the thermomechanically processed alloys and for alloys with different PFZ widths in order to clarify the mechanism of fatigue crack nucleation within the soft PFZ.

5. It is suggested that a study be conducted of Hornbogen's model which states that fracture toughness increases with the (PFZ width)$^{\frac{1}{2}}$. However, it is also necessary to examine the limit of PFZ width that can improve the fracture toughness without a reduction in tensile property values.

REFERENCES

[1] Starke, E. Aluminum alloys of 70's: Scientific solutions to engineering problems. Mat. Sci. and Eng. 29(1977), p. 99.

[2] Kelly, A. Precipitation hardening. Progress in Mat. Sci., Vol. 10, No. 3, 1963.

[3] Nock, J. High strength aluminum alloys. J. of Metals, March, 1963, p. 216.

[4] Laird, C. Fatigue. Mat. Sci. and Eng. 25(1976), p. 187.

[5] Friedel, J. Dislocations, 1964, p. 67.

[6] Bamford, W. The use of fatigue crack growth technology in fracture control plans for nuclear components. ASTM STP 738, 1981, p. 281.

[7] Hopkins, S. Prediction of structural crack growth behavior under fatigue loading. ASTM STP 738, 1981, p. 255.

[8] ASM Committee. Heat treatment aluminum alloys. Metals Handbook, Vol. 2, p. 271.

[9] ASTM: Standard test method for constant-load-amplitude fatigue crack growth rates above 10^{-8}m/cycle. ASTM E647-81.

[10] ASTM: Standard recommended practice for constant-amplitude low cycle fatigue testing. ASTM E606-77.

[11] MTS: Series 643.6X tension compression grips. Hardware Product Manual (1980).

[12] Strawley, J. Wide range stress intensity factor expressions for ASTM E-399 standard fracture toughness specimen. Int. J. of Fracture 12(1976), p. 475.

[13] ASTM E-8: Standard method of tension testing of metallic materials. ASTM E8-79, p. 160.

[14] Thomas, G. Aging characteristics of aluminum alloys. J. of Inst. of Metals, 88(1959), p. 81.

[15] Guinier, A. Precipitation phenomenon in supersaturated solid solutions. J. of Metals, 1956, p. 673.

[16] Unwin, P. The origin of grain boundary precipitate free zone. Acta. Met. 17(1969), p. 1363.

[17] Cornish, A. Precipitation in neighbourhood of grain boundaries in an Al-Zn-Mg alloy. J. of Inst. of Metals, 97(1969), p. 44.

[18] Starke, E. The causes and effects of "denuded" or "precipitate free" zones of grain boundaries in aluminum-base alloys. J. of Metals, January 1970, p. 54.

[19] Nicholson, R. The nucleation of precipitates: the system Al-Zn-Mg. Acta Met., 13(1965), p. 403.

[20] Sedriks, A. Deformation within precipitate free zones in an aged Al-Zn-Mg alloy. Trans. ASM, 62(1969), p. 815.

[21] Abe, M. Influence of the precipitate free zone width on the tensile properties of an Al-6Zn-1.2Mg alloy. Met. Trans. 4(1973), p. 1499.

[22] Lütejering, G. Influence of grain size on the fracture of aluminum alloys. Fracture, Vol. 2, 1977, p. 7.

[23] Welpman, K. Influence of TMT on fracture properties of aluminum alloys. Fracture, Vol. 2, 1977, p. 195.

[24] Cornish, A. The effect of variable quenching conditions on the relationship between the stress-corrosion resistance, tensile properties, and microstructure of high-purity Al-Zn-Mg alloy. J. of Inst. of Metals, 99(1971), p. 377.

[25] Ostermann, F. Thermomechanical processing and fatigue of aluminum alloys. ASTM STP 467, 1974, p. 169.

[26] McEvily, A. Effect of thermomechanical processing on the fatigue and stress corrosion properties of Al-Zn-Mg alloy. Trans. ASM 60(1967), p. 661.

[27] Di Russo, E. Thermomechanical treatments on high strength Al-Zn-Mg-(Cu) alloys. Met. Trans. 4(1973), p. 1133.

[28] Ostermann, F. Improved fatigue resistance of 7075 aluminum alloys through thermomechanical processing. Met. Trans., 2(1971), p. 2897.

[29] Di Russo, E. A new thermo-mechanical procedures for improving the ductility and toughness of Al-Zn-Mg-Cu alloys in transverse direction. Mat. Sci. and Eng., 14 (1974), p. 23.

[30] Alder, P. Influence of microstructure on mechanical properties and stress corrosion susceptibility of 7075 aluminum alloy. Met. Trans. 3(1971), p. 3191.

[31] Ryu, J. Effect of two-step aging on fatigue and stress corrosion resistance in 7075 aluminum alloy. J. of Korean Inst. of Metals, 19(1981), p. 310.

[32] Nunomura, S. Fatigue and microstructure of 7075 aluminum alloy. Light Metal, Japan, 28(1978), p. 547.

[33] Weissmann, S. Extension of the fatigue life of metal crystals through control of substructure. Tran. JIM, 9(1968), p. 1004.

[34] Kiritani, M. Defect structures in fatigued Al-6.5 At. Pct Zn alloy. Met Trans. 3(1972), p. 1229.

[35] Lu, M. The influence of aging and thermomechanical treatment on the fatigue properties of an Al-6.5 at % Zn alloy. Mat. Sci. and Eng., 32(1978), p. 41.

[36] Basquin, O. The exponential law of endurance test. Proc. ASTM, 10(1910), p. 625.

[37] Tavernelli, J. Experimental support for generalized equation predicting low cycle fatigue. Tran. ASME. J. of Basic Eng., 84(1962), p. 553.

[38] Manson, S. Discussion of Ref. 37 Trans. ASME. J. Basic Eng., 84(1962), p. 537.

[39] Fine, M. Fatigue crack initiation and near threshold crack growth. Fatigue and Microstructure, ASM, 1978, p. 245.

[40] Glysler, A. Correlation between microstructure and fatigue fracture. Strength of Metals and Alloys, Vol. 2, 5th Int. Conference, 1979, p. 27.

[41] Fujita, F. Dislocation theory of fracture of crystals. Acta Met., 6(1958), p. 543.

[42] Laird, C. A theory of crack nucleation in high strain fatigue. Int. J. Fracture Mechanics, 4(1968), p. 219.

[43] Newmann, P. Coarse slip model of fatigue. Acta Met., 17 (1969), p. 1219.

[44] Lynch, S. A new model for initiation and growth of fatigue cracks. Metal Science, 9(1975), p. 401.

[45] Mughrabi, H. Microscopic mechanism of metal fatigue strength of metals and alloys. 5th Int. Conference, Vol. 3, 1979, p. 27.

[46] McEvily, A. The effect of non-uniform precipitation on the fatigue properties of an age-hardening alloy. Trans. AIME, 227(1963), p. 452.

[47] Grove, C. Effect of titanium additions on aging characteristics of an Al-Zn-Mg alloy. Met. Trans., 4(1973), p. 1023.

[48] Polmear, I. The properties of commercial Al-Zn-Mg alloys: practical implications of trace elements of silver. J. of Inst. of Metals, 89(1960), p. 193.

[49] Chen, C. Microstructure study on the effect of titanium in the aging treatment of an Al-Zn-Mg alloy. Met. Trans., 9A (1978), p. 553.

[50] Polmear, I. The aging characteristics of complex Al-Zn-Mg alloys. J. of Inst. of Metal, 1960, p. 51.

[51] Sanders, R. The effect of grain refinement on the low cycle fatigue behavior of an aluminum-zinc-magnesium alloy. Mat. Sci. and Eng., 28(1977), p. 53.

[52] Waldman, J. The effect of ingot processing treatment on the grain size and properties of Al alloy 7075. Met. Trans., 5(1974), p. 573.

[53] Starke, E. Cyclic plastic deformation and microstructure. Fatigue and microstructure, ASM (1977), p. 205.

[54] Sanders, T. The relationship of microstructure to monotonic and cyclic straining of two age-hardening aluminum alloy. Met. Trans., 7A(1976), p. 1407.

[55] Singh, V. Effect of prior treatment on the low cycle fatigue behavior of aluminum alloy. RR 58 at 423K. Int. J. Fatigue, Jan. 1980, p. 12.

[56] Sanders, R. The effect of intermediate thermomechanical treatment on the fatigue properties of a 7050 aluminum alloy. Met. Trans., Vol. 9A(1978), p. 1087.

[57] Hyatt, M. New aluminum aircraft alloys for 1980's. Metallurgia, Vol. 42(1977), p. 81.

[58] Kuo, V. The effect of ITMT's and P/M processing on the microstructure and mechanical properties of the X7091 alloy. Met. Trans., 14A(1983), p. 435.

[59] Avitzur, B. Discussion of Improved fatigue resistance of Al-Zn-Mg-Cu(7075) alloys through thermomechanical processing. Met. Trans., 4(1973), p. 383.

[60] Mehrpay, F. Effect of thermomechanical treatment on fatitue strength in 7075-Al. Met. Trans., 7A(1976), p. 761.

[61] Rack, H. Thermomechanical treatment of high purity 6061 aluminum alloy. Met. Trans. 8A(1977), p. 335.

[62] McEvily, A. Current aspects of fatigue. Metal Science, August 1977, p. 274.

[63] Beevers, C. Fatigue crack growth characteristics at low stress intensities of metals and alloys. Metal Science, August 1977, p. 362.

[64] Kirby, B. Slow fatigue crack growth and threshold behavior in air and vacuum of commercial aluminum alloys. Fatigue of Eng. Material and Structure, 1(1979), p. 203.

[65] Haddad, M. Review of new development in crack propagation studies. American Society for Testing and Material, 1981, p. 65.

[66] Beevers, C. Some aspects of fatigue crack growth in metals and alloys. Fracture, Vol. 1, 1977, p. 239.

[67] Tomkins, B. Fatigue crack propagation: an analysis. Philosophical Mag., 8(1968), p. 1041.

[68] Paris, P. A critical analysis of crack propagation laws. Trans. ASME, December 1963, p. 528.

[69] Suresh, S. Mechanisms of slow fatigue crack growth in high strength aluminum alloy: Role of microstructure and environment. Met. Trans., 15A(1984), p. 369.

[70] Staley, J. How microstructure affects fatigue and fracture of aluminum alloys. Fracture Mechanics, 1978, p. 671.

[71] Petit, J. Effect of microstructure on crack growth in a high strength aluminum alloy. Proc. of 4th E.C.F. Conference, 1979, p. 426.

[72] Staley, J. Improving fatigue resistance of aluminum aircraft alloy. Communication from Alcoa Technical Center, 1977, p. 11.

[73] Forsyth, P. The relationship between fatigue crack behavior and microstructure in 7178 aluminum alloy. Int. J. Fatigue, January 1981, p. 17.

[74] Lindigkeit, J. The effect of microstructure on the fatigue crack propagation behavior of Al-Zn-Mg-Cu alloy. Met. Trans., 12A(1981), p. 1613.

[75] Laird, C. The influence of metallurigcal structure on the mechanisms of fatigue crack propagation. ASTM STP 415, 1967, p. 131.

[76] Plumbridge, W. Fatigue resistance and structure. Fatigue of Eng. Materials and Structure, 2(1980), p. 361.

[77] Nageswararao, M. Fatigue crack propagation in Stage I in aluminum-zinc-magnesium alloy. Met. Trans., 7A(1976) p. 1847.

[78] Morris, W. Fatigue crack initiation and early crack propagation in Al 2219-T851. Met. Trans., 7A(1976), p. 1161.

[79] Stoenesifer, F. Effect of grain size and temperature on fatigue crack propagation in A533 steel. Eng. Fract. Mech., 10(1978), p. 305.

[80] Wei, R. Fatigue crack propagation in high strength aluminum alloy. Int. J. of Fracture Mechanics, 4(1968), p. 159.

[81] Miller, K. Fatigue under complex stress. Metal Science, Aug. 1977, p. 109.

[82] Knott, J. Effects of overloads on fatigue crack propagation: Aluminum alloy. Metal Science, August 1977, p. 399.

[83] Branco, M. An analysis of the influence of mean stress intensity and environment on fatigue crack growth in a new high strength aluminum alloy. J. of Testing and Evaluation, 3(1975), p. 407.

[84] Zurek, A. The effect of grain size on fatigue growth of short cracks. Met. Trans, 14A(1982), p. 1697.

[85] Anthony, W. The dependence of fatigue crack growth rate on grain size. Met. Trans., 4(1973), p. 1173.

[86] Lindigkeit, J. The effect of grain size on the fatigue crack propagation behavior of age-hardened alloys in inert and corrosive environment. Acta Met., 27(1979), p. 1717.

[87] Kang, T. The effect of pre-stress cycles on fatigue crack growth: An analysis of crack growth mechanism. Eng. Fracture Mechanics, 6(1974), p. 631.

[88] McClintock, F. Discussion to fracture mode transition for a crack traversing a plate. J. Basic Engineering, 82(1960) p. 417.

[89] Schijve, J. The effect of pre-strain on fatigue crack growth and crack closure. Eng. Fracture Mechanics, 8(1976), p. 575.

[90] Schutte, K. Influence of monotonic and cyclic predeformation on fatigue crack propagation of high strength aluminum alloys. Eng. Fracture Mechanics, 13(1980), p. 1009.

[91] Awatani, J. A study on the effect of stacking fault energy on fatigue crack propagation as deduced from dislocation patterns. Met. Trans., 10A(1979), p. 503.

[92] Saxena, A. Low cycle fatigue, fatigue crack propagation and substructure in a series of polycrystalline Cu-Al alloys. Met. Trans., 6A(1975), p. 1809.

[93] Avery, D. Fracture of solids. Interscience Publishers, (1962), p. 339.

[94] Laird, C. Effect of dislocation substructures on fatigue fracture. Met. Trans., 8A(1977), p. 851.

[95] Kirman, I. The relation between microstructure and toughness in 7075 aluminum alloy. Met. Trans., 2(1971), p. 1761.

[96] Bowles, C. On the formation of fatigue striation. Int. J. Fracture Mech., 8(1972), p. 75.

[97] McClintock, F. Discussion. ASTM STP 415 (1967), p. 170.

[98] Tomkins, B. Micromechanism of fatigue crack growth at high stress. Metal Science, Aug. 1980, p. 408.

[99] Irving, P. Prediction of fatigue crack growth rates: Theory, mechanisms, and experimental results. Metal Science, Aug. 1977, p. 351.

[100] Katz, Y. Micromechanisms of fatigue crack growth exposed to load transient effects. Metal Science, 15(1981), p. 317.

[101] Beevers, C. Micromechanism of fatigue crack growth at low stress intensities. Metal Science, Aug. 1980, p. 418.

[102] Kaisand, L. Relationship between low-cycle fatigue and fatigue crack growth rate properties. J. of Testing and Evaluation, 7(1979), p. 270.

[103] Hahn, G. Metallurgical factors affecting fracture toughness of aluminum alloys. Met. Trans., 6A(1975), p. 653.

[104] Knott, J. Micromechanisms of fracture and the fracture toughness of engineering alloy. Fracture, Vol. 1, 1977, p. 61.

[105] Kawabata, T. Ductile fracture in the interior of precipitate free zone in an Al-6.0% Zn-2.6% Mg alloy. Acta Met., 24 (1976), p. 817.

[106] Gräf, M. Observation of ductile intercrystalline fracture of an Al-Zn-Mg alloy. Acta Met., 25(1977), p. 883.

[107] Santner, J. A study of fracture in high purity 7075 aluminum alloy. Met. Trans., 9A(1978), p. 769.

[108] Thompson, D. The effects of alloying and processing on the fracture characteristics of aluminum sheet. Eng. Fracture Mechanics, 7(1975), p. 389.

[109] Hornbogen, E. Fracture toughness of precipitation hardened alloys containing narrow soft zones at grain boundaries. Acta Met., 25(1977), p. 877.

[110] Ludka, G. The influence of microstructure and strength of fracture mode and toughness of 7XXX series aluminum alloy. Met. Tran., 13A(1982), p. 411.

[111] Reimann, W. Improved fracture resistance of 7075 through thermomechanical processing. Eng. Fracture Mechanics, 5(1973), p. 67.

[112] Beachem, C. An electron fractographic study of the influence of plastic strain condition upon ductile rupture process in metals. Trans. ASM, 56(1963), p. 319.

[113] Hunter, M. Fractography and microstructure of aluminum alloys 7075-T651 and 7075-T7351. ASTM STP 436, 1968, p. 196.

[114] Garrett, G. The influence of compositional and microstructural variations on the mechanism of static fracture in aluminum alloys. Proc. of 2nd Int. Conf. on Mechanical Behavior, 1976, p. 488.

[115] Burghard, H. The influence of precipitate morphology on microvoid growth and coalescence in tensile fracture. Met. Trans., 5(1974), p. 2083.

[116] Lütering, G. Fatigue and fracture of aluminum alloy. Aluminum transformation technology and applications, 1978, p. 171.

[117] Weissmann, S. Dislocation substructure and extension of fatigue life in metal crystal. Trans. ASM, 59(1966), p. 709.

[118] McMillan, J. Application of electron fractography to fatigue studies. ASTM STP 436, 1968, p. 89.

[119] Hosford, W. Effect of stress during aging on the precipitation of θ' in Al-4 wt pct Cu. Met. Trans. A, Vol. 6A, March 1975, p. 487.

[120] ASM. Metals Handbook Ninth Edition. Properties and Selection: Nonferrous alloys and pure metals, p. 44.

[121] Sanders, T. Review of fatigue and fracture research on high-strength aluminum alloys. ASM Fatigue and Microstructure, 1979, p. 467.

BIBLIOGRAPHY

Abe, M. Influence of the precipitate free zone width on the tensile properties of an Al-6Zn-1.2Mg alloy. Met. Trans., 4(1973), p. 1499.

Alder, P. Influence of microstructure on mechanical properties and stress corrosion susceptibility of 7075 aluminum alloy. Met. Trans., 3(1971), p. 3191.

Anthony, W. The dependence of fatigue crackgrowth rate on grain size. Met. Trans., 4(1973), p. 1173.

ASM. Metals Handbook Ninth Edition. Properties and Selection: Nonferrous alloys and pure metals, p. 44.

ASM Committee. Heat treatment aluminum alloys. Metals Handbook, Vol. 2, p. 271.

ASTM: Standard recommended practice for constant-amplitude low cycle fatigue testing. ASTM E606-77.

ASTM E-8: Standard method of tension testing of metallic materials. ASTM E8-79, p. 160.

ASTM: Standard test method for constant-load-amplitude fatigue crack growth rates above 10^{-8}m/cycle. ASTM E647-81.

Avery, D. Fracture of solids. Interscience Publishers (1962), p. 339.

Avitzur, B. Discussion of improved fatigue resistance of Al-Zn-Mg-Cu (7075) alloys through thermomechanical processing. Met. Trans., 4(1973), p. 383.

Awatani, J. A study on the effect of stacking fault energy on fatigue crack propagation as deduced from dislocation patterns. Met. Trans., 10A(1979), p. 503.

Bamford, W. The use of fatigue crack growth technology in fracture control plans for nuclear components. ASTM STP 738, 1981, p. 281.

Basquin, O. The exponential law of endurance test. Proc. ASTM, 10(1910), p. 625.

Beachem, C. An electron fractographic study of the influence of plastic strain condition upon ductile rupture process in metals. Trans. ASM, 56(1963), p. 319.

Beevers, C. Fatigue crack growth characteristics at low stress intensities of metals and alloys. Metal Science, August 1977, p. 362.

Beevers, C. Some aspects of fatigue crack growth in metals and alloys. Fracture, Vol. 1, 1977, p. 239.

Beevers, C. Micromechanism of fatigue crack growth at low stress intensities. Metal Science, August 1980, p. 418.

Bowles, C. On the formation of fatigue striation. Int. J. Fracture Mech., 8(1972), p. 75.

Branco, M. An analysis of the influence of mean stress intensity and environment on fatigue crack growth in a new high strength aluminum alloy. J. of Testing and Evaluation, 3(1975), p. 407.

Burghard, H. The influence of precipitate morphology on microvoid growth and coalescence in tensile fracture. Met. Trans., 5(1974), p. 2083.

Chen, C. Microstructure study on the effect of titanium in the aging treatment of an Al-Zn-Mg alloy. Met. Trans., 9A(1978), p. 553.

Cornish, A. The effect of variable quenching conditions on the relationship between the stress-corrosion resistance, tensile properties, and microstructure of high-purity Al-Zn-Mg alloy. J. of Inst. of Metals, 99(1971), p. 377.

Cornish, A. Precipitation in neighbourhood of grain boundaries in an Al-Zn-Mg alloy. J. of Inst. of Metals, 97(1969), p. 44.

Di Russo, E. Thermomechanical treatments on high strength Al-Zn-Mg-(Cu) alloys. Met. Trans., 4(1973), p. 1133.

Di Russo, E. New thermomechanical procedures for improving the ductility and toughness of Al-Zn-Mg-Cu alloys in transverse direction. Mat. Sci. and Eng., 14(1974), p. 23.

Fine, M. Fatigue crack initiation and near threshold crack growth. Fatigue and Microstructure, ASM, 1978, p. 245.

Forsyth, P. The relationship between fatigue crack behavior and microstructure in 7178 aluminum alloy. Int. J. Fatigue, January 1981, p. 17.

Friedel, J. Dislocations, 1964, p. 67.

Fujita, F. Dislocation theory of fracture of crystals. Acta Met., 6(1958), p. 543.

Garrett, G. The influence of compositional and microstructural variations on the mechanism of statis fracture in aluminum alloys. Proc. of 2nd Int. Conf. on Mechanical Behavior, 1976, p. 488.

Gräf, M. Observation of ductile intercrystalline fracture of an Al-Zn-Mg alloy. Acta Met., 25(1977), p. 883.

Glysler, A. Correlation between microstructure and fatigue fracture. Strength of Metals and Alloys, Vol. 2, 5th Int. Conference, 1979, p. 27.

Grove, C. Effect of titanium additions on aging characteristics of an Al-Zn-Mg alloy. Met. Trans., 4(1973), p. 1023.

Guinier, A. Precipitation phenomenon in supersaturated solid solutions. J. of Metals, 1956, p. 673.

Haddad, M. Review of new development in crack propagation studies. American Society for Testing and Material, 1981, p. 65.

Hahn, G. Metallurgical factors affecting fracture toughness of aluminum alloys. Met. Trans., 6A(1975), p. 653.

Hopkins, S. Prediction of structural crack growth behavior under fatigue loading. ASTM STP 738, 1981, p. 255.

Hornbogen, E. Fracture toughness of precipitation hardened alloys containing narrow soft zones at grain boundaries. Acta Met., 25(1977), p. 877.

Hosford, W. Effect of stress during aging on the precipitation of θ' in Al-4 wt pct Cu. Met. Trans. A, Vol. 6A, March 1975, p. 487.

Hunter, M. Fractography and microstructure of aluminum alloys 7075-T651 and 7075-T7351. ASTM STP 436, 1968, p. 196.

Hyatt, M. New aluminum aircraft alloys for 1980's. Metallurgia, Vol. 42(1977), p. 81.

Irving, P. Prediction of fatigue crack growth rates: Theory, mechanisms, and experimental results. Metal Science, August 1977, p. 351.

Kaisand, L. Relationship between low-cycle fatigue and fatigue crack growth rate properties. J. of Testing and Evaluation, 7(1979), p. 270.

Kang, T. The effect of pre-stress cycles on fatigue crack growth: An analysis of crack growth mechanism. Eng. Fracture Mechanics, 6(1974), p. 631.

Katz, Y. Micromechanisms of fatigue crack growth exposed to load transient effects. Metal Science, 15(1981), p. 317.

Kawabata, T. Ductile fracture in the interior of precipitate free zone in an Al-6.0% Zn-2.6% Mg alloy. Acta Met., 24(1976), p. 817.

Kelly, A. Precipitation hardening. Progress in Mat. Sci., Vol. 10, No. 3, 1963.

Kirby, B. Slow fatigue crack growth and threshold behavior in air and vacuum of commercial aluminum alloys. Fatigue of Eng. Material and Structure, 1(1979), p. 203.

Kiritani, M. Defect structures in fatigued Al-6.5 At. Pct. Zn alloy. Met. Trans. 3(1972), p. 1229.

Kirman, I. The relation between microstructure and toughness in 7075 aluminum alloy. Met. Trans., 2(1971), p. 1761.

Knott, J. Micromechanisms of fracture and the fracture toughness of engineering alloy. Fracture, Vol. 1, 1977, p. 61.

Knott, J. Effects of overloads on fatigue crack propagation: Aluminum alloy. Metal Science, August 1977, p. 399.

Kuo, V. The effect of ITMT's and P/M processing on the microstructure and mechanical properties of the X7091 alloy. Met. Trans., 14A(1983), p. 435.

Laird, C. The influence of metallurgical structure on the mechanisms of fatigue crack propagation. ASTM STP 415, 1967, p. 131.

Laird, C. A theory of crack nucleation in high strain fatigue. Int. J. Fracture Mechanics, 4(1968), p. 219.

Laird, C. Effect of dislocation substructures on fatigue fracture. Met. Trans., 8A(1977), p. 851.

Laird, C. Fatigue. Mat. Sci. and Eng. 25(1976), p. 187.

Lindigkeit, J. The effect of grain size on the fatigue crack propagation behavior of age-hardened alloys in inert and corrosive environment. Acta Met., 27(1979), p. 1717.

Lindigkeit, J. The effect of microstructure on the fatigue crack propagation behavior of Al-Zn-Mg-Cu alloy. Met. Trans., 12A(1981), p. 1613.

Lu, M. The influence of aging and thermomechanical treatment on the fatigue properties of an Al-6.5 at % Zn alloy. Mat. Sci. and Eng., 32(1978), p. 41.

Ludka, G. The influence of microstructure and strength of fracture mode and toughness of 7XXX series aluminum alloy. Met. Trans., 13A(1982), p. 411.

Lütejering, G. Influence of grain size on the fracture of aluminum alloys. Fracture, Vol. 2, 1977, p. 7.

Lütering, G. Fatigue and fracture of aluminum alloy. Aluminum transformation technology and applications, 1978, p. 171.

Lynch, S. A new model for initiation and growth of fatigue cracks. Metal Science, 9(1975), p. 401.

Manson, S. Discussion of Ref. 37. Trans. ASME. J. Basic Eng., 84(1962), p. 537.

McClintock, F. Discussion to fracture mode transition for a crack traversing a plate. J. Basic Engineering, 82(1960), p. 417.

McClintock, F. Discussion. ASTM STP 415 (1967), p. 170.

McEvily, A. The effect of non-uniform precipitation on the fatigue properties of an age-hardening alloy. Trans. AIME, 227(1963), p. 452.

McEvily, A. Effect of thermomechanical processing on the fatigue and stress corrosion properties of Al-Zn-Mg alloy. Trans. ASM 60(1967), p. 661.

McEvily, A. Current aspects of fatigue. Metal Science, August 1977, p. 274.

McMillan, J. Application of electron fractography to fatigue studies. ASTM STP 436, 1968, p. 89.

Mehrpay, F. Effect of thermomechanical treatment on fatigue strength in 7075-Al. Met. Trans., 7A(1976), p. 761.

Miller, K. Fatigue under complex stress. Metal Science, August 1977, p. 109.

Morris, W. Fatigue crack initiation and early crack propagation in Al 2219-T851. Met. Trans., 7A(1976), p. 1161.

MTS: Series 643.6X tension compression grips. Hardware Product Manual (1980).

Mughrabi, H. Microscopic mechanism of metal fatigue strength of metals and alloys. 5th Int. Conference, Vol. 3, 1979, p. 27.

Nageswararao, M. Fatigue crack propagation in Stage I in aluminum-zinc-magnesium alloy. Met. Trans., 7A(1976), p. 1847.

Newmann, P. Coarse slip model of fatigue. Acta Met., 17(1969), p. 1219.

Nicholson, R. The nucleation of precipitates: the system Al-Zn-Mg. Acta Met., 13(1965), p. 403.

Nock, J. High strength aluminum alloys. J. of Metals, March, 1963, p. 216.

Nunomura, S. Fatigue and microstructure of 7075 aluminum alloy. Light Metal, Japan, 28(1978), p. 547.

Ostermann, F. Improved fatigue resistance of 7075 aluminum alloys through thermomechanical processing. Met. Trans., 2(1971), p. 2897.

Osterman, F. Thermomechanical processing and fatigue of aluminum alloys. ASTM STP 467, 1974, p. 169.

Paris, P. A critical analysis of crack propagation laws. Trans. ASME, December 1963, p. 528.

Petit, J. Effect of microstructure on crack growth in a high strength aluminum alloy. Proc. of 4th E.C.F. Conference, 1979, p. 426.

Plumbridge, W. Fatigue resistance and structure. Fatigue of Eng. Materials and Structure, 2(1980), p. 361.

Polmear, I. The aging characteristics of complex Al-Zn-Mg alloys. J. of Inst. of Metal, 1960, p. 51.

Polmear, I. The properties of commercial Al-Zn-Mg alloys: practical implications of trace elements of silver. J. of Inst. of Metals, 89(1960), p. 193.

Rack, H. Thermomechanical treatment of high purity 6061 aluminum alloy. Met. Trans., 8A(1977), p. 335.

Reimann, W. Improved fracture resistance of 7075 through thermomechanical processing. Eng. Fracture Mechanics, 5(1973), p. 67.

Ryu, J. Effect of two-step aging on fatigue and stress corrosion resistance in 7075 aluminum alloy. J. of Korean Inst. of Metals, 19(1981), p. 310.

Sanders, R. The effect of grain refinement on the low cycle fatigue behavior of an aluminum-zinc-magnesium alloy. Mat. Sci. and Eng., 28(1977), p. 53.

Sanders, R. The effect of intermediate thermomechanical treatment on the fatigue properties of a 7050 aluminum alloy. Met. Trans., Vol. 9A(1978), p. 1087.

Sanders, T. The relationship of microstructure to monotonic and cyclic straining of two age-hardening aluminum alloy. Met. Trans., 7A(1976), p. 1407.

Sanders, T. Review of fatigue and fracture research on high-strength aluminum alloys. ASM Fatigue and Microstructure, 1979, p. 467.

Santner, J. A study of fracture in high purity 7075 aluminum alloy. Met. Trans., 9A(1978), p. 769.

Saxena, A. Low cycle fatigue, fatigue crack propagation and sub-structure in a series of polycrystalline Cu-Al alloys. Met. Trans., 6A(1975), p. 1809.

Schijve, J. The effect of pre-strain on fatigue crack growth and crack closure. Eng. Fracture Mechanics, 8(1976), p. 575.

Schutte, K. Influence of monotonic and cyclic predeformation on fatigue crack propagation of high strength aluminum alloys. Eng. Fracture Mechanics, 13(1980), p. 1009.

Sedriks, A. Deformation within precipitate free zones in an aged Al-Zn-Mg alloy. Trans. ASM, 62(1969), p. 815.

Singh, V. Effect of prior treatment on the low cycle fatigue behavior of aluminum alloy. RR 58 at 423K. Int. J. Fatigue, Jan. 1980, p. 12.

Staley, J. Improving fatigue resistance of aluminum aircraft alloy. Communication from Alcoa Technical Center, 1977, p. 11.

Staley, J. How microstructure affects fatigue and fracture of aluminum alloys. Fracture Mechanics, 1978, p. 671.

Starke, E. The causes and effects of "denuded" or "precipitate free" zones of grain boundaries in aluminum-base alloys. J. of Metals, January 1970, p. 54.

Starke, E. Aluminum alloys of 70's: Scientific solutions to engineering problems. Mat. Sci. and Eng. 29(1977), p. 99.

Starke, E. Cyclic plastic deformation and microstructure. Fatigue and microstructure, ASM (1977), p. 205.

Stoenesifer, F. Effect of grain size and temperature on fatigue crack propagation in A533 steel. Eng. Fract. Mech., 10(1978), p. 305.

Strawley, J. Wide range stress intensity factor expressions for ASTM E-399 standard fracture toughness specimen. Int. J. of Fracture 12(1976), p. 475.

Suresh, S. Mechanisms of slow fatigue crack growth in high strength aluminum alloy: Role of microstructure and environment. Met. Trans., 15A(1984), p. 369.

Tavernelli, J. Experimental support for generalized equation predicting low cycle fatigue. Tran. ASME. J. of Basic Eng., 84(1962), p. 553.

Thomas, G. Aging characteristics of aluminum alloys. J. of Inst. of Metals, 88(1959), p. 81.

Thompson, D. The effects of alloying and processing on the fracture characteristics of aluminum sheet. Eng. Fracture Mechanics, 7(1975), p. 389.

Tomkins, B. Fatigue crack propagation: an analysis. Philosophical Mag., 8(1968), p. 1041.

Tomkins, B. Micromechanism of fatigue crack growth at high stress. Metal Science, August 1980, p. 408.

Unwin, P. The origin of grain boundary precipitate free zone. Acta Met. 17(1969), p. 1363.

Waldman, J. The effect of ingot processing treatment on the grain size and properties of Al alloy 7075. Met. Trans., 5(1974), p. 573.

Wei, R. Fatigue crack propagation in high strength aluminum alloy. Int. J. of Fracture Mechanics, 4(1968), p. 159.

Weissman, S. Dislocation substructure and extension of fatigue life in metal crystal. Trans. ASM, 59(1966), p. 709.

Weissman, S. Extension of the fatigue life of metal crystals through control of substructure. Tran. JIM, 9(1968), p. 1004.

Welpman, K. Influence of TMT on fracture properties of aluminum alloys. Fracture, Vol. 2, 1977, p. 195.

Zurek, A. The effect of grain size on fatigue growth of short cracks. Met. Trans., 14A(1982), p. 1697.

APPENDICES

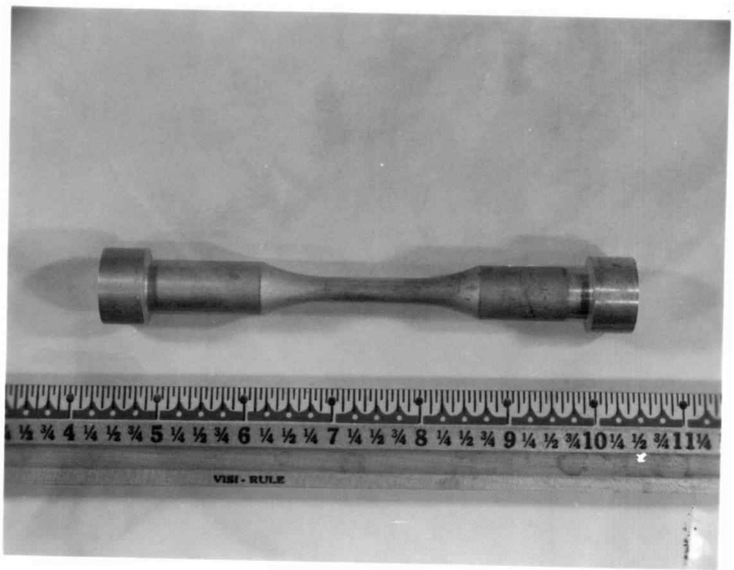

APPENDIX 1. The shape of flat-end smooth fatigue specimen

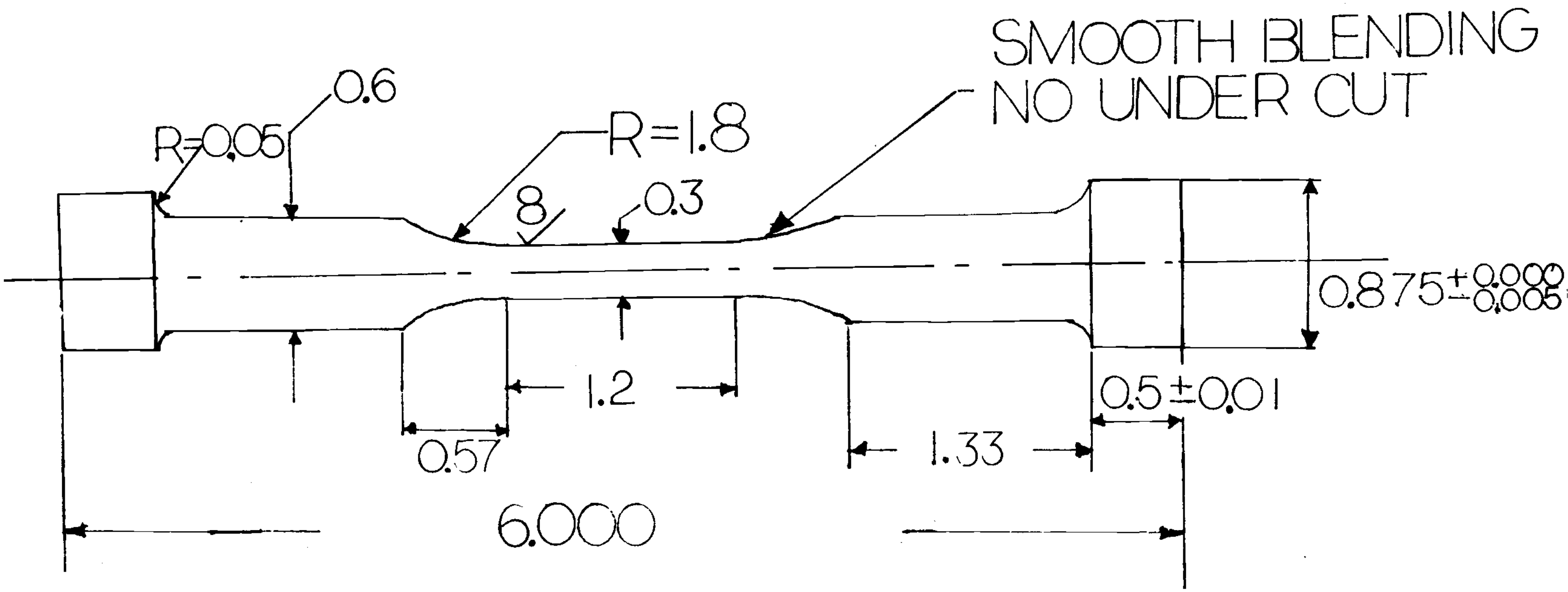

APPENDIX 2. The dimensions of flat-end smooth fatigue specimen (inches)

APPENDIX 3. The shape of special grip for fatigue crack propagation test

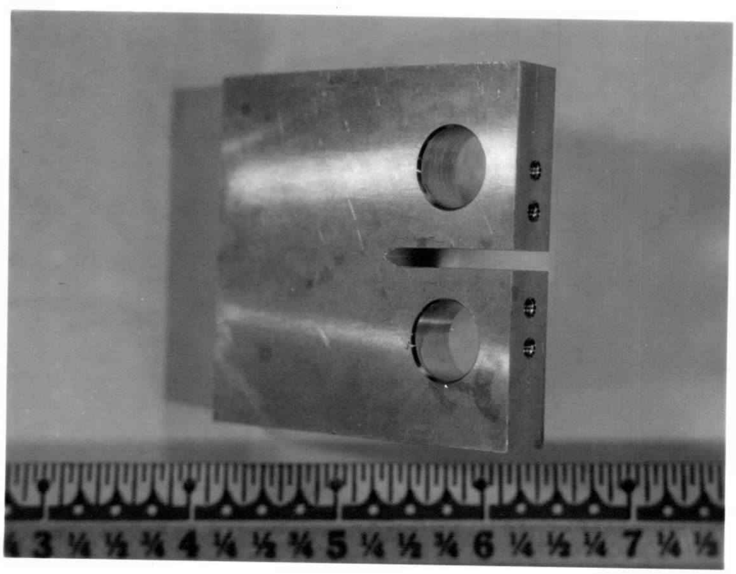

APPENDIX 4. The shape of compact tension specimen for fatigue crack propagation test

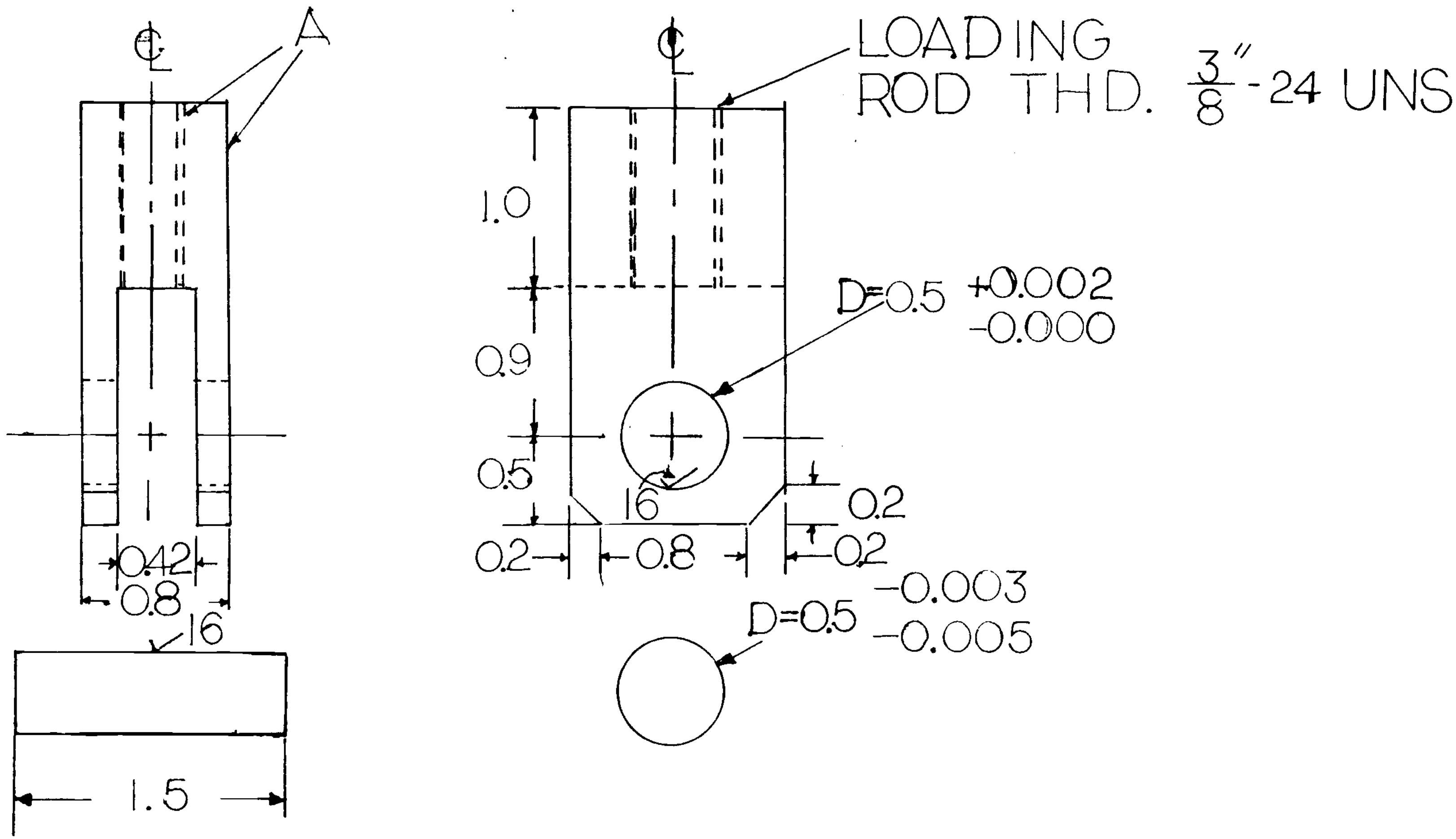

APPENDIX 5. The dimensions of clevis and pin for fatigue crack propagation test (inches)

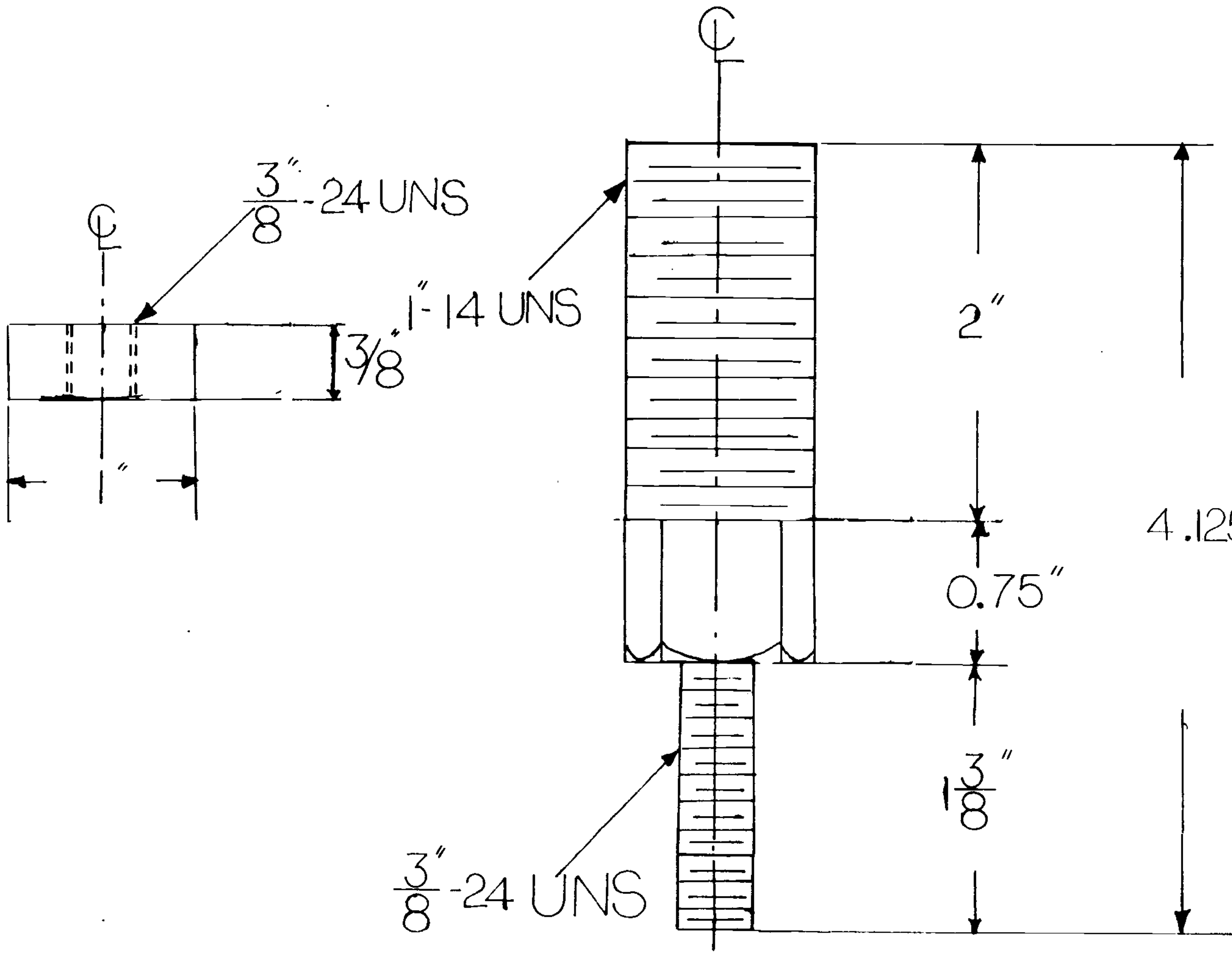

APPENDIX 6. The dimensions of the adapter for MTS (inches)

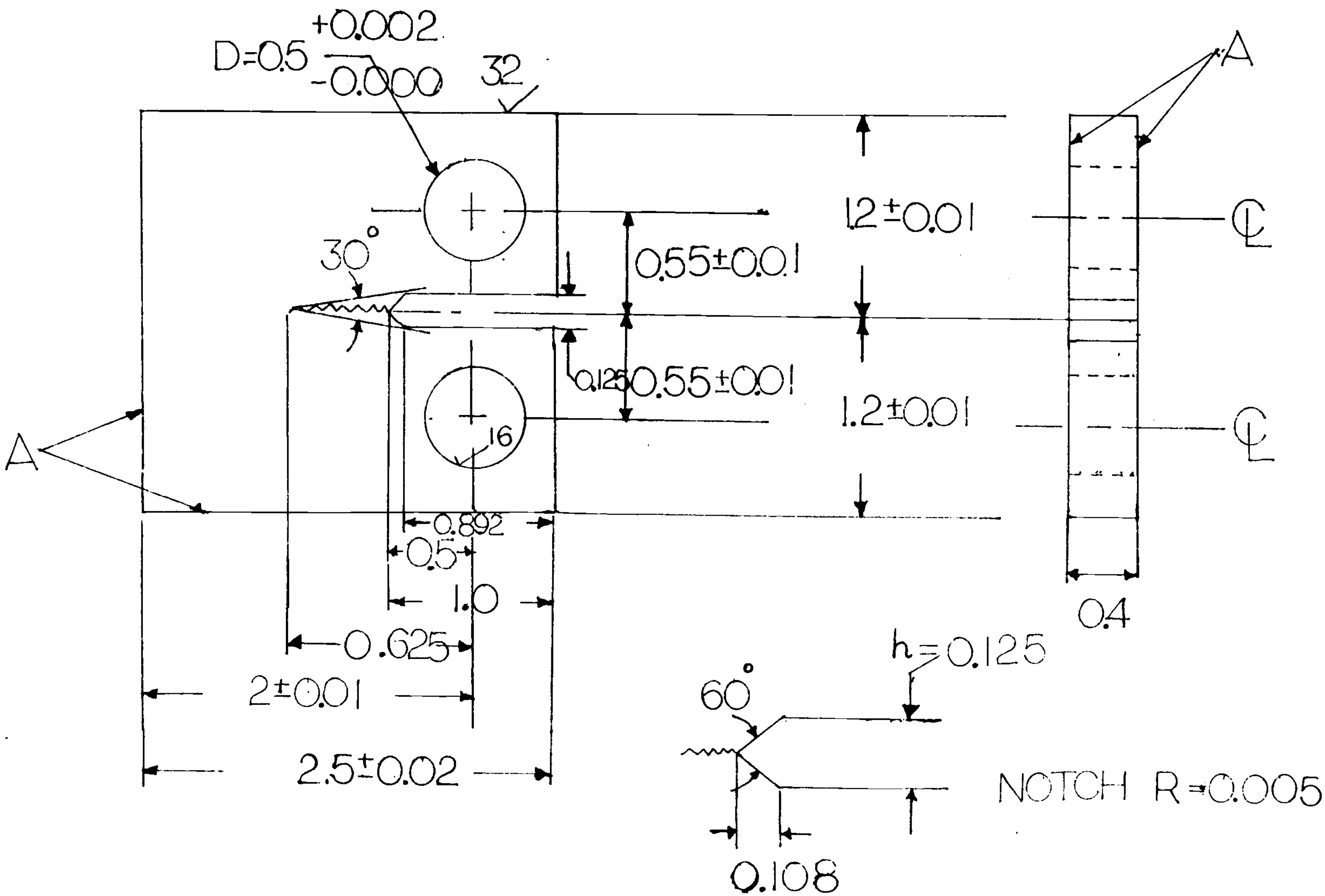

APPENDIX 7. The dimensions of compact tension specimen for fatigue crack propagation test (inches)

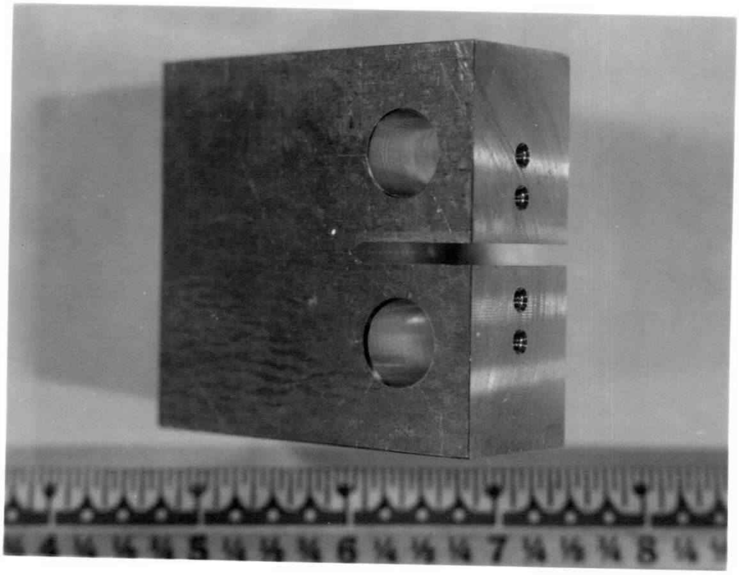

APPENDIX 8. The shape of compact tension specimen for K_{IC} test

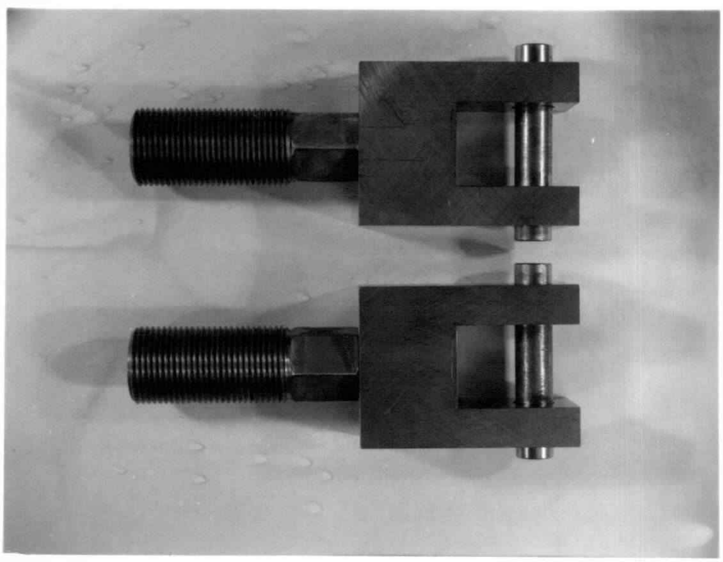

APPENDIX 9. The shape of special grip for K_{IC} test

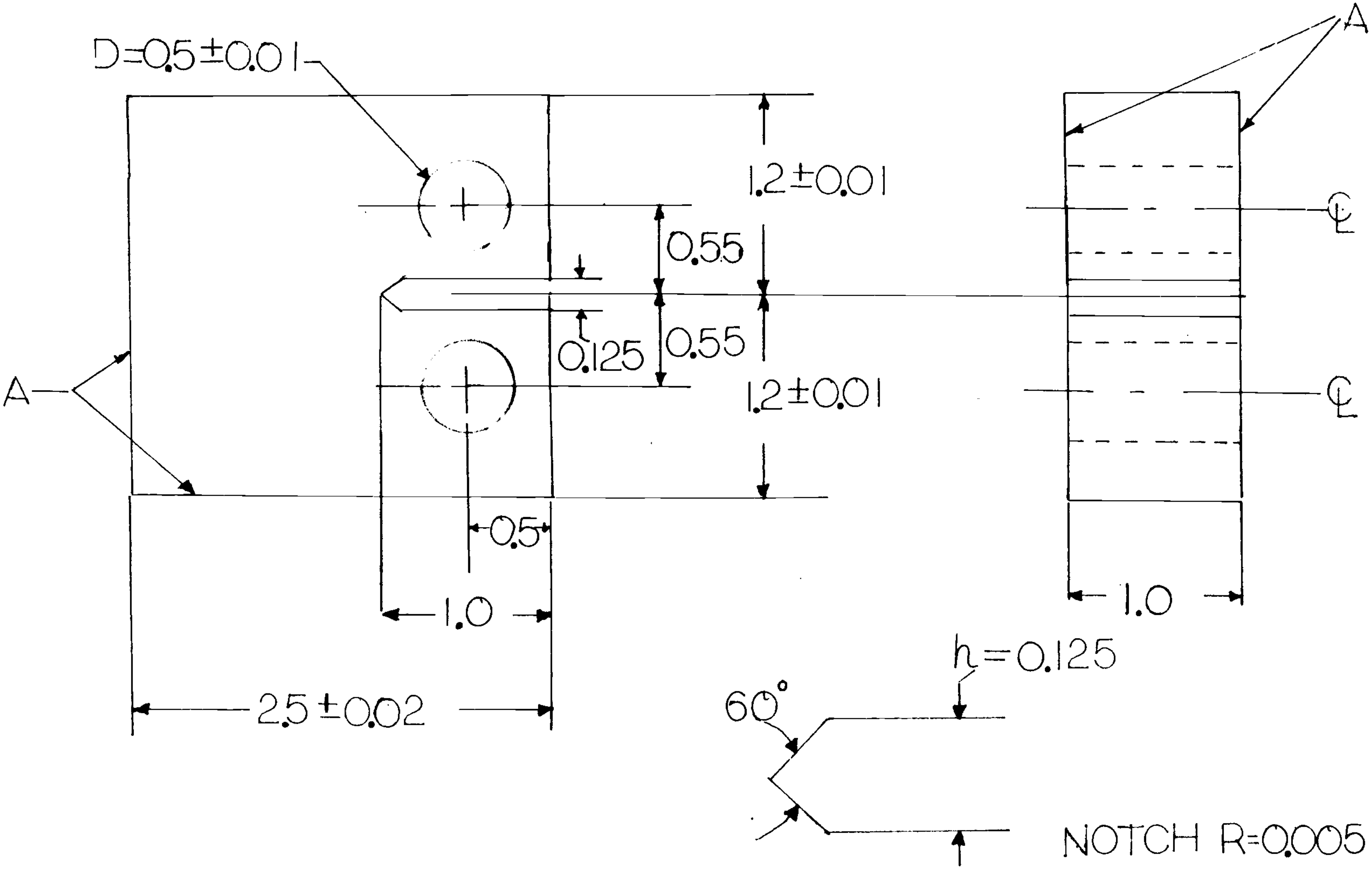

APPENDIX 10. The dimensions of compact tension specimen for K_{IC} test (inches)

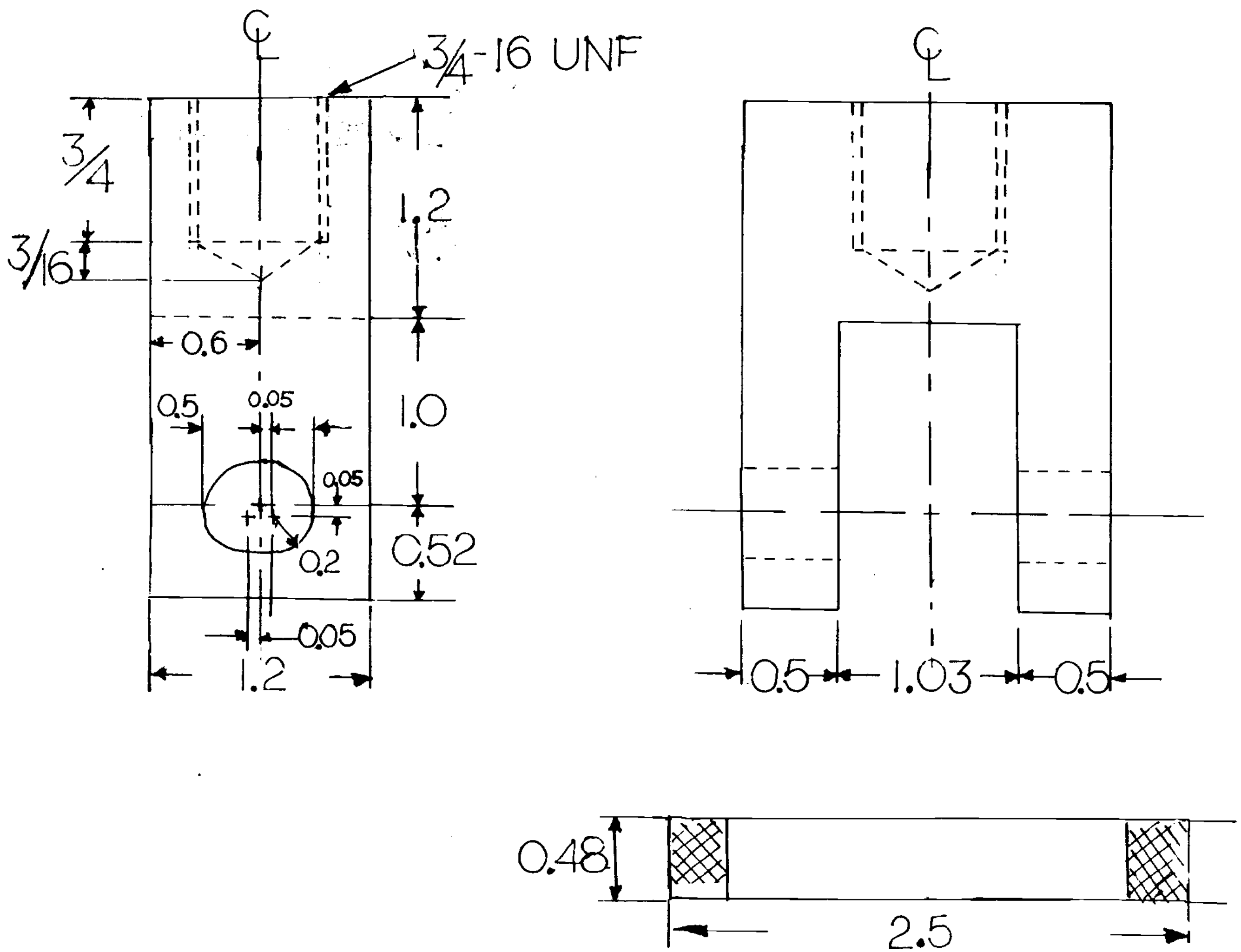

APPENDIX 11. The dimensions of clevis and pin for K_{IC} test (inches)

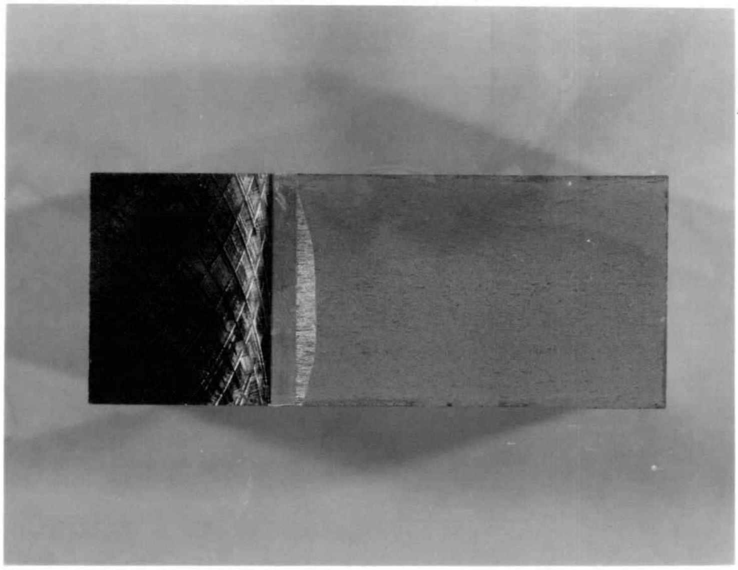

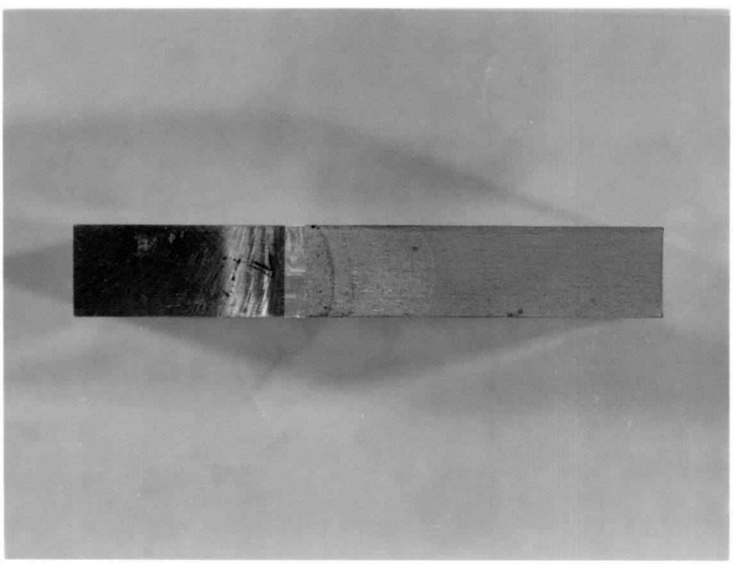

APPENDIX 12. Fractographs of compact tension specimens showing fatigue pre-crack

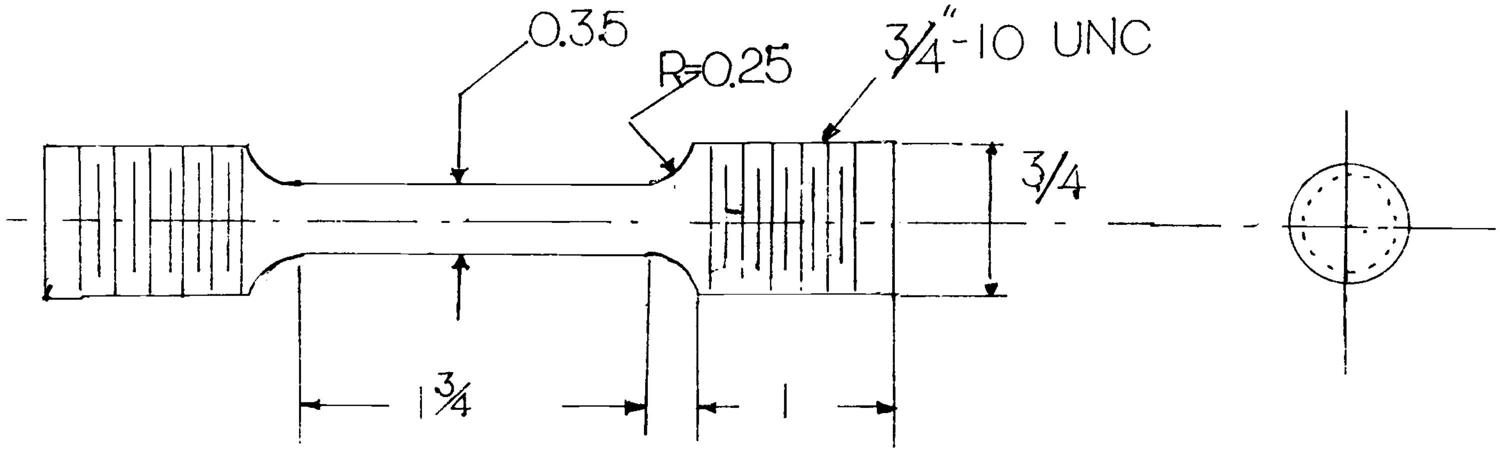

APPENDIX 13. The dimensions of standard tensile test specimen according to ASTM E-8 (inches)

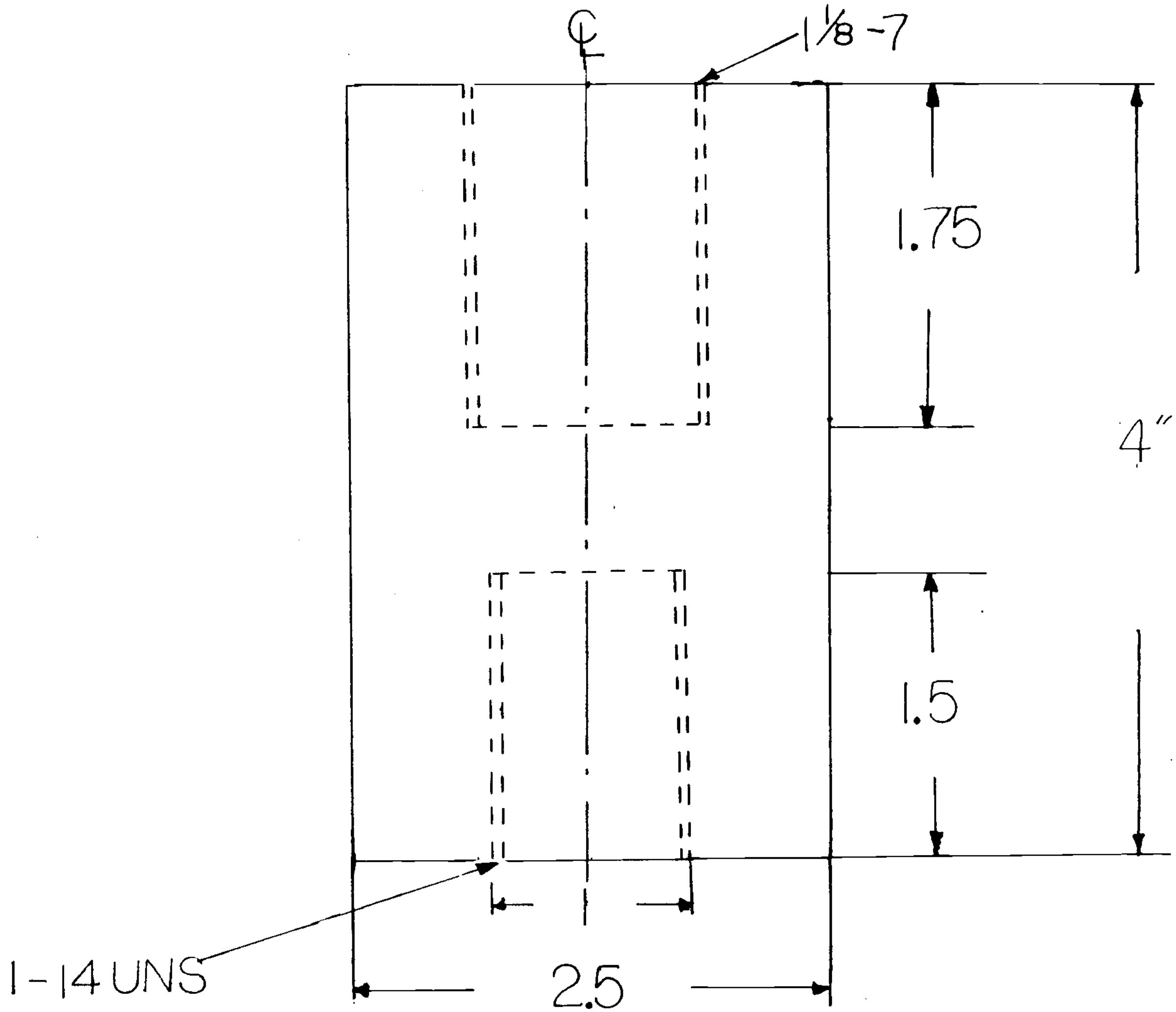

APPENDIX 14. The dimensions of special adapter for tensile test of flat-end smooth fatigue specimen (inches)

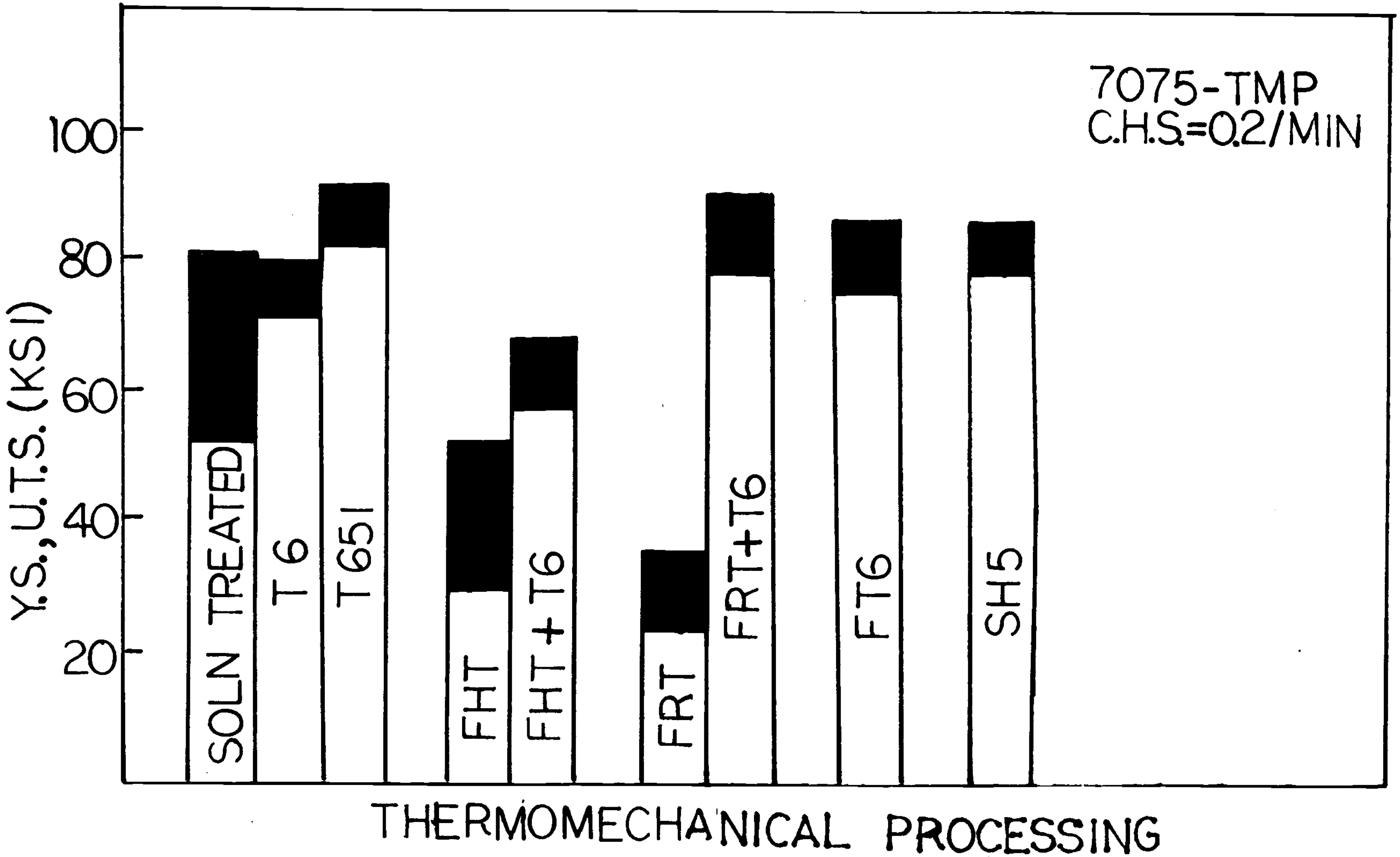

APPENDIX 15. Y.S. and U.T.S. of 7075 aluminum alloys subjected to various thermomechanical processings

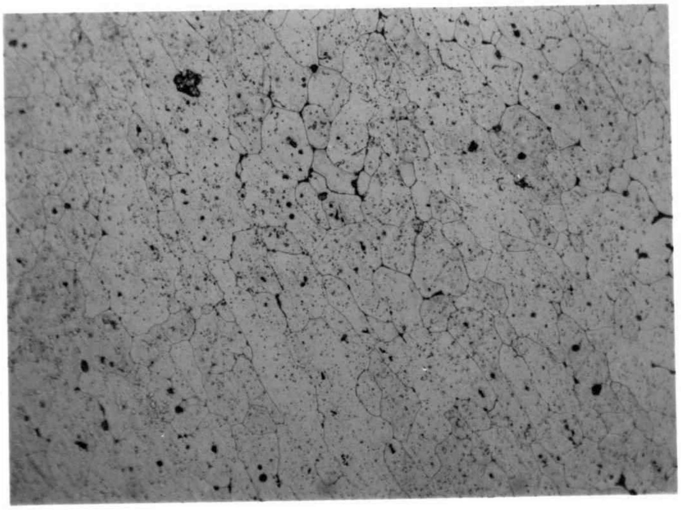

APPENDIX 16. Microstructure of 7075-PFZ#1 (100X)

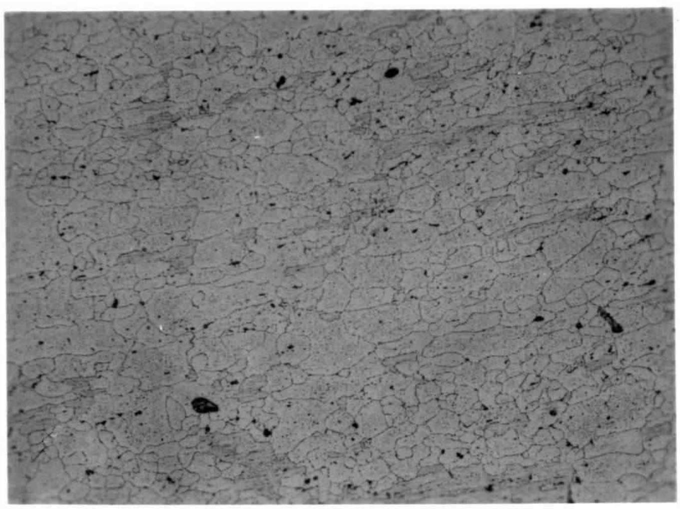

APPENDIX 17. Microstructure of 7075-PFZ#2 (100X)

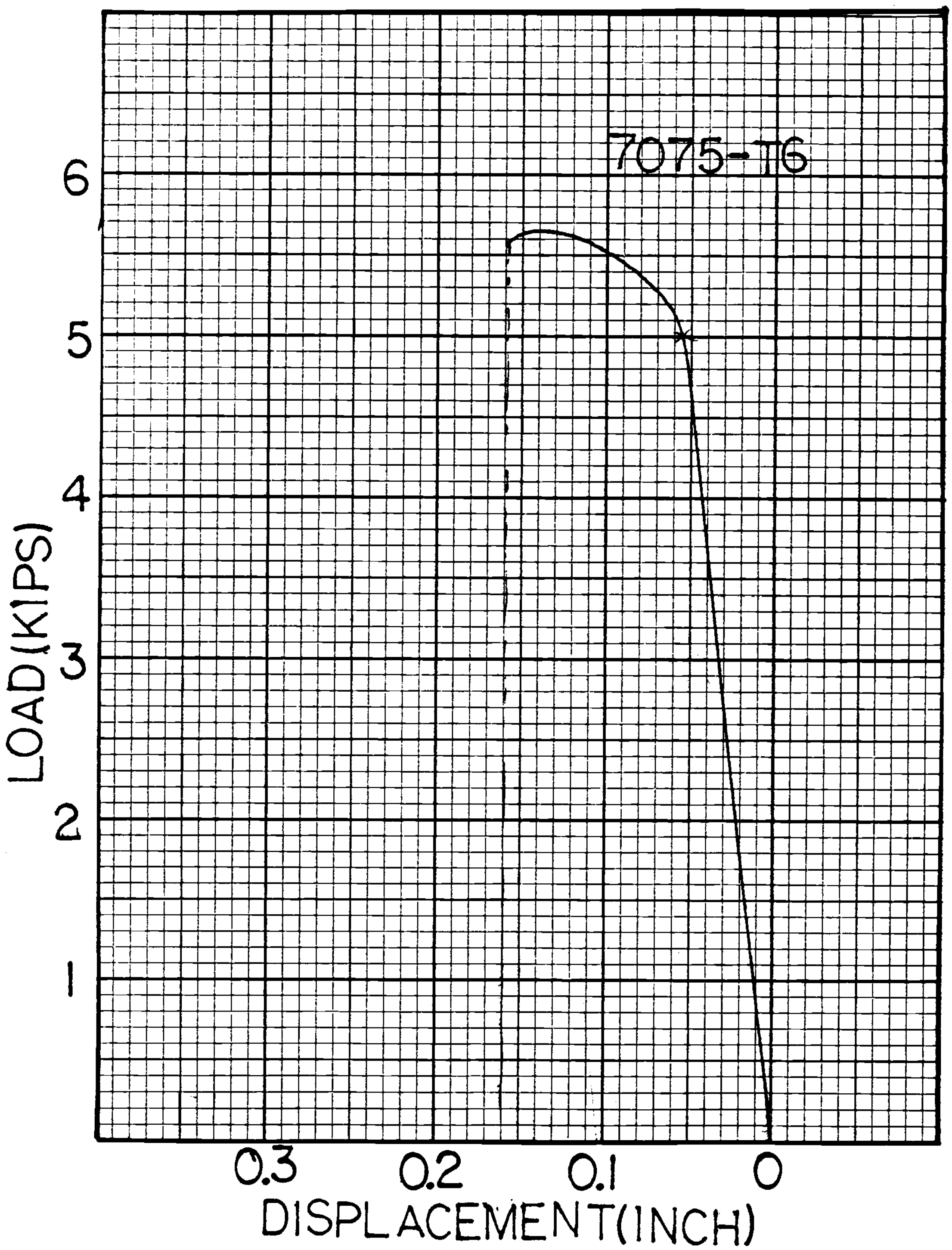

APPENDIX 18. Load versus displacement of 7075-T6 aluminum alloy

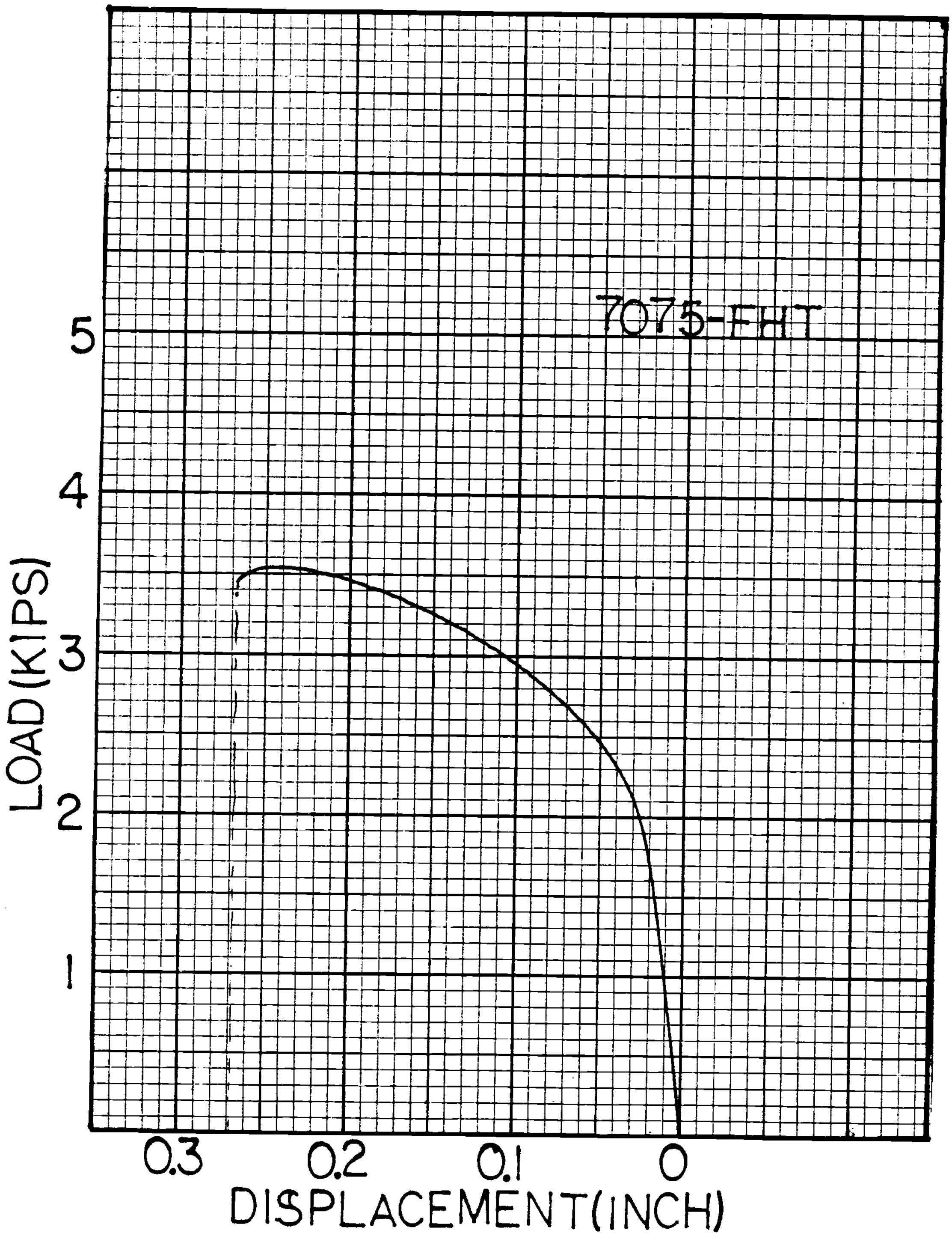

APPENDIX 19. Load versus displacement of 7075-FHT before T6 tempering

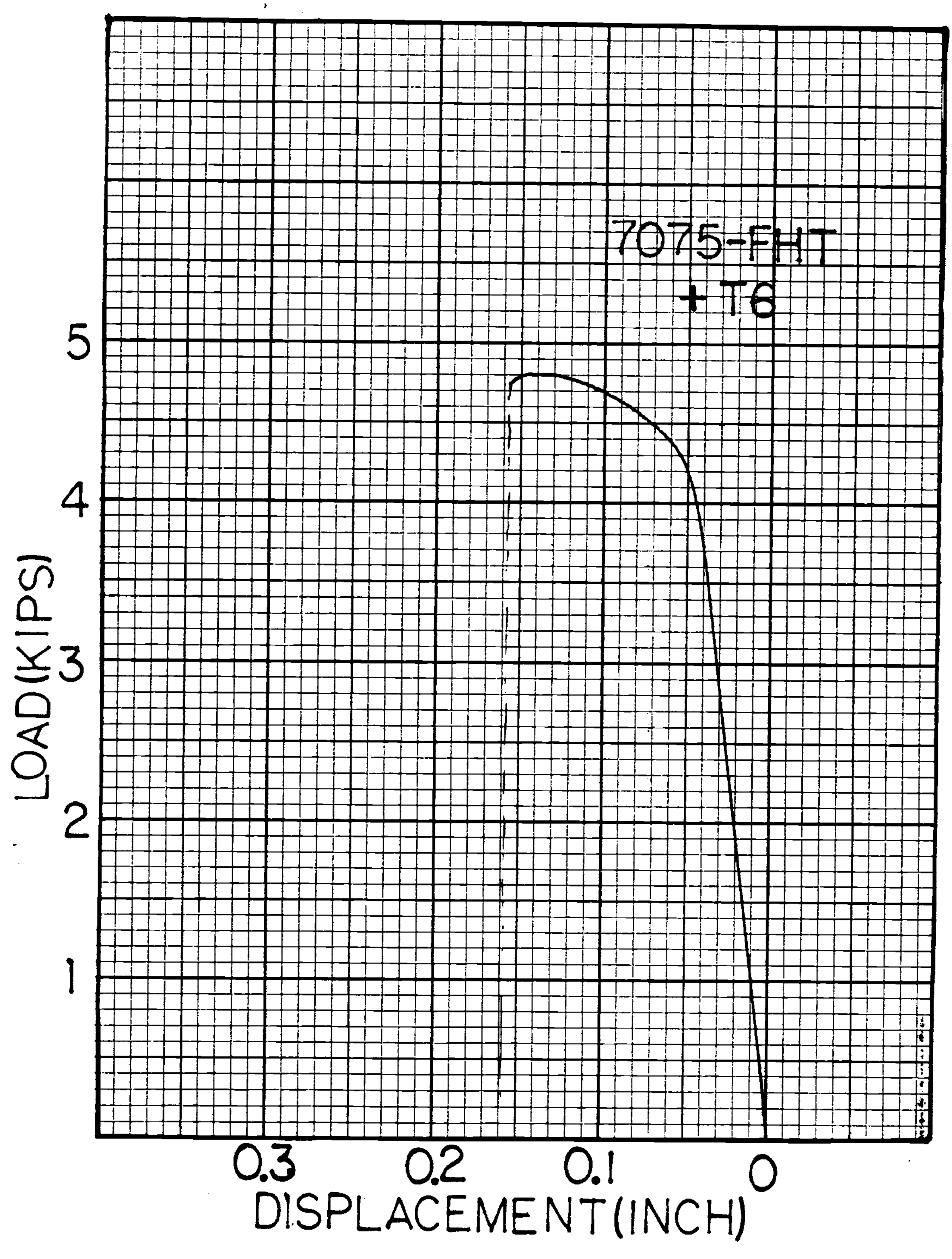

APPENDIX 20. Load versus displacement of 7075-FHT after T6 tempering

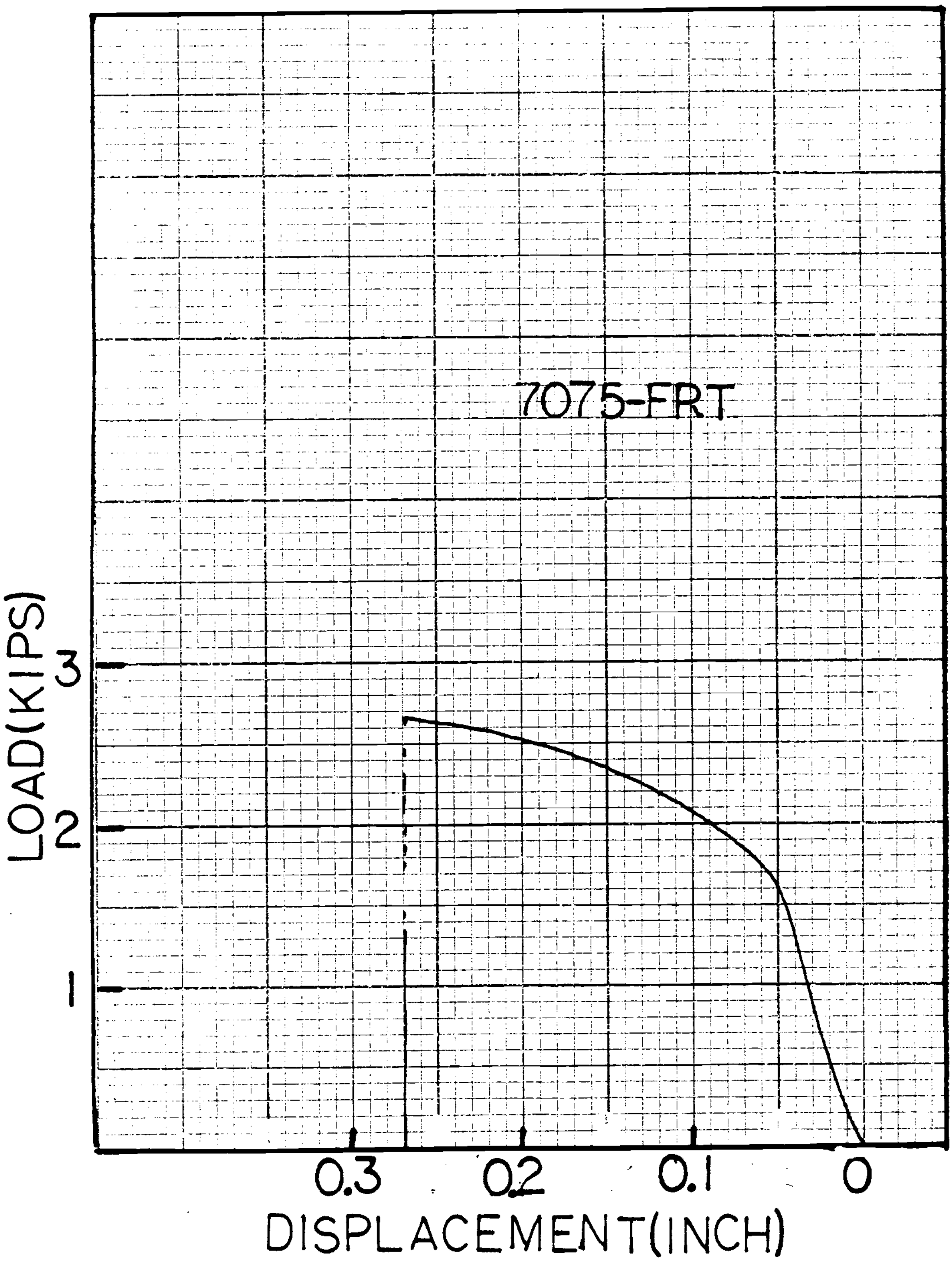

APPENDIX 21. Load versus displacement of 7075-FRT before T6 tempering

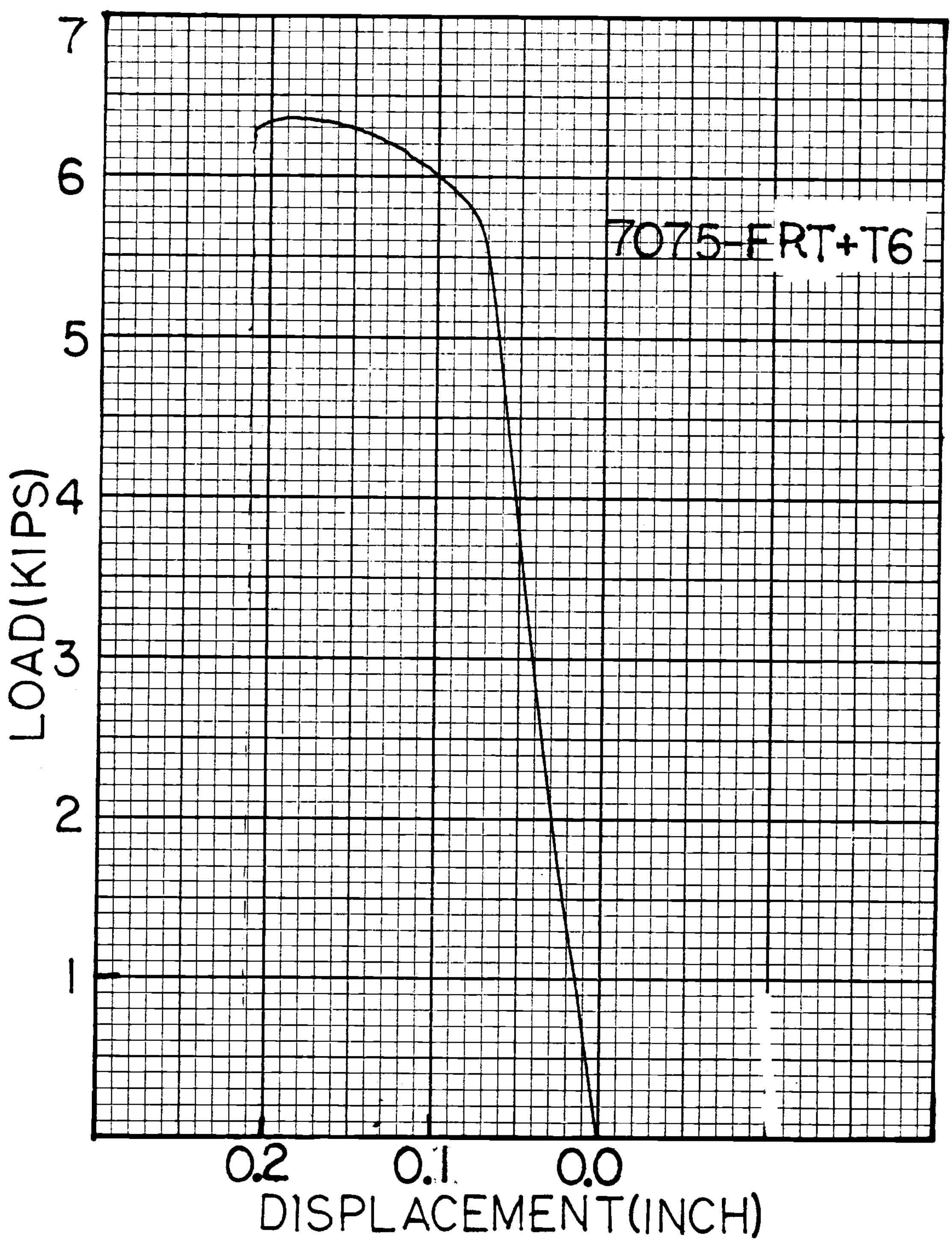

APPENDIX 22. Load versus displacement of 7075-FRT after T6 tempering

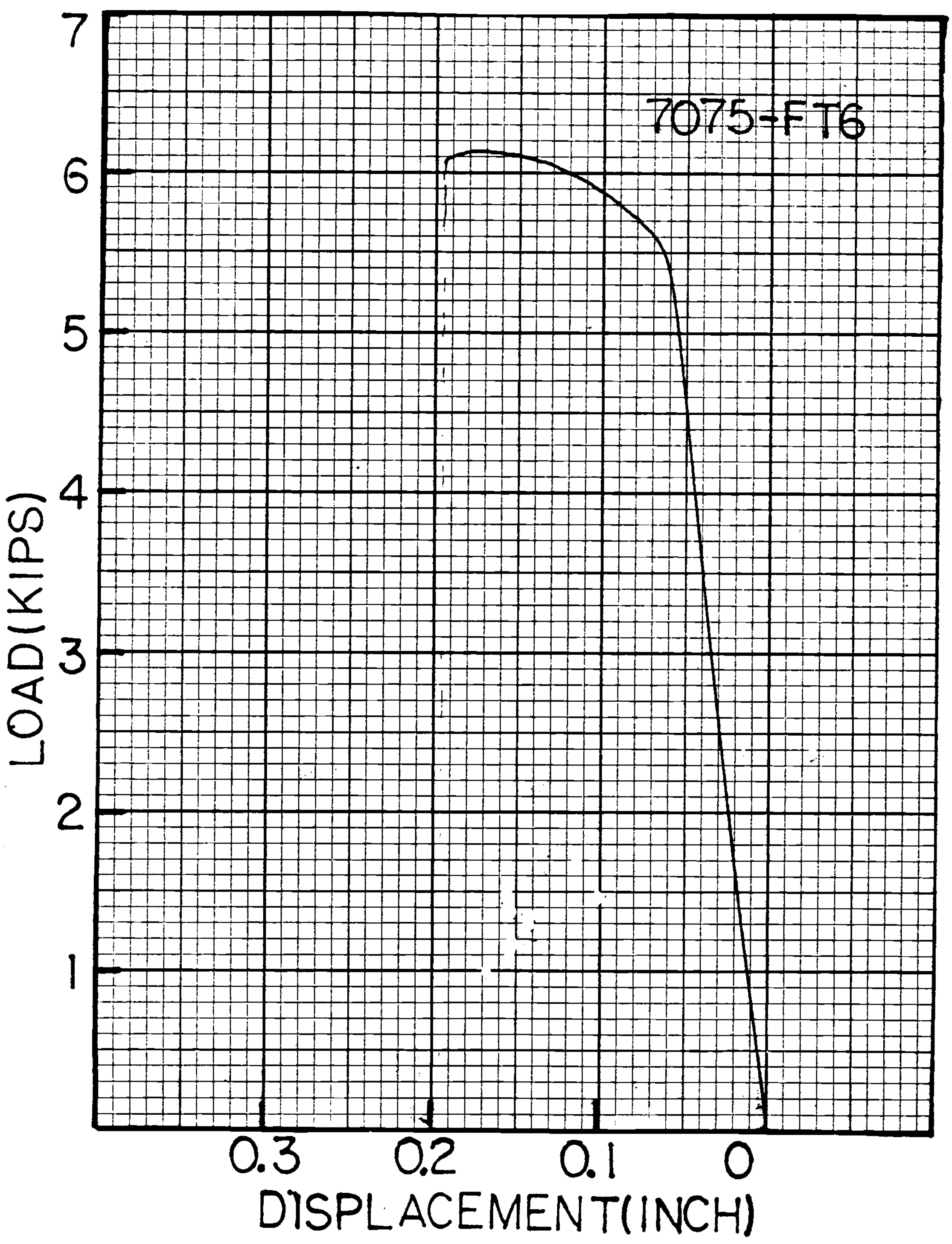

APPENDIX 23. Load versus displacement of 7075-FT6

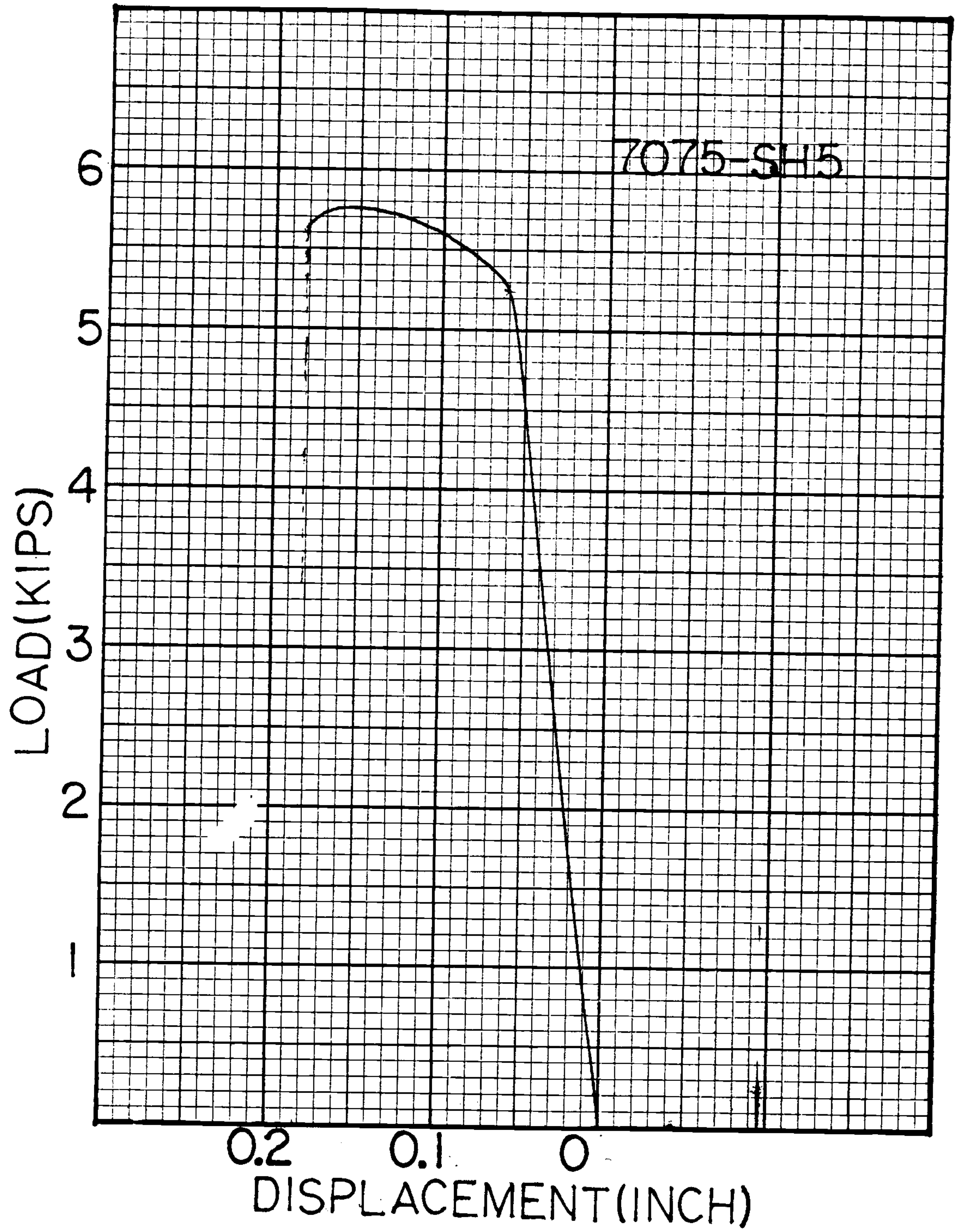

APPENDIX 24. Load versus displacement of 7075-SH5

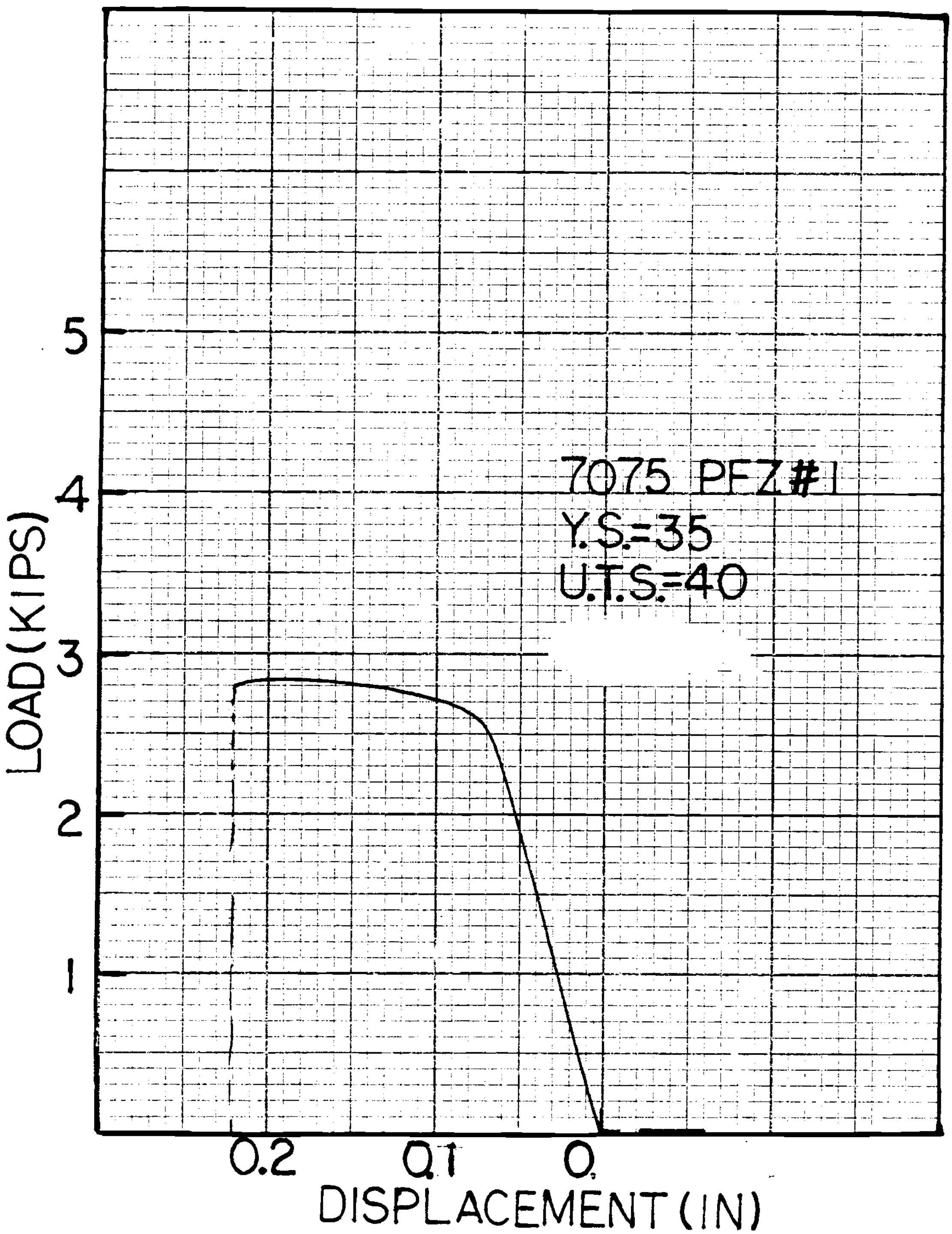

APPENDIX 25. Load versus displacement of 7075-PFZ#1

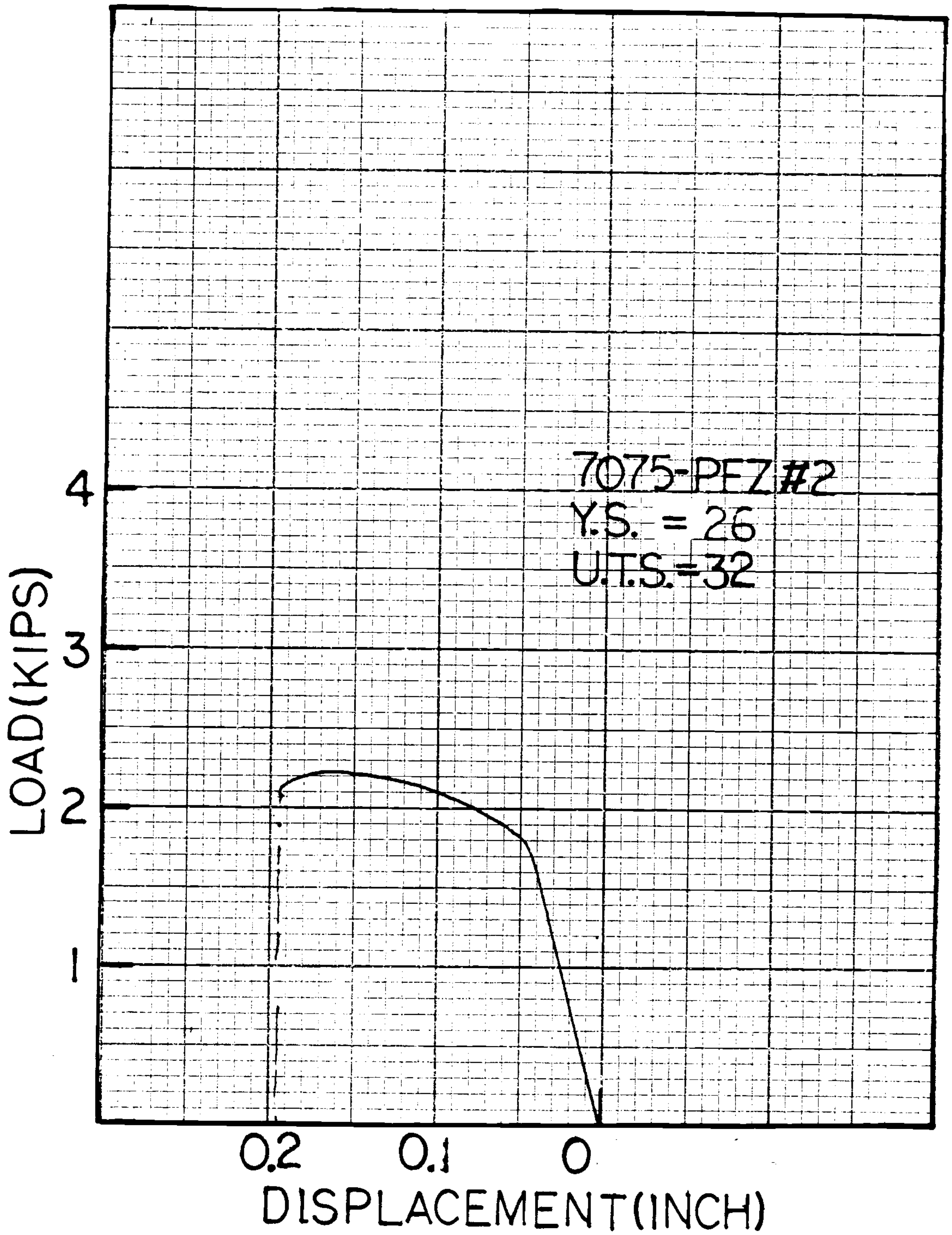

APPENDIX 26. Load versus displacement of 7075-PFZ#2

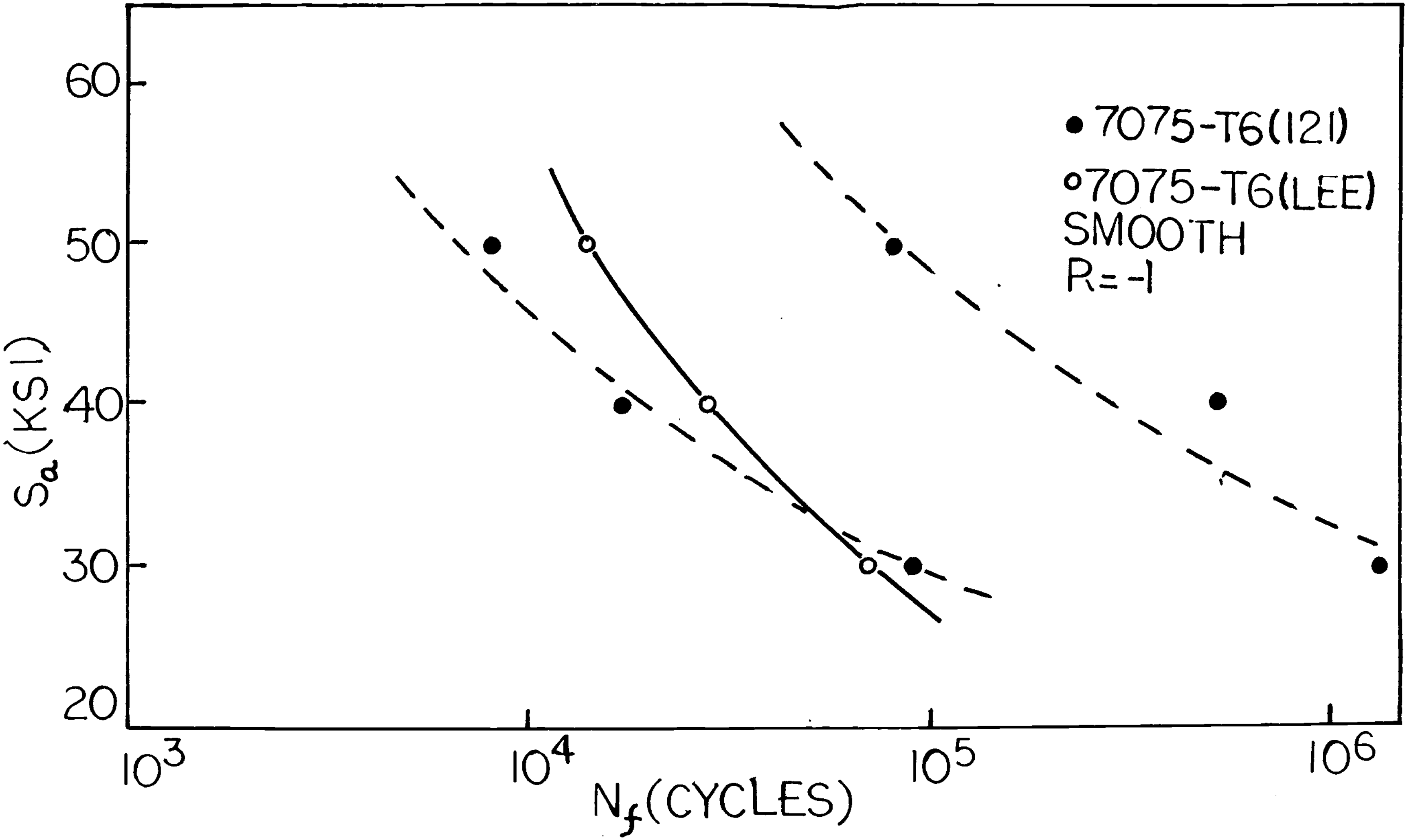

APPENDIX 27. Stress amplitude versus fatigue life of 7075-T6 of this investigation compared with literature values

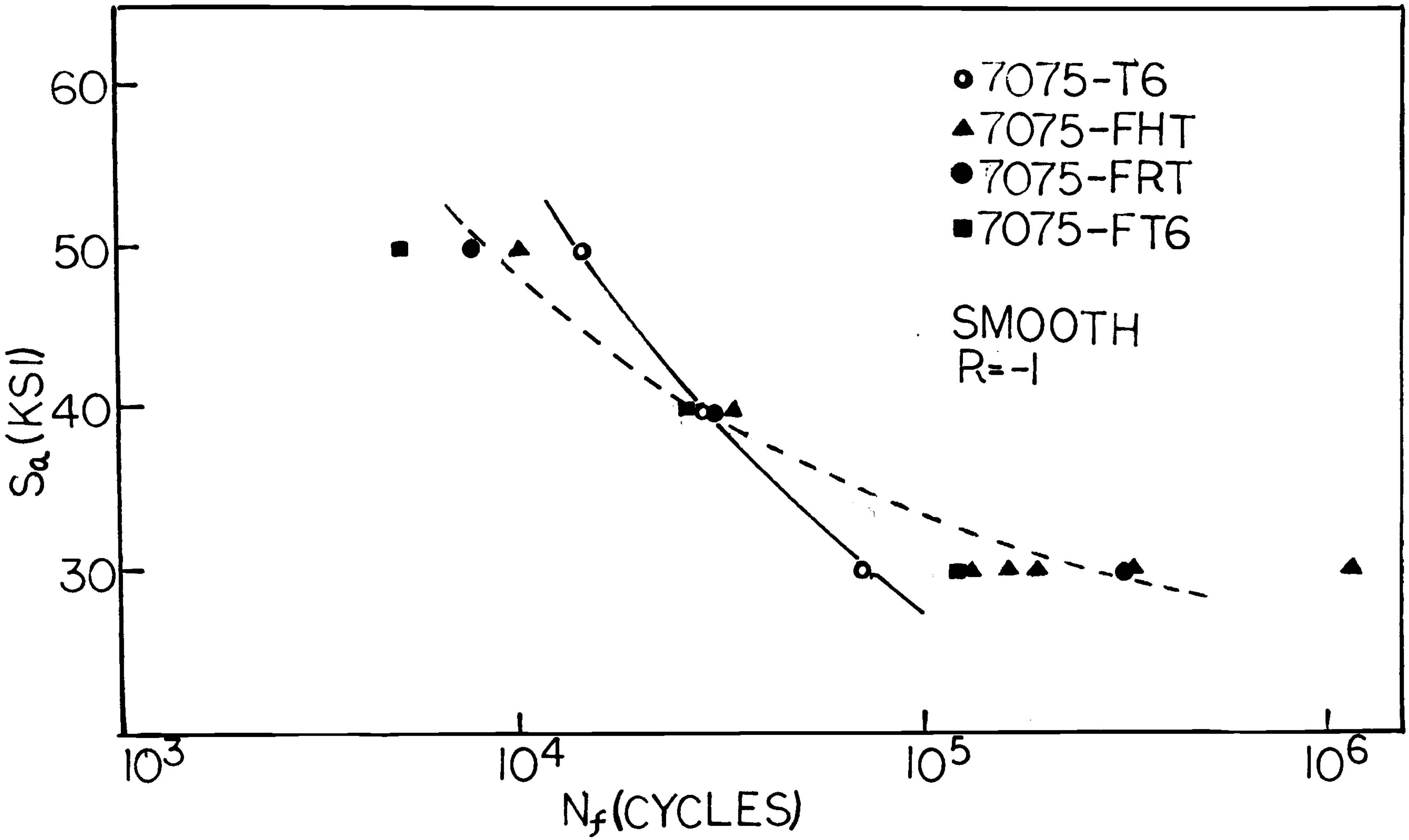

APPENDIX 28. Stress amplitude versus fatigue life of 7075 aluminum alloy cyclically loaded compared with S-N curve of 7075-T6

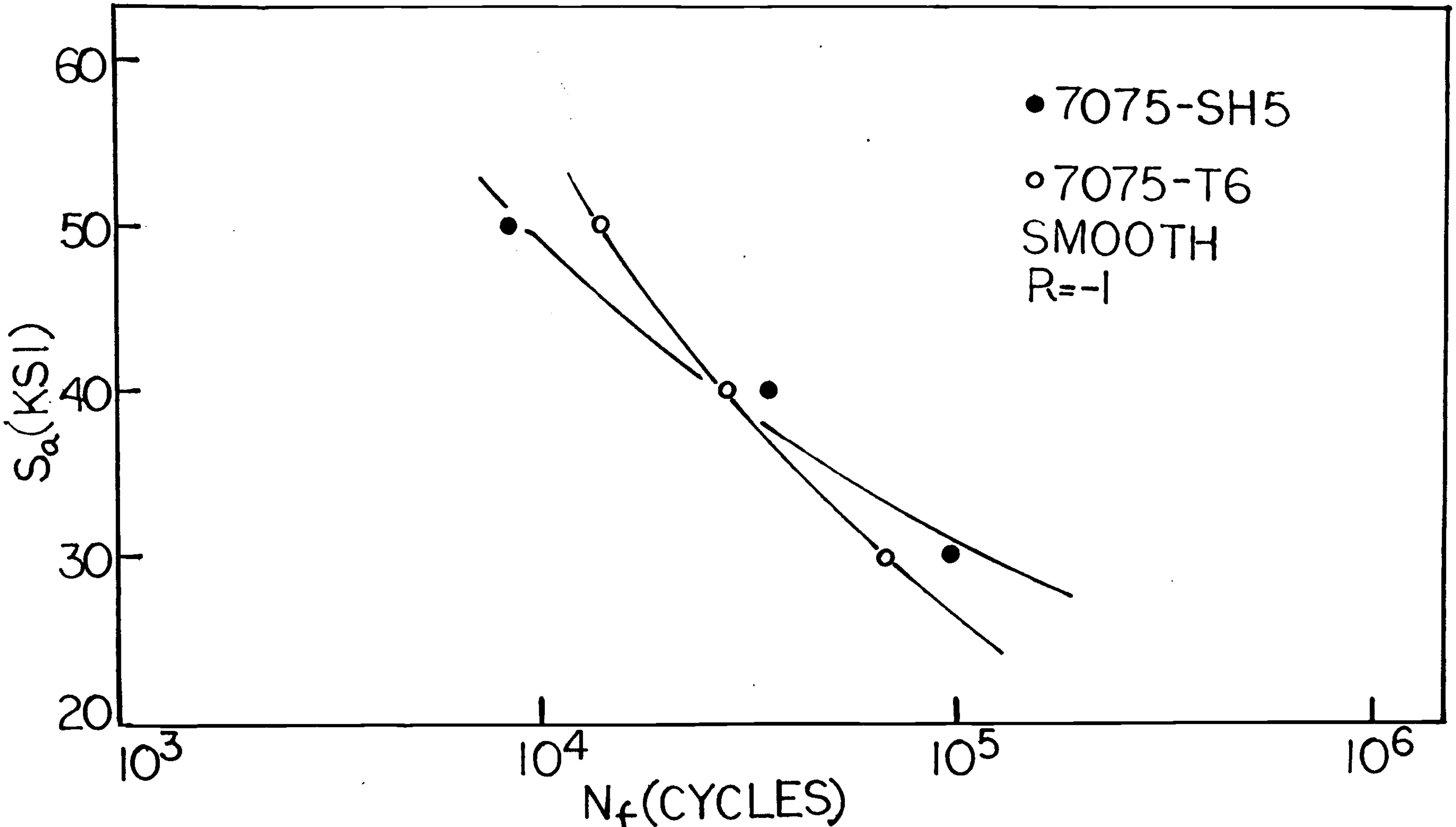

APPENDIX 29. Stress amplititude versus fatigue life of 7075 aluminum alloy stretched 5% plastically at 150°C compared with S-N curve of 7075-T6

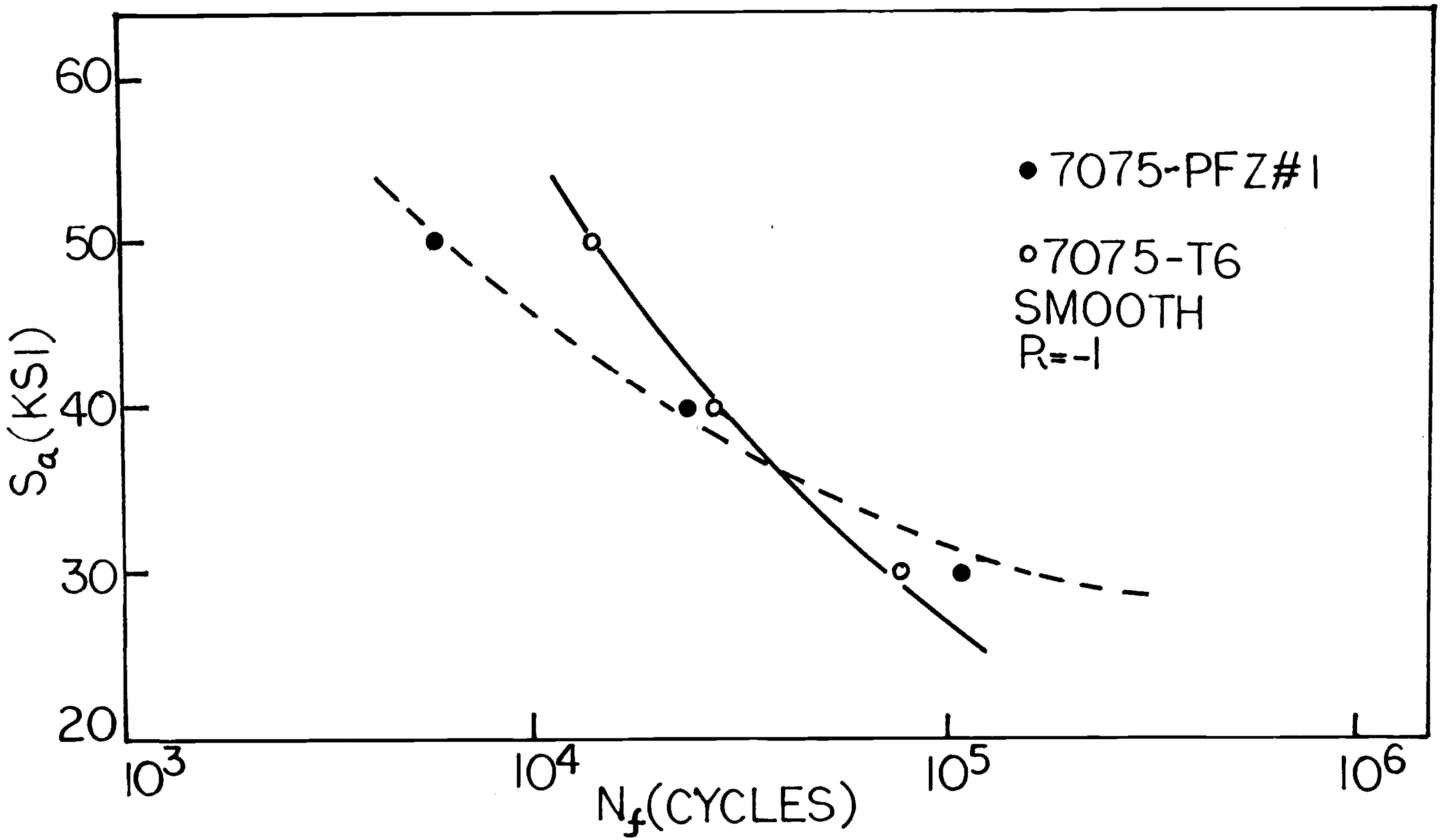

APPENDIX 30. Stress amplitude versus fatigue life of 7075-PFZ#1 aluminum alloy with PFZ of 800Å compared with S-N curve of 7075-T6

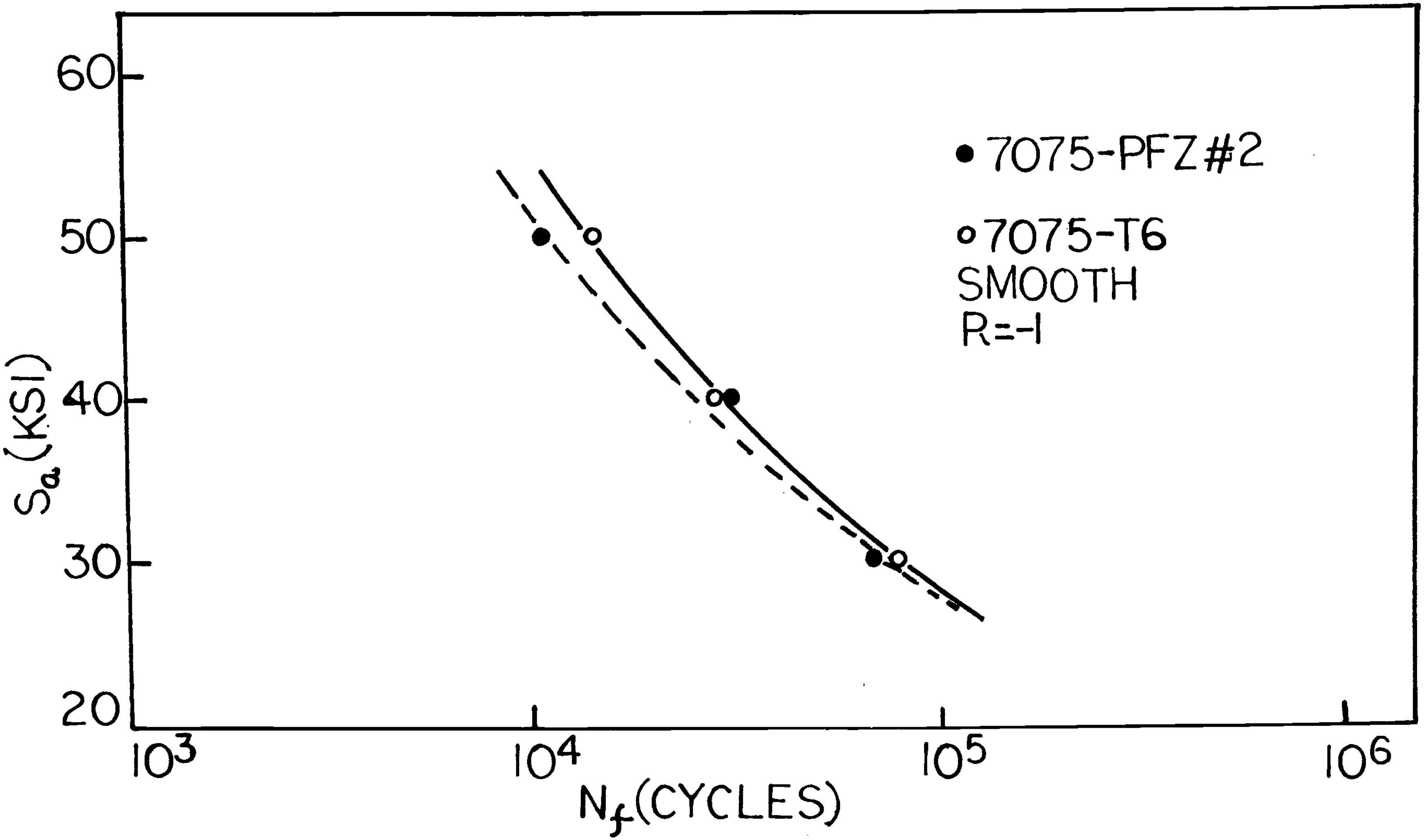

APPENDIX 31. Stress amplitude versus fatigue life of 7075-PFZ#2 with PFZ of 2000Å compared with S-N curve of 7075-T6

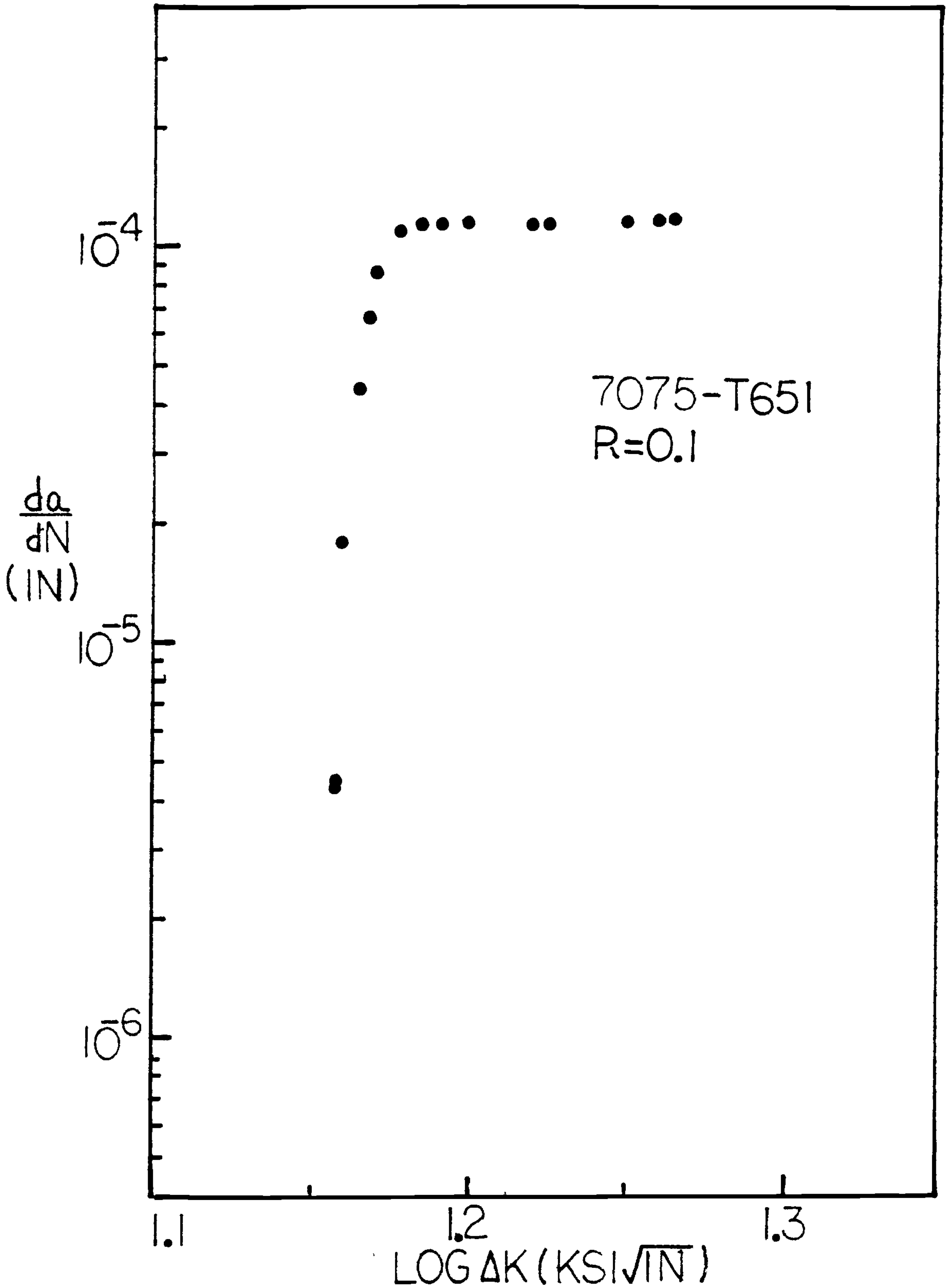

APPENDIX 32. Fatigue crack propagation rate versus stress intensity factor range of 7075-T651 aluminum alloy

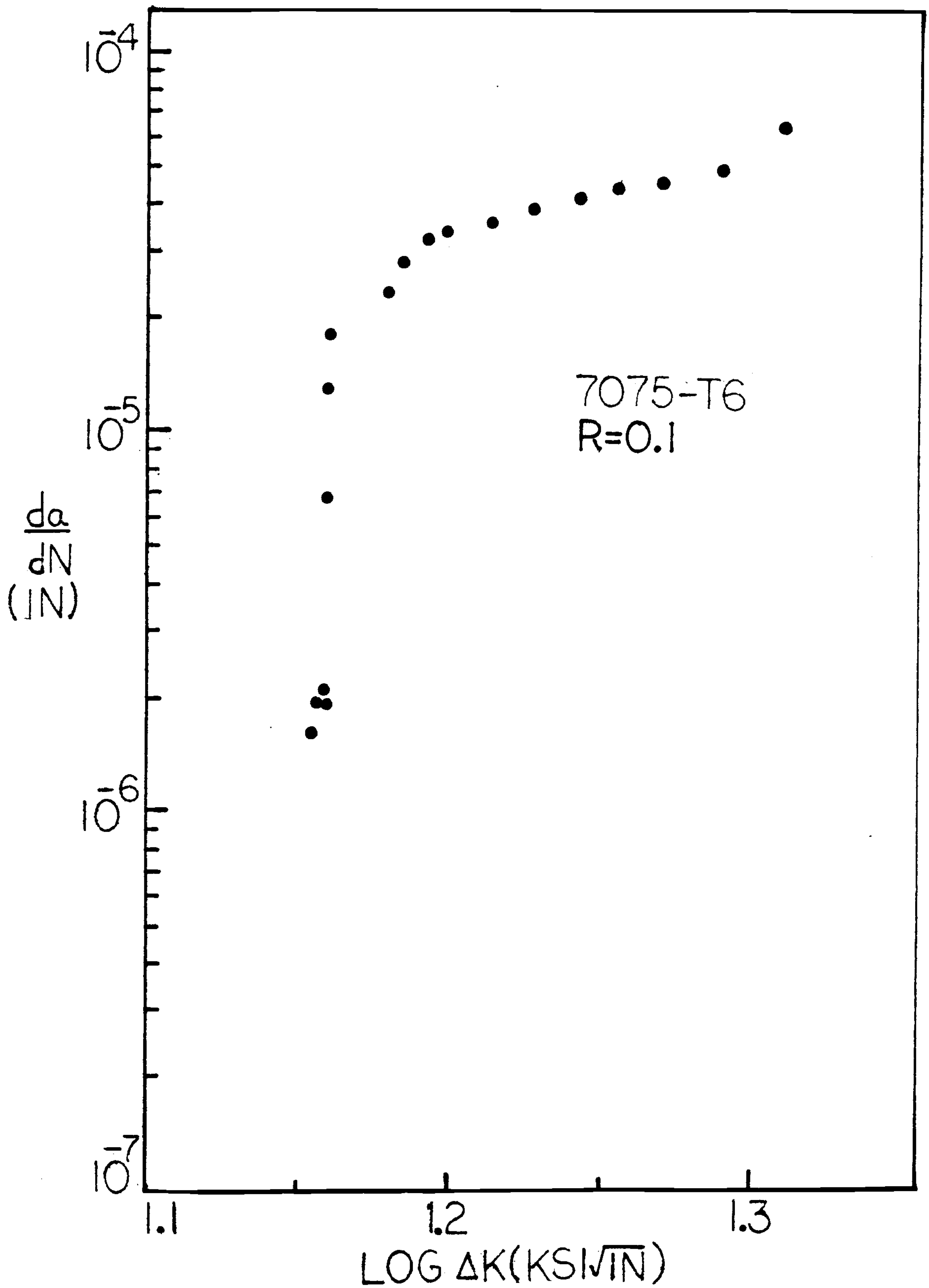

APPENDIX 33. Fatigue crack propagation rate versus stress intensity factor range of 7075-T6 aluminum alloy

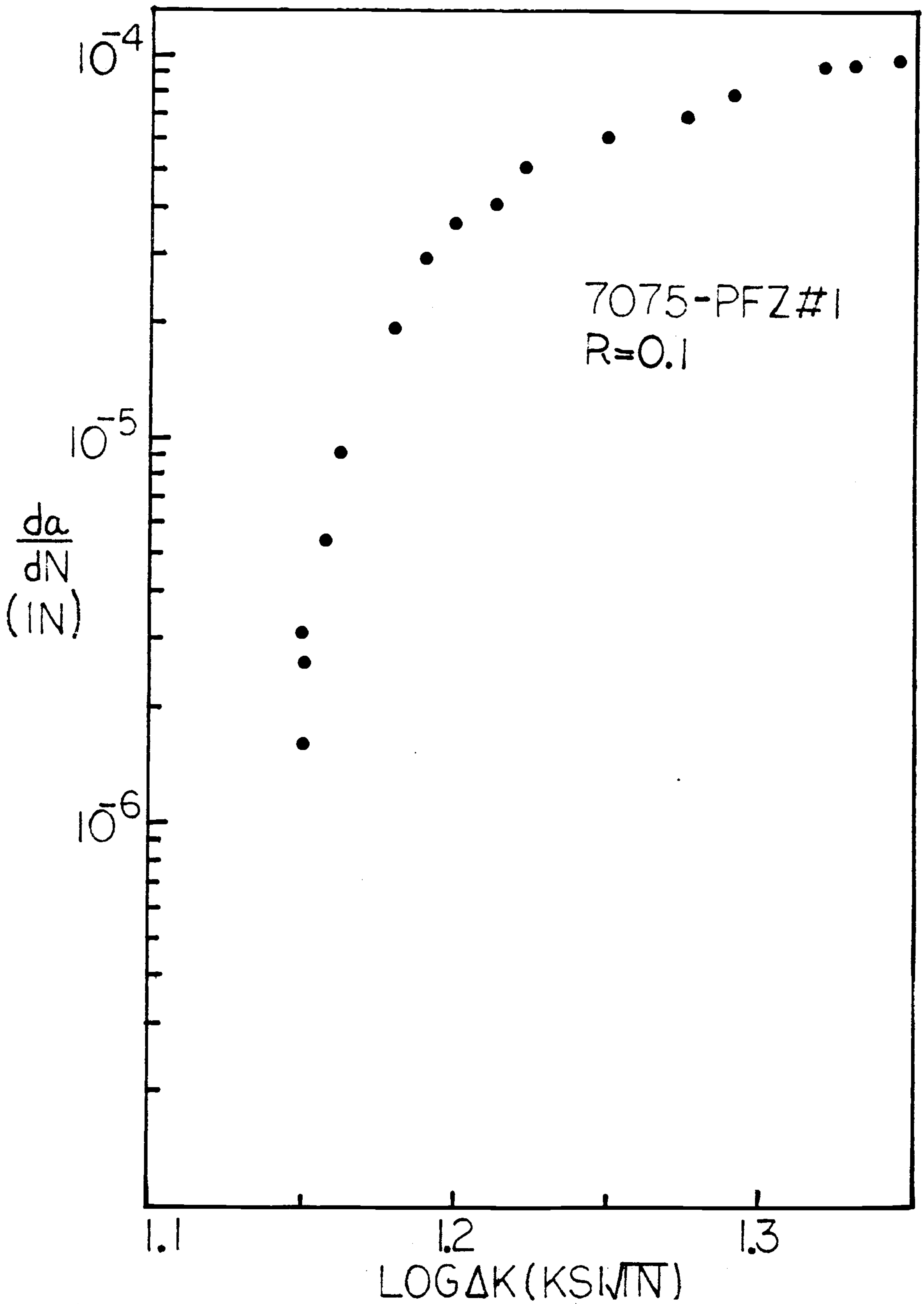

APPENDIX 34. Fatigue crack propagation rate versus stress intensity factor range of 7075-PFZ#1 aluminum alloy

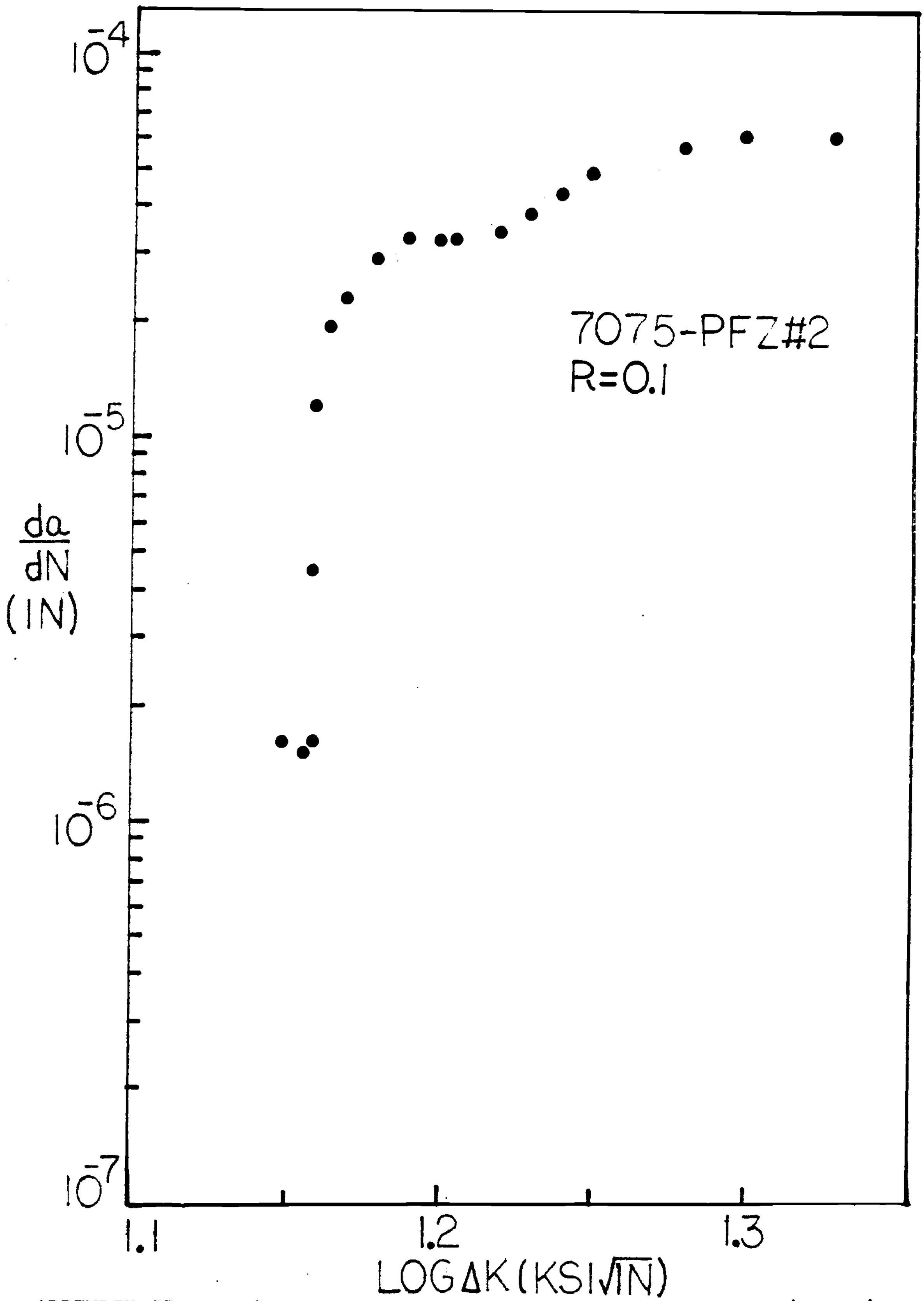

APPENDIX 35. Fatigue crack propagation rate versus stress intensity factor range of 7075-PFZ#2 aluminum alloy

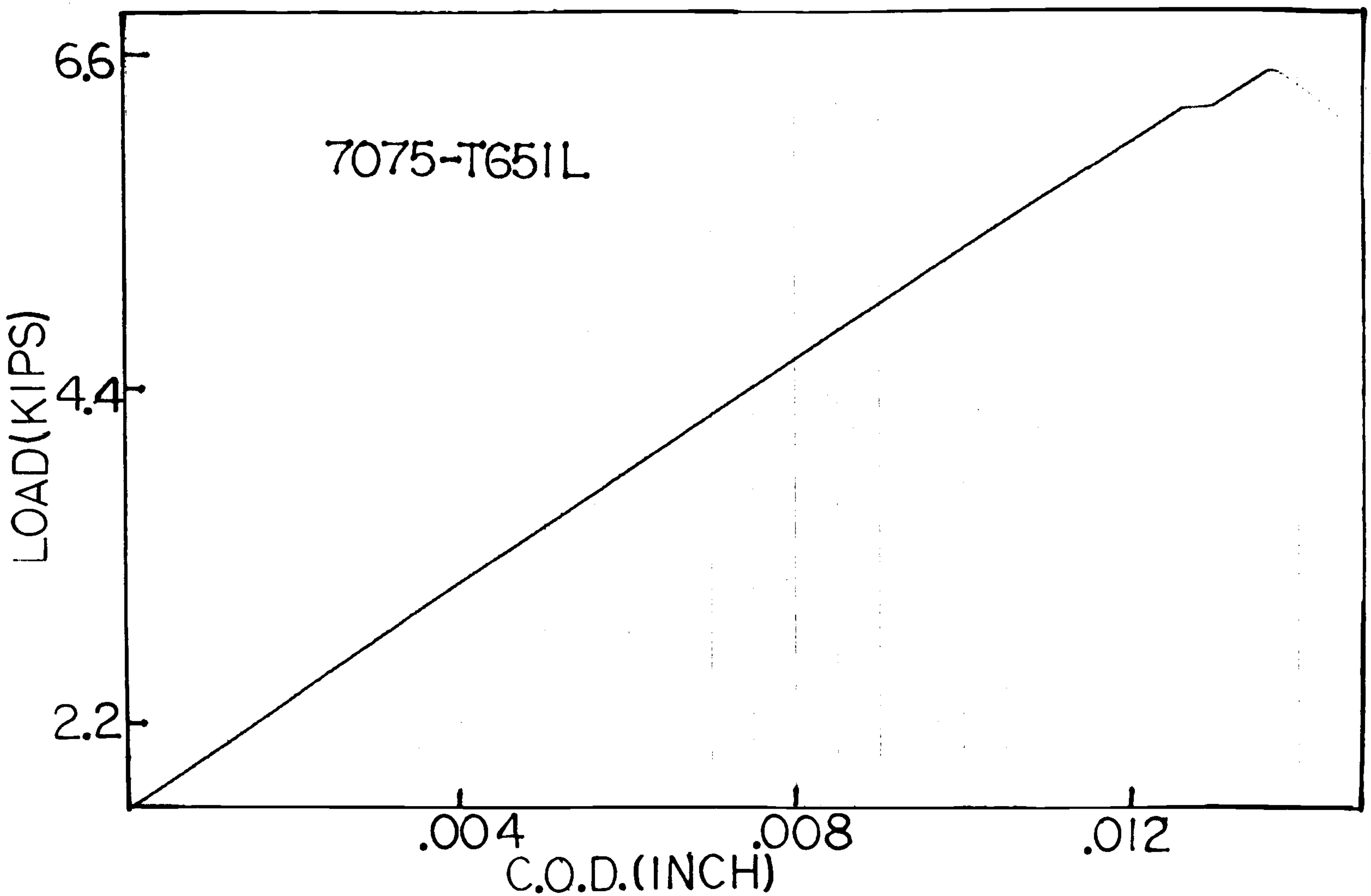

APPENDIX 36. Load versus crack opening distance of 7075-T651L for fracture toughness

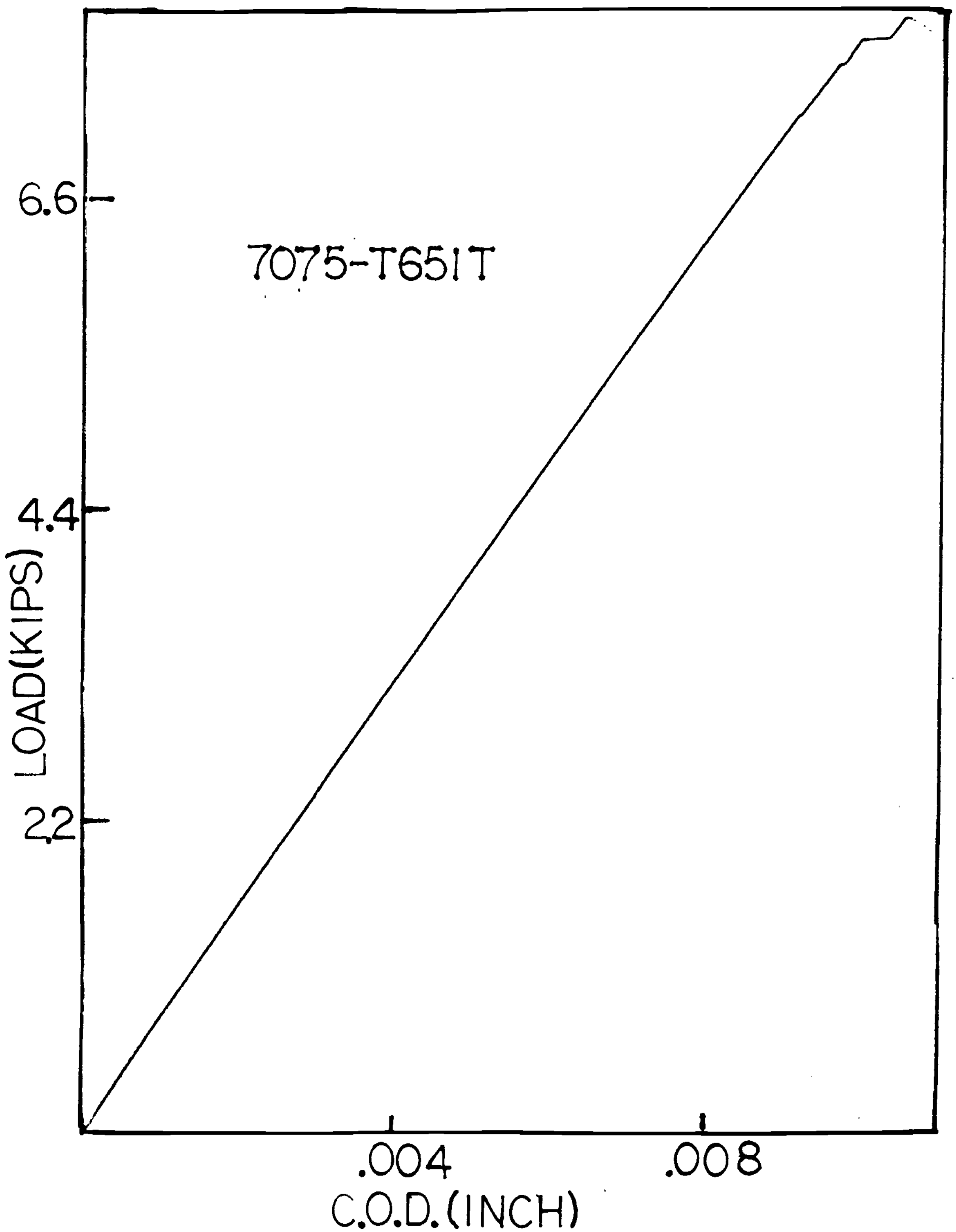

APPENDIX 37. Load versus crack opening distance of 7075-T651T for fracture toughness

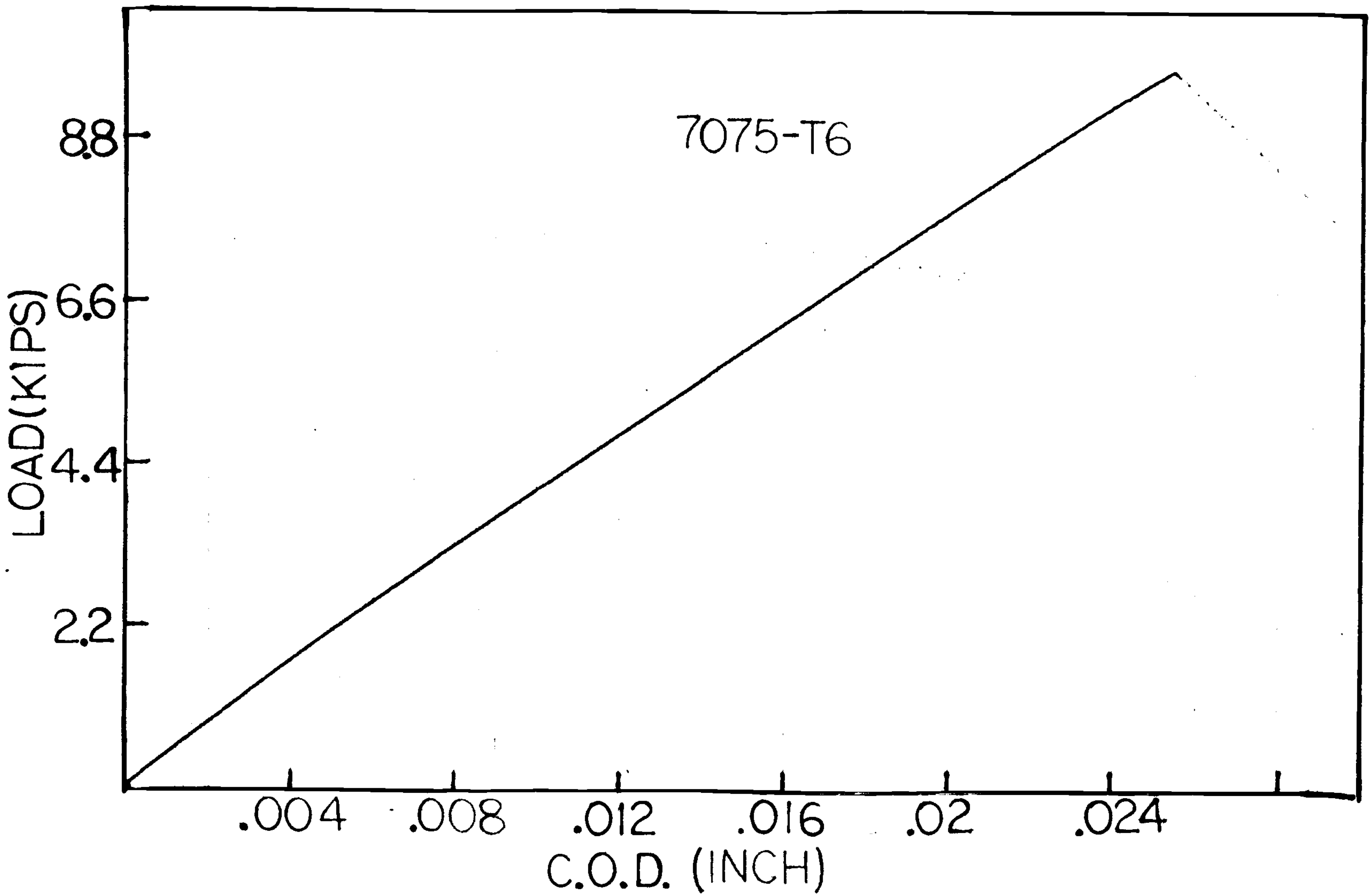

APPENDIX 38. Load versus crack opening distance of 7075-T6 for fracture toughness

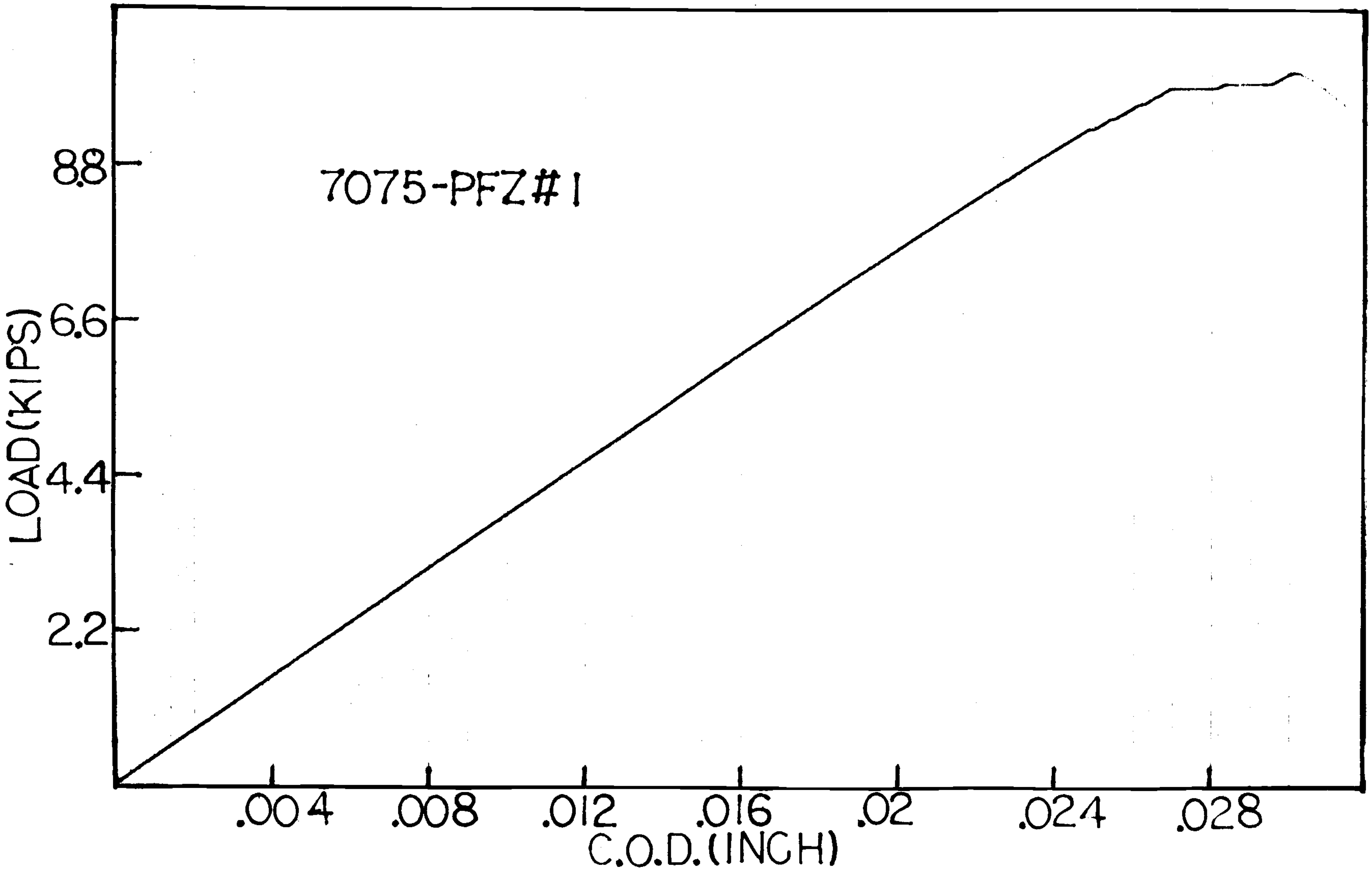

APPENDIX 39. Load versus crack opening distance of 7075-PFZ#1 for fracture toughness

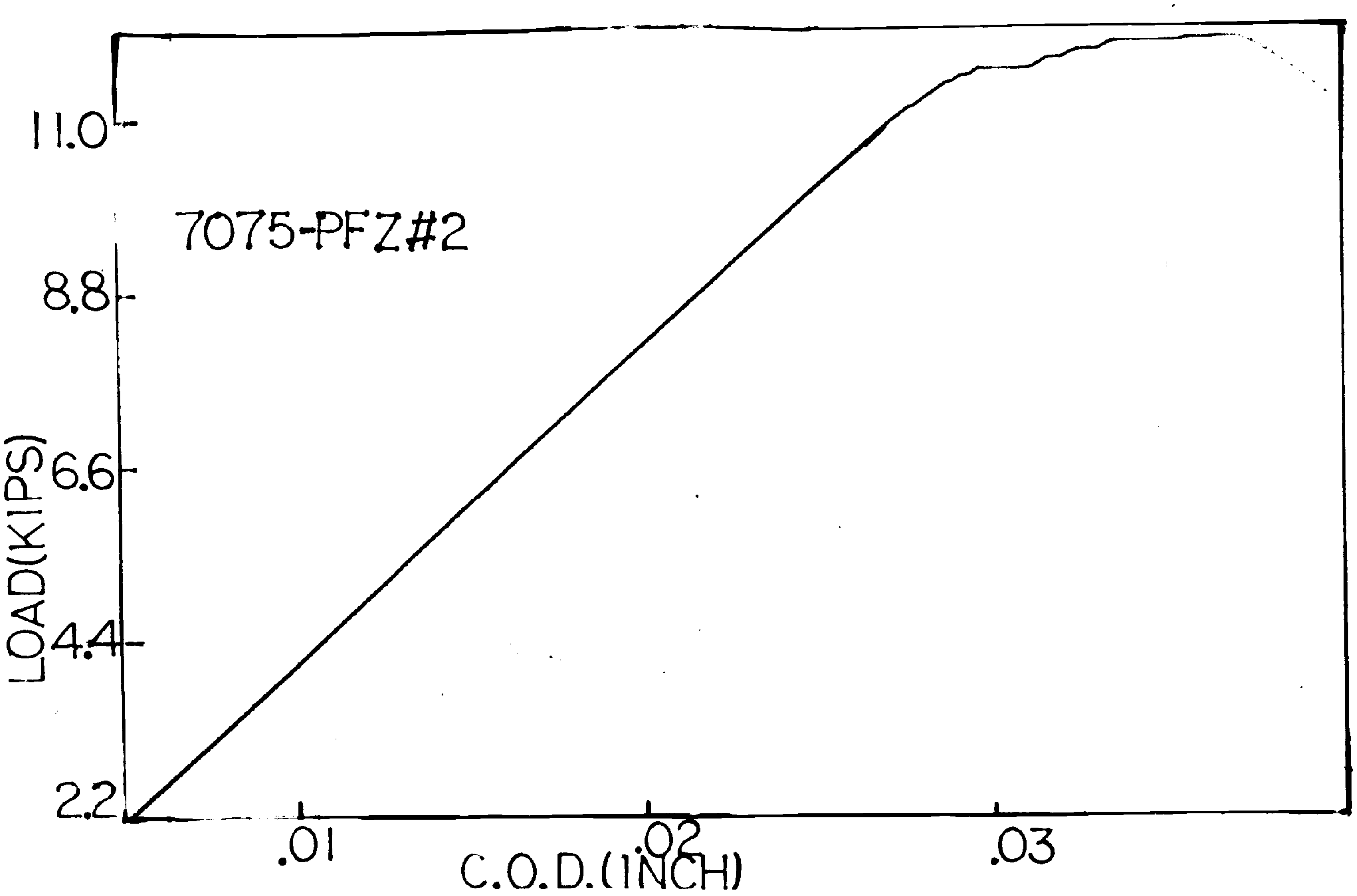

APPENDIX 40. Load versus crack opening distance of 7075-PFZ#2 for fracture toughness

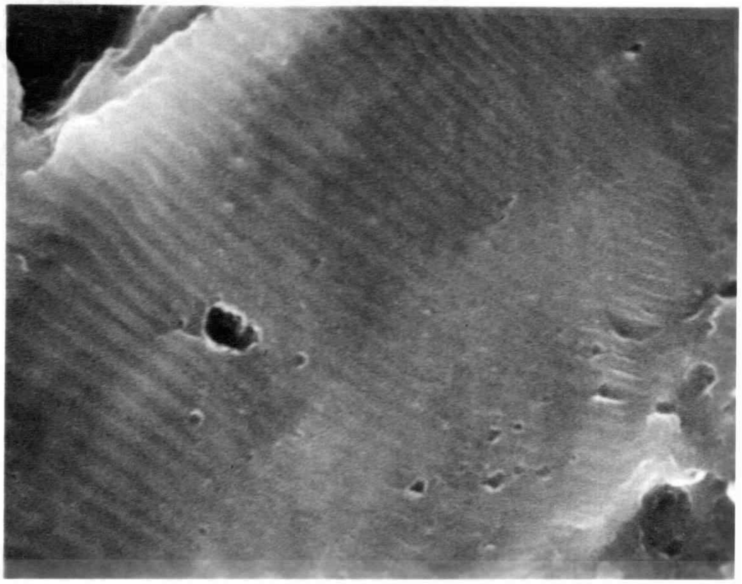

APPENDIX 41. Fatigue striation of 7075-T6 at $\Delta K=17$ Ksi$\sqrt{in}$, 6000X

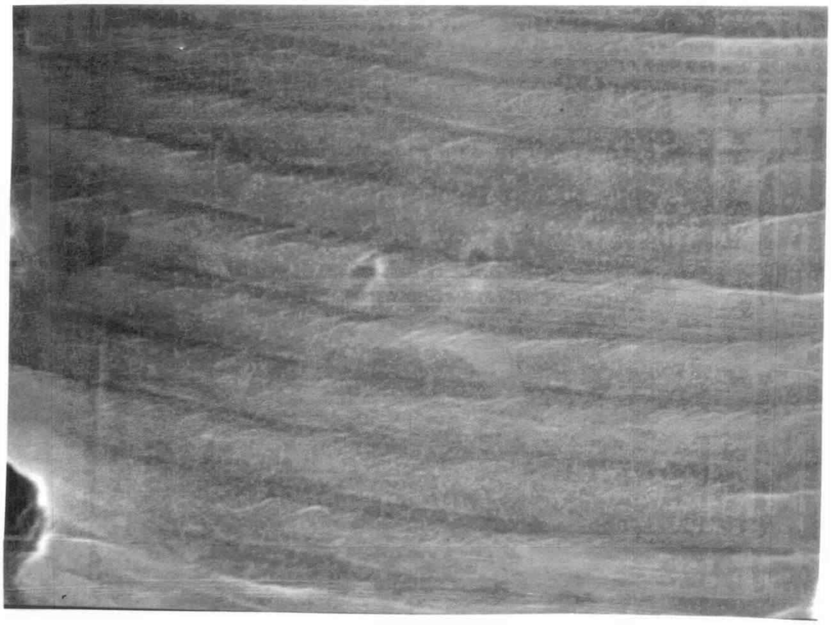

APPENDIX 42. Fatigue striation of 7075-T651 at $\Delta K=17$ Ksi$\sqrt{in}$, 6000X

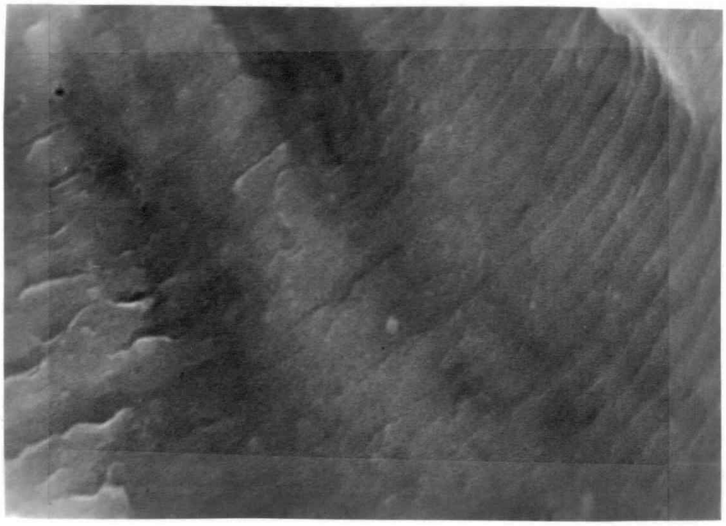

APPENDIX 43. Fatigue striation of 7075-PFZ#1 at ΔK=17 Ksi$\sqrt{in}$, 6000X

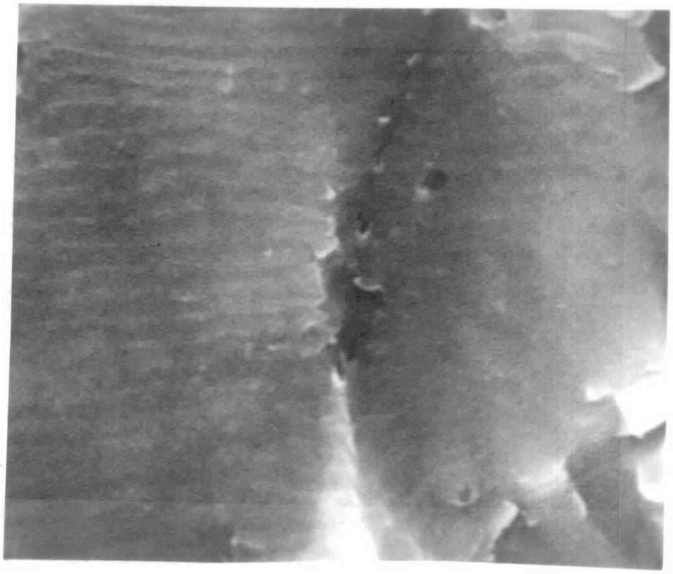

APPENDIX 44. Fatigue striation of 7075-PFZ#2 at ΔK=17 Ksi$\sqrt{in}$, 6000X

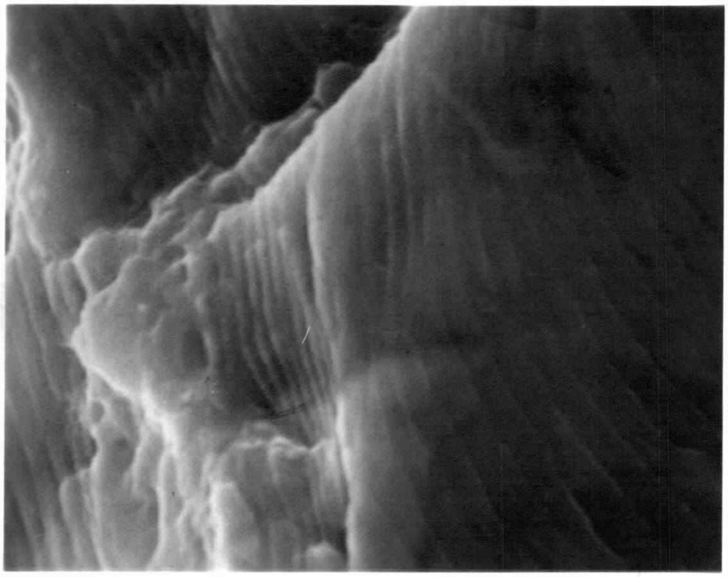

APPENDIX 45. SEM of 7075-T6 showing various striation spacings in different orientation of grains (6000X)

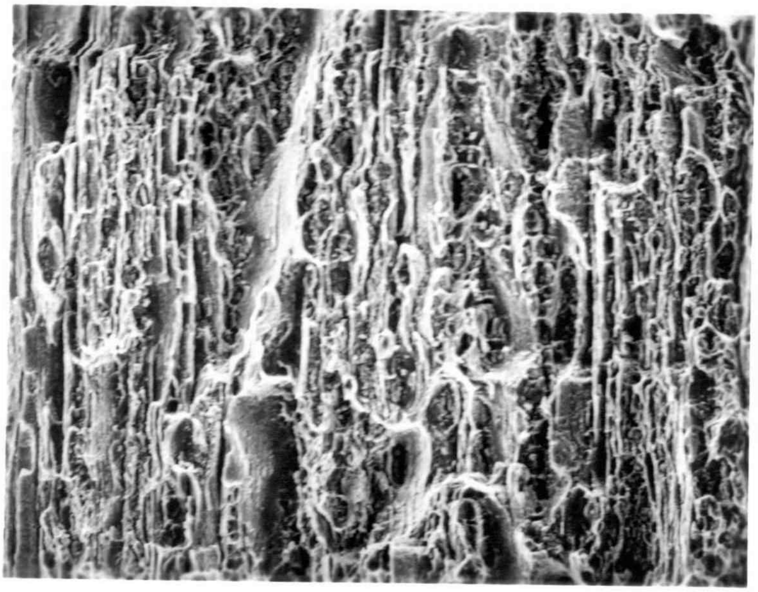

APPENDIX 46. SEM fractograph of 7075-T6 (500X)

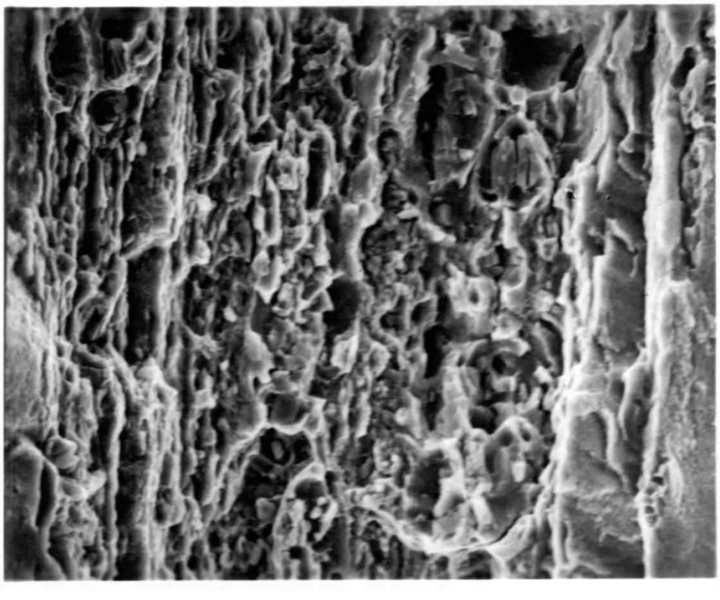

APPENDIX 47. SEM fractograph of 7075-T651 (500X)

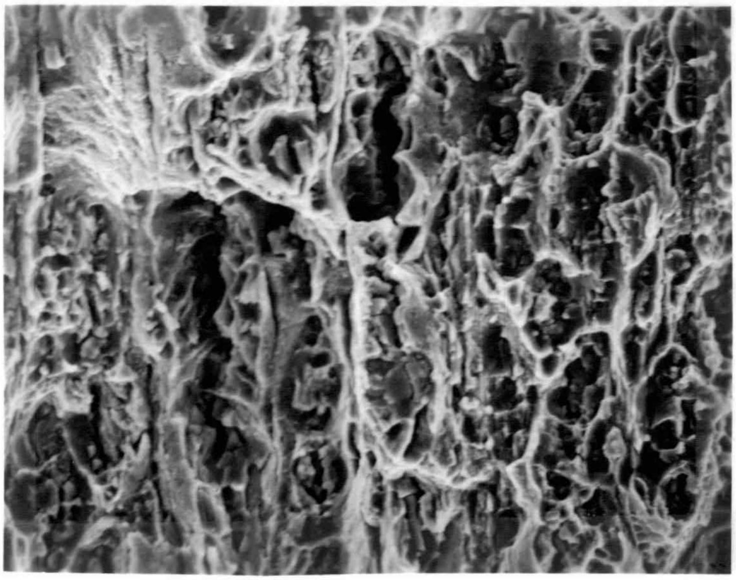

APPENDIX 48. SEM fractograph of 7075-PFZ#1 (500X)

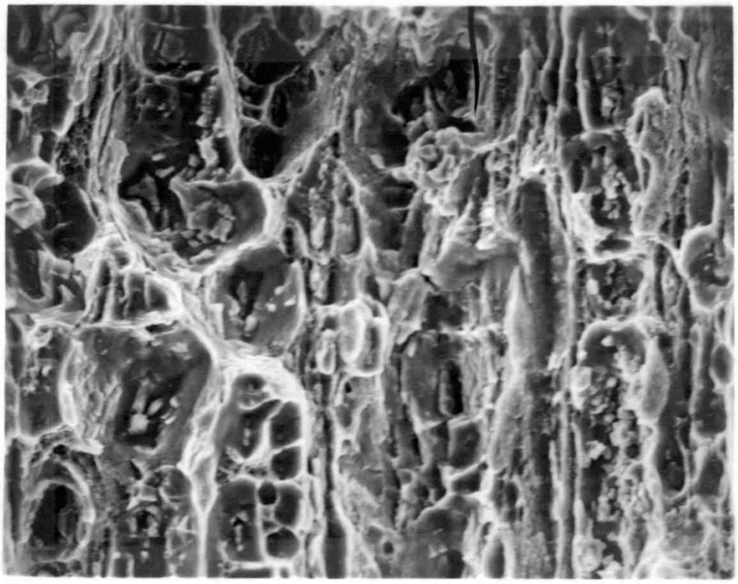

APPENDIX 49. SEM fractograph of 7075-PFZ#2 (500X)

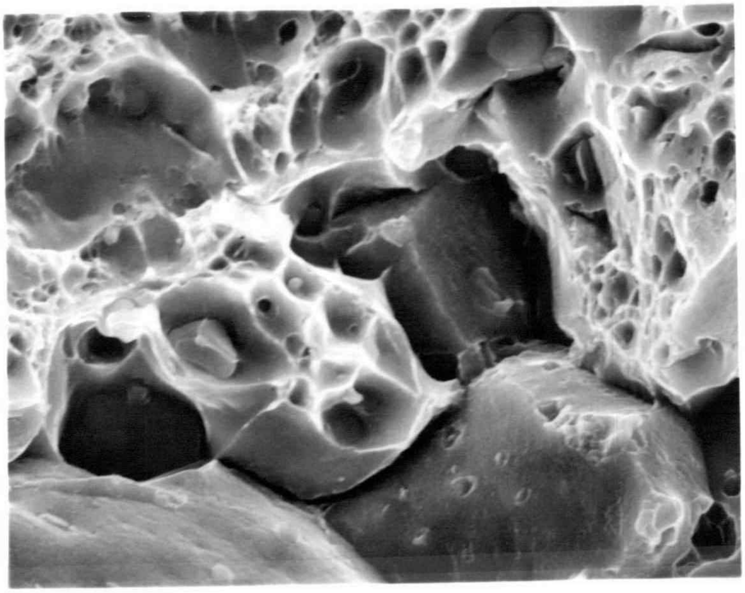

APPENDIX 50. Scanning electron micrograph of PFZ#1 subjected to tensile test showing intergranular fracture mode, 2000X

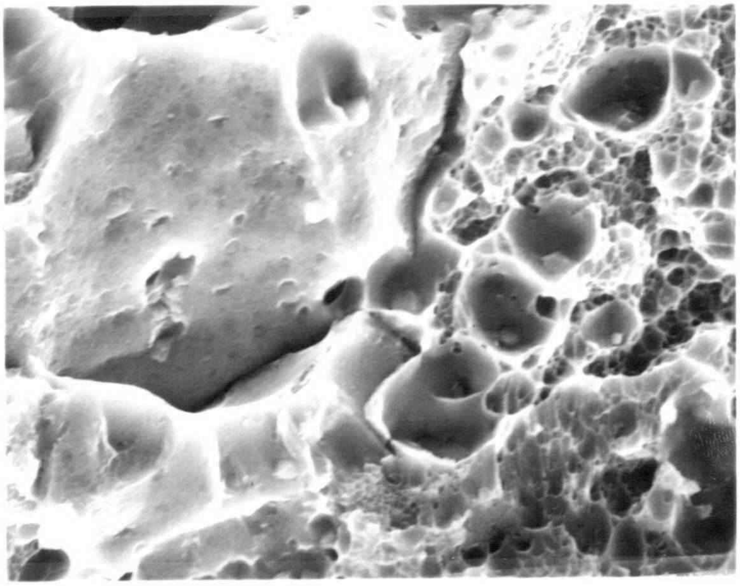

APPENDIX 51. Scanning electron micrograph of PFZ#2 subjected to tensile test showing ductile dimple mode of fracture, 2000X

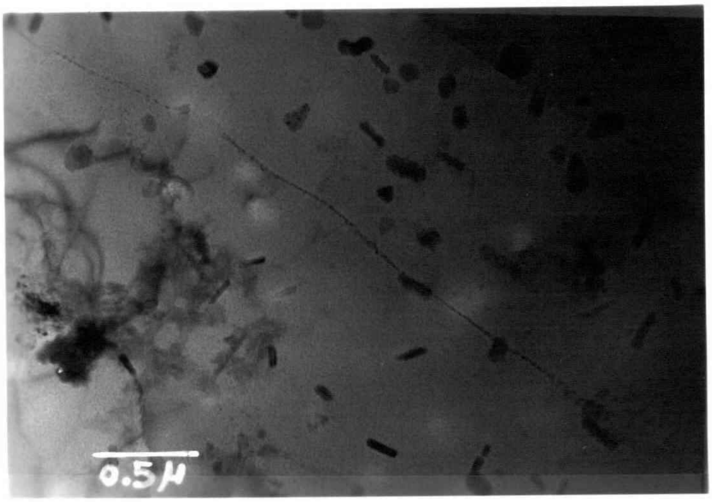

APPENDIX 52. Transmission electron micrograph of cyclically preloaded alloy at high temperature showing dislocations passing through the coherent precipitates

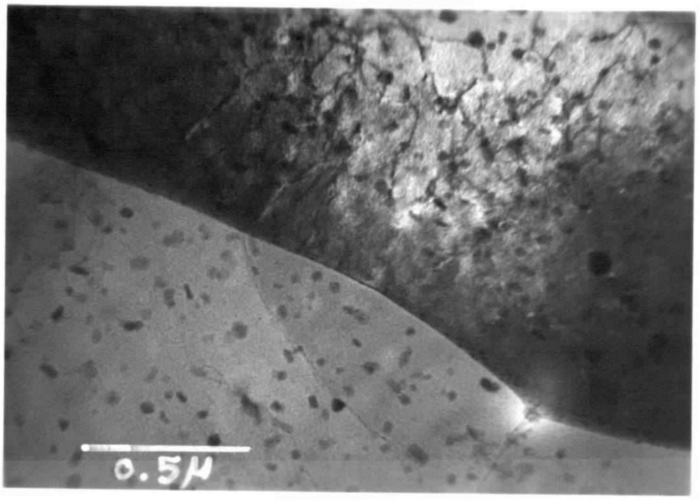

APPENDIX 53. Transmission electron micrograph of 7075-FRT showing high dislocation density in the matrix without precipitate free zone

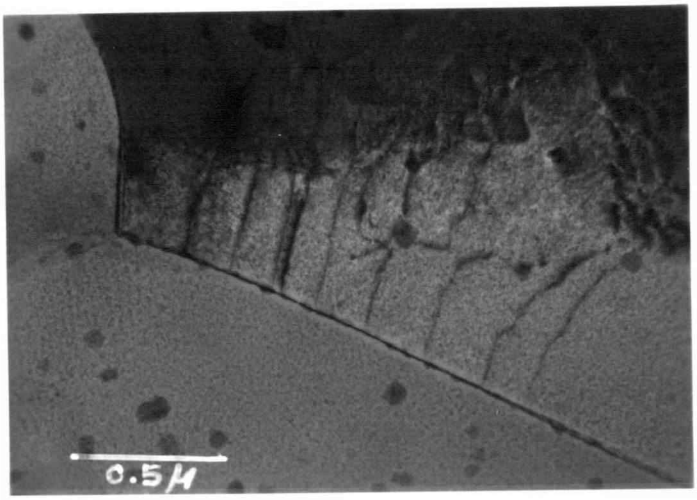

APPENDIX 54. Transmission electron micrograph of 7075-FRT showing dislocations generated from the grain boundary by cyclic loading of 7 Ksi

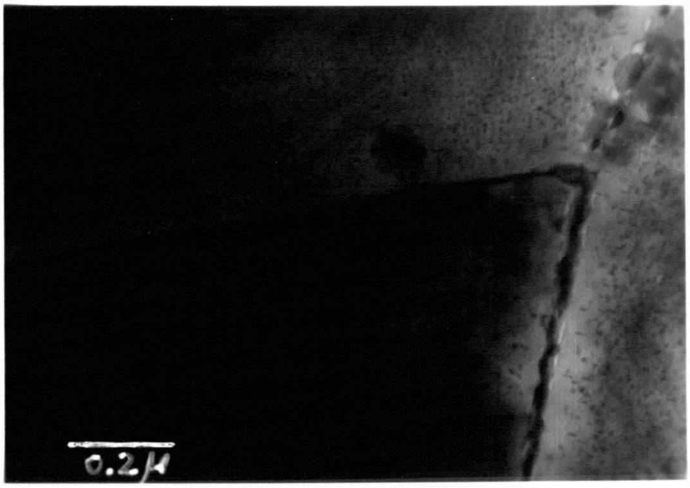

APPENDIX 55. Transmission electron micrograph of 7075-PFZ#1, 73000X

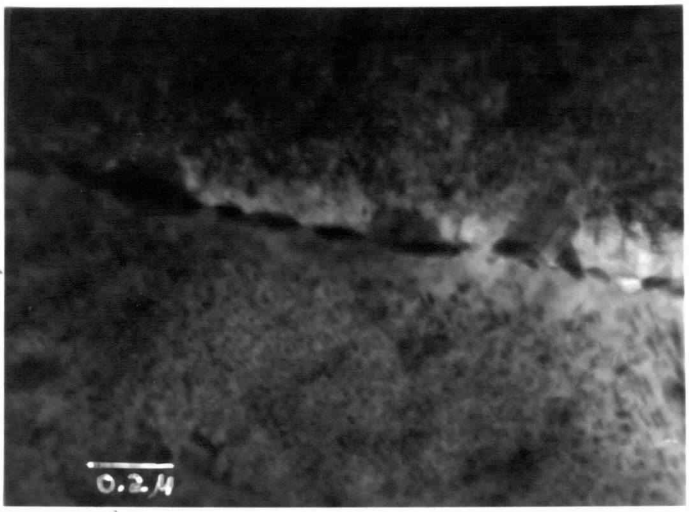

APPENDIX 56. Transmission electron micrograph of 7075-PFZ#2, 57000X

APPENDIX 57. Transmission electron micrograph of 7075-FHT after cyclic pre-loading with 50 Ksi showing heavy slip band

```
100 OPEN4,4:CMD4
110 DIMA(30),N(30),BB(3),DN(30),DK(30),ID(7),AA(10),NN(10)
120 READ ID$,NP,TY
130 READ PN,PX,F,B,W,AM
140 READ EV$,TE$,YS$,KI$
150 FOR I=1TONP
160 READ A(I),N(I)
170 NEXT I
180 REM**CRACK LENTH DATA IS ONLY ACTUAL PROPAGATED CRACK
190 R=PN/PX
200 PRINT "ID=";ID$,"NP=";NP,"TY=";TY
210 PRINT "PN=";PN,"PX=";PX,"F=";F,"B=";B,"W=";W,"AM=";AM
220 PRINT "EV=";EV$,"TE=";TE$,"YS=";YS$,"KI=";KI$
230 PRINT"R=";R
235 PRINT"#","N.OF C",      "CRACK LENGTH","A(REG)","REG.P"      ,"DELTA K","DA/DN"
240 FOR I=1TONP
250 A(I)=A(I)+AM
260 NEXT I
270 K=0
280 PI=3.1416
290 PP=PX-PN
300 FOR I=1TO3
310 PRINT I,N(I),A(I)
320 NEXT I
330 NP=NP-6
340 FORI=1TONP
```

APPENDIX 58. BASIC program for fatigue crack propagation rate with respect to ΔK by seven point polynomial method

```
350 L=0
360 K=K+1
370 K1=K+6
380 FORJ=KTOK1
390 L=L+1
400 AA(L)=A(J)
410 NN(L)=N(J)
420 NEXT J
430 C1=.5*(NN(1)+NN(7))
440 C2=.5*(NN(7)-NN(1))
450 SX=0
460 S2=0
470 S3=0
480 S4=0
490 SY=0
500 YX=0
510 Y2=0
520 FOR J=1TO7
530 X=(NN(J)-C1)/C2
540 YY=AA(J)
550 SX=SX+X
560 S2=S2+X^2
570 S3=S3+X^3
580 S4=S4+X^4
590 SY=SY+YY
600 YX=YX+X*YY
```

```
610 Y2=Y2+YY*X^2

620 NEXT J

630 DE=7.0*(S2*S4-S3^2)-SX*(SX*S4-S2*S3)+S2*(SX*S3-S2^2)

640 T2=SY*(S2*S4-S3^2)-YX*(SX*S4-S2*S3)+Y2*(SX*S3-S2^2)

650 BB(1)=T2/DE

660 T3=7.0*(YX*S4-Y2*S3)-SX*(SY*S4-Y2*S2)+S2*(SY*S3-YX*S2)

670 BB(2)=T3/DE

680 T4=7.0*(S2*Y2-S3*YX)-SX*(SX*Y2-S3*SY)+S2*(SX*YX-S2*SY)

690 BB(3)=T4/DE

700 YB=SY/7.0

710 RS=0

720 TS=0

730 FOR J=1TO7

740 X=(NN(J)-C1)/C2

750 YH=BB(1)+BB(2)*X+BB(3)*X^2

760 RS=RS+(AA(J)-YH)^2

770 TS=TS+(AA(J)-YB)^2

780 NEXT J

790 R2=1.0-RS/TS

800 DN(I)=BB(2)/C2+2.0*BB(3)*(NN(4)-C1)/C2^2

810 X=(NN(4)-C1)/C2

820 AR=BB(1)+BB(2)*X+BB(3)*X^2

830 S=1E+10

840 SN=0

850 QQ=I+3

860 T=AR/W
```

```
870 FT=((2+T)*(0.886+4.64*T-13.32*T^2+14.72*T^3-5.6*T^4))/(1-T)^1.5

880 S=YS*SQR(PI*W*(1-T))/2

888 LIST

890 DK(I)=(FT*PP)/(B*SQR(W))

900 AX=DK(I)/(1-R)

910 IF AX>=S THEN 920

920 PRINT QQ,N(QQ),A(QQ),AR,R2,    DK(I) ,DN(I)

930 NEXT I

940 J=NP+4

950 K=NP+6

960 FOR I=JTOK

970 PRINT I,N(I),A(I)

980 NEXT I

990 DATA T-651,24,1

1000 DATA .154,1.43,10,.4,2,.5000

1010 DATA AIR,25C,75KSI,COMPACT

1020 DATA .194,1080,.197,1680,.1998,2040,.2008,2520,.2016,3000

1030 DATA .2058,3480,.2074,3960,.2080,4200,.2084,4320,.230,4440

1040 DATA .240,4560,.250,4680,.270,4800,.280,4920,.30,5040

1050 DATA .320,5160,.330,5280,.340,5400,.360,5520,.380,5640

1060 DATA .40,5760,.45,6000,.510,6240,.540,6360

2000 PRINT#4

READY.
```

ID$=T-6 NP= 24 TY= 1

PN= .16 PX= 1.43 F= 10 B= .4 W= 2 AM= .5

EV=AIR TE=20C YS=75KSI KI=COMPACT

R= .111888112

#	N.OF C	CRACK LENGTH	A(REG)	REG.P	DELTA K	DA/DN
1	0	.694				
2	1800	.6942				
3	2400	.695				
4	3600	.697	.696801452	.994760122	14.2914101	1.58625843E-06
5	4200	.698	.698193149	.998205214	14.316969	1.93429334E-06
6	6600	.7038	.70342741	.993763434	14.4135423	2.04887865E-06
7	7200	.7048	.70484445	.996745225	14.4398092	1.87658913E-06
8	7800	.7062	.706131108	.742710577	14.4637049	6.72618461E-06
9	8400	.7066	.706104762	.948040053	14.4632151	1.13571429E-05
10	9000	.708	.714028572	.984042419	14.6113403	1.825E-05

APPENDIX 59. Crack propagation rate computed by seven point polynomial method for 7075-T6

11	9600	.73	.729304762	.966035581	14.9017849	2.32261904E-05
12	10200	.75	.747657143	.982831777	15.2597092	2.76309524E-05
13	10800	.77	.765904762	.989443343	15.626034	3.19047619E-05
14	11400	.78	.783809523	.992602263	15.9963706	3.27380953E-05
15	12000	.8	.802857143	.995633188	16.4031015	3.57142858E-05
16	12600	.83	.826190477	.993564993	16.9207676	3.80952381E-05
17	13200	.85	.851904762	.997828447	17.5183661	4.16666667E-05
18	13800	.88	.877142857	.997754491	18.1353827	4.3452381E-05
19	14400	.9	.902380953	.998819641	18.7857803	4.46428572E-05
20	15000	.93	.929523811	.998423956	19.5265245	4.88095238E-05
21	15600	.96	.958710295	.999435751	20.3761723	5.26745631E-05
22	16200	.99				
23	16800	1.03				
24	17280	1.06				

ID$=T-651 NP= 24 TY= 1

PN= .16 PX= 1.43 F= 10 B= .4 W= 2 AM= .5

EV=AIR TE=20C YS=75KSI KI=COMPACT

R= .111888112

#	N.OF C	CRACK LENGTH	A(REG)	REG.P	DELTA K	DA/DN
1	1080	.694				
2	1680	.697				
3	2040	.6998				
4	2520	.7008	.700853236	.971233306	14.3659599	4.51484662E-06
5	3000	.7016	.702830847	.966907911	14.4024998	4.32171497E-06
6	3480	.7058	.704716745	.963845542	14.4374398	4.40687563E-06
7	3960	.7074	.708471715	.612220476	14.5072864	1.8142402E-05
8	4200	.708	.713819984	.7686531	14.6074193	4.3824125E-05
9	4320	.7084	.717152138	.930775438	14.670198	6.83414724E-05
10	4440	.73	.724296104	.973082751	14.8058303	8.99850786E-05

APPENDIX 60. Crack propagation rate computed by seven point polynomial method for 7075-T651

11	4560	.74	.739009524	.980995626	15.0897908	1.06904762E-04
12	4680	.75	.753485715	.989625033	15.3755498	1.20476191E-04
13	4800	.77	.766190477	.996279762	15.6318568	1.25000001E-04
14	4920	.78	.783333334	.992486338	15.9863748	1.30952381E-04
15	5040	.8	.800952381	.992165242	16.3618086	1.27976191E-04
16	5160	.82	.815238095	.989536622	16.6750063	1.25E-04
17	5280	.83	.83	.987755102	17.0074426	1.30952381E-04
18	5400	.84	.843809524	.992866407	17.3269991	1.33928572E-04
19	5520	.86	.859415585	.99873606	17.698694	1.45546373E-04
20	5640	.88	.878652501	.999504088	18.1733153	1.69083255E-04
21	5760	.9	.900990831	.999809294	18.7490301	1.91593084E-04
22	6000	.95				
23	6240	1.01				
24	6360	1.04				

ID$=PFZ#1 NP= 24 TY= 1

PN= .16 PX= 1.43 F= 10 B= .4 W= 2 AM= .5

EV=AIR TE=20C YS=75KSI KI=COMPACT

R= .111888112

#	N.OF C	CRACK LENGTH	A(REG)	REG.P	DELTA K	DA/DN
1	0	.588				
2	480	.686				
3	600	.687				
4	1800	.693	.691720858	.537861292	14.198518	2.14924083E-05
5	2520	.695	.694306025	.988523037	14.2457035	3.22379003E-06
6	3360	.696	.696581768	.988375305	14.28738	2.62416181E-06
7	5400	.701	.696621429	.930676624	14.2881075	1.62775866E-06
8	8400	.7044	.702068458	.91012093	14.3884013	5.39038398E-06
9	9960	.706	.710363126	.941768539	14.5426104	9.254448E-06
10	12600	.73	.742329353	.970085619	15.1547513	1.94050953E-05

APPENDIX 61. Crack propagation rate computed by seven point polynomial method for 7075-PFZ#1

11	13440	.76	.756036327	.994509473	15.4265828	2.92840223E-05
12	14280	.78	.782264441	.997121968	15.9639671	3.59739285E-05
13	14760	.8	.801337576	.997657772	16.3701478	4.02012352E-05
14	15600	.84	.835399126	.994524016	17.1313676	5.10351486E-05
15	16200	.865	.868473164	.995570854	17.9198298	5.98557605E-05
16	16800	.9	.906342945	.995850783	18.8911374	6.90996381E-05
17	17160	.94	.931227648	.994340409	19.574554	7.87197146E-05
18	17760	.98	.983838657	.99323062	21.1568103	9.19183454E-05
19	17880	.99	.995480919	.989691927	21.5353032	9.20644726E-05
20	18000	1.01	1.00493617	.990765128	21.8510283	9.708291E-05
21	18120	1.02	1.01952381	.993961352	22.3535033	9.82142856E-05
22	18240	1.03				
23	18360	1.04				
24	18480	1.05				

ID$=PFZ#2 NP= 24 TY= 1

PN= .16 PX= 1.43 F= 10 B= .4 W= 2 AM= .5

EV=AIR TE=20C YS=75KSI KI=COMPACT

R= .111888112

#	N.OF C	CRACK LENGTH	A(REG)	REG.P	DELTA K	DA/DN
1	5640	.694				
2	6240	.696				
3	7080	.697				
4	8040	.698	.698228833	.976061845	14.317625	1.59344104E-06
5	8520	.6982	.699142676	.977022931	14.3344357	1.50501445E-06
6	10200	.7024	.701715942	.984833078	14.3818875	1.49645858E-06
7	12000	.7044	.704247815	.977477164	14.4287433	1.47083302E-06
8	13800	.706	.706940415	.705696775	14.4787575	4.35874933E-06
9	15000	.7078	.712743154	.837070919	14.5871963	1.20505448E-05
10	15600	.71	.71798789	.962327124	14.6859917	1.95449944E-05

APPENDIX 62. Crack propagation rate computed by seven point polynomial method for 7075-PFZ#2

11	16200	.73	.729177922	.969853927	14.899346	2.26834253E-05
12	16800	.75	.746876191	.98599677	15.2442693	2.89642858E-05
13	17400	.77	.767142857	.99343832	15.651286	3.27380953E-05
14	18000	.78	.786666667	.994092827	16.0565186	3.33333334E-05
15	18600	.81	.807142858	.99388753	16.4965301	3.39285715E-05
16	19200	.83	.826666668	.990722968	16.9315678	3.80952381E-05
17	19800	.85	.850952382	.992643328	17.495693	4.28571428E-05
18	20400	.87	.874285714	.997116494	18.0639178	4.88095239E-05
19	21000	.91	.905238095	.99851552	18.8616652	5.83333334E-05
20	21600	.94	.948095239	.983497103	20.0603949	6.07142858E-05
21	22200	.99	.989772837	.985972506	21.3483458	5.94267697E-05
22	22800	1.04				
23	23400	1.05				
24	23640	1.06				

	P<Q>	K<IC>
T651L	6.27	22.2654727
T651T	7.7	25.1019545
T6	9.68	39.7386721
PFZ#1	9.9	34.8272788
PFZ#2	11.66	38.8949787

```
1 OPEN4,4:CMD4
100 REM***DK AS KSI/IN^.5
110 REM***DP,SA AND SM IS EXPRESSED AS KIPS
112 PRINT SPC(30);"P<Q>"; SPC(20);"K<IC>"
115 FOR X=1TO5
120 READ ID$,P,B,W,A
150 L=A/W
160 FL=(2+L)*(.866+4.64*L-13.32*L^2+14.72*L^3-5.6*L^4)/(1-L)^1.5
175 K=P*FL/(B*W^.5)
180 PRINT ID$,SPC(10);P,SPC(10);K
300 NEXT X
400 DATA T651L,6.27,1.0,2,.525
410 DATA T651T,7.70,1.0,2,.4625
420 DATA T6, 9.68,1.0,2,.636
430 DATA PFZ#1,9.9,1.0,2,.518
440 DATA PFZ#2,11.66,1.0,2,.479
888 LIST
999 PRINT#4
```

APPENDIX 63. BASIC program for plane strain fracture toughness using Strawley's equation